Kristian Rye Jensen (s072237)

Shape Optimization for Electrical Impedance Tomography

Master's Thesis, March 2013

KRISTIAN RYE JENSEN (s072237)

Shape Optimization for Electrical Impedance Tomography

Master's Thesis, March 2013

Supervisors:

Main supervisor: Kim Knudsen, Associate Professor at DTU Mathematics

Jens Gravesen, Associate Professor at DTU Mathematics

Anton Evgrafov, Associate Professor at DTU Mathematics

DTU - Technical University of Denmark, Kgs. Lyngby - 2013

Shape Optimization for Electrical Impedance Tomography

This report was prepared by:
Kristian Rye Jensen (s072237)

Advisors:
Main supervisor: Kim Knudsen, Associate Professor at DTU Mathematics
Jens Gravesen, Associate Professor at DTU Mathematics
Anton Evgrafov, Associate Professor at DTU Mathematics

DTU Mathematics
Technical University of Denmark
Matematiktorvet, Building 303B
2800 Kgs. Lyngby
Denmark
Tel: +45 4525 3031
Fax: +45 4588 1399

MAT-INSTADM@mat.dtu.dk

Project period:	September 2012 - March 2013
ECTS:	30
Education:	MSc Eng
Field:	Mathematical Modelling and Computations
Class:	Confidential
Remarks:	This report is submitted as partial fulfillment of the requirements for graduation in the above education at the Technical University of Denmark.
Copyrights:	©Kristian Rye Jensen, 2013

Table of Contents

List of Figures

List of Tables

List of Symbols

$\lvert \cdot \rvert$	Euclidean norm
$a.e.$	almost everywhere
β	Noise level.
$\mathcal{N}_i^k$	B-spline of order k
C_c^∞	Space of smooth functions with compact support
$\boldsymbol{p}_i$	Control points in $\mathbb{R}^2$, ($\mathbb{C}$)
D_a	The annulus
$\mathbb{D}$	The unit disc
f	Dirichlet-data
$\hat{f}$	Approximated dirichlet data.
$\tilde{f}$	Transformed dirichlet data
g	Neumann-data
Γ_{I}	Boundary of inclusion
Γ_{II}	Outer boundary
$\tilde{g}$	Transformed Neumann data
$H^{1/2}(\partial\Omega)$	The space $W^{1/2,2}(\partial\Omega)$
$H^1(\Omega)$	The space $W^{k,2}(\Omega)$
$H^{-1/2}(\partial\Omega)$	The space $W^{-1/2,2}(\partial\Omega)$
$H^{-1}(\Omega)$	The space $W^{-1,2}(\Omega)$
$\left\langle \cdot, \cdot \right\rangle$	Inner product or dual pairing
$J(\boldsymbol{p})$	Objective function control point optimization
$J(r_i)$	Objective function radius optimization
Ξ	Knot vector
λ	Regularization parameter

$L(\gamma)$	Length of the curve γ.
L^p	Space of p-integrable functions
ν	Outwards pointing unit normal
n_{cp}	Number of control points
n_{el}	Number of elements
$N(x,y)$	Neumann function
$\|\cdot\|$	Norm
Ω	Open bounded domain in $\mathbb{R}^2$ with smooth boundary
$\partial\Omega$	Boundary of Ω
φ	Normal trace of u to Γ_{I}
$\boldsymbol{p}^*$	Optimal vector of control points.
Ψ_α	Automorphism of the unit disc
r_i	Radius of the inner circular inclusion.
r_i^*	Optimal radius of the inner circular inclusion.
σ	Electrical conductivity
K_N	Single layer potential with normal derivative of Neumann kernel
S_N	Single layer potential with Neumann kernel
$\mathbb{S}_k^{\boldsymbol{\Xi}}$	Space of linear combinations of B-splines of order k and knot vector $\boldsymbol{\Xi}$
u	Electrical potential
$W^{1/2,2}(\partial\Omega)$	The space given by the trace of $W^{1,2}(\Omega)$
$W^{k,p}(\Omega)$	Sobolev space for functions with k weak derivatives in $L^p(\Omega)$
$W^{-1/2,2}(\partial\Omega)$	Continuous dual space of $W^{1/2,2}$

Abstract

This thesis presents a solution of an inverse boundary value problem for harmonic functions arising in Eletrical Impedance Tomography. The concerned problem is regarding shape optimization of perfectly conducting circular inclusions using B-splines. In the thesis a representation of the harmonic electrical potential using boundary integrals is set up as to make a Neumann to Dirichlet (current to voltage) map on the outer boundary, represented by the unit circle. The Cauchy data obtained is hereby associated with the shape and location of the perfectly conducting inclusion. The geometry and governing functions have been approximated by B-splines and the Boundary Element Method (BEM) has been used to discretize the equations with regards to implementation in MATLAB.

The forward problem has been set up, as to given the boundary of the perfectly conducting inclusion and an applied current obtain the voltage distribution on the outer boundary. The algorithm has been tested using a solution obtained from separation of variables and seen to approximate the analytical solutions for both a concentric and a non-concentric circular inclusion. The Cauchy data for the non-concentric case have been found using a conformal map from the concentric to the non-concentric case.

The inverse problem of optimizing the shape of the inclusion, that is optimizing the control points for the boundary, represented by B-splines, has seen to satisfactory detect and approximate the circular boundary, when applying curve speed regularization. For this purpose the Interior-point algorithm has been used from MATLABs optimization framework.

Preface

This thesis has been submitted as a partial fulfillment for the requirements of obtaining the degree of M.Sc. Eng. in Mathematical Modelling and Computations at the Technical University of Denmark and when submitted also fulfill the requirement for obtaining the degree of M.Sc. in Mathematical Sciences from Korea Advanced Institute of Science and Technology (KAIST) on the socalled Dual-degree agreement between KAIST department of Mathematical Sciences and DTU Mathematics. The work has been done from September 2012 to March 2013 at DTU Mathematics. The project has been supervised by Kim Knudsen (main supervisor), Jens Gravesen and Anton Evgrafov all associate professors from DTU Mathematics. The content of the thesis is based on an idea from the supervisors, who are from different mathematical fields and this has led to a thesis combining mathematical theory from the fields of geometry optimization, the theory of inverse problems in medical imaging and numerical implementations.

The intended reader is people like myself with the prerequisites I had before I started the project, i.e. a person who has a background in applied mathematics combined with some knowledge of engineering.

The main contributors to this project has been my advisors and I would like to send my appreciations for always having time to explain and discuss topics and ideas.

I also want to say thanks to my advisor at KAIST, associate professor Lim, Mikyoung who helped me choosing courses and guided me through my one year stay at KAIST.

_____

Kristian Rye Jensen (s072237)

Chapter **1**
Introduction

This chapter will give an account for the motivation, goals and outline regarding the topic of the thesis, namely shape optimization for electrical impedance tomography (EIT).

1.1 Motivation

Electrical Impedance Tomography is an experimental imaging technique, where electrical impedance is a reference to the complex ratio of the voltage to current in an alternating current (AC) curcuit [24], i.e. the imaging part is by evaluating the voltage and current to get an idea of different conductivities in the domain of interest. In medical imaging there are numerous different imaging tools for physicians to apply, these consists of nuclear imaging tools such as X-ray CT (*computed tomography*), SPECT (*single photon emission computed tomography*) and PET (*positron emission tomography*), also non-nuclear, such as MR (*magnetic resonance*) imaging and ultra sound are some of the most used in practic. So with so many different choices why is it necessary to study and obtain methods for a new one, such as EIT?

One reason is that different imaging devices illustrates different properties, e.g. X-Ray CT is highly applicable for imaging of the spatial distribution, whereas other nuclear imaging techniques are better illustrating the biological differences in tissues. EIT images are based on biological tissues different ability to conduct an electric current. This means that there are other available medical imaging techniques for illustrating the same properties. However EIT is a noninvasive procedure which means that it is not invading healthy tissue, furthermore it does not need any big machinery since it at most requires some electrodes, a battery, and a computer to run reconstruction algorithms on the data. Therefore it would be very usefull in the ICU (intesive care unit), where some patients probably cannot be moved to be put in an X-ray CT scanner or be recipients of some ionization radiation for imaging. *Dräger* as one of the first has made a commercialised EIT system called *PulmoVista® 500* for lung monitoring of ICU patients with Acute Lung Injury (ALI) where this is used to monitor the mechanical ventilation of the diseased lung as to make sure it does not overinflate the lung, which could lead to damage of cellular structure [8]. An image of the output of such a device is seen in figure 1.1.

Measurements of the system is obtained by putting on a belt of 16 electrodes, combined with a computer and then recursively induce current at two electrodes and measure the corresponding voltages at the rest of the electrodes, after which current is induced through the next pair of electrodes and so forth. They are using the *Finite Element Method* for the image reconstruction, and can quickly measure and obtain the images.
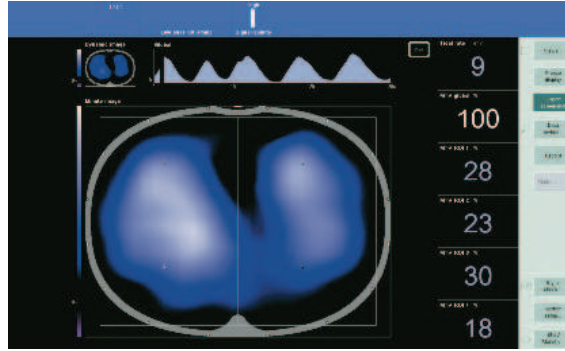
Figure 1.1: The image of the lungs from the EIT machine called PulmoVista® 500 from Dräger[8].

Something else to image could be cancer tumours, since cancer tissue has a higher conductivity than normal tissue. For the destruction of this malicious tissue in a best way, done by laser or ultrasound, the shape of the tumour would be of importance as to not affect healthy tissue.

Shape optimization is how to find the optimal shape of a given object, and in this thesis it will be to find the optimal shape of an inclusion, i.e. a domain with different conductivity compared to the background conductivity. In practice it could be used to determine the shape of a cancer knot, to properly remove this without ruining healthy tissue.

For shape optimization and isogeometric analysis the building blocks are the *B-splines*, *Basis splines* or *spline*, which are piecewise polynomial curves and can take an arbitrarily polynomial degree over an interval, and change the degree locally which for the right information should be able to represent any simple curve.

1.2 Goals

The goal of this thesis is to combine these topics, e.g. to use knowledge of the equations of EIT to mathematically formulate at first a forward problem, on how to obtain the map from current to voltage given that the conductivity distribution is known, thereafter the inverse problem on shape optimization from the knowledge of boundary current and voltage. Mathematical theory for Boundary Integral Equation (BIE), B-splines and usage of the Boundary Element Method (BEM) will be utilized and implemented in MATLAB as the used programming language.

1.3 Outline

The outline of this thesis will initially in Chapter 2 give some preliminaries as the toolbox for further reading, it will explain the governing equations, the simplification of the problem related to this work and describe the tools for the isogeometric analysis of B-splines with regards to the shape optimization problem. Chapter 3 will introduce the Neumann function as a kernel for the constructed boundary integral equations, which will be set up for the problem of an annular domain, i.e. where the inclusion is a concentric circle. Chapter 4 will generalise the described integral equations and the discretization and implementation of the forward problem, which will be tested with a solution for the concentric circle inclusion found by separation of variables, done in Appendix A.2. In Chapter 5 some theory from Complex Analysis will be explained in the context of the usage in this work. Here the concentric circle is mapped conformally to a non-concentric circle to obtain Cauchy-data (both Neumann and Dirichlet, e.g. the current and voltage distribution at the boundary) to obtain other test data. In Chapter 6 the inverse problem of the shape optimization is explained with corresponding noise and regularization. At last Chapter 7 and 8 will discuss the work with future extensions and conclude on the thesis.

<div align="right">

Chapter **2**

</div>

<div align="right">

Preliminaries

</div>

In this chapter mathematically and physical preliminaries will be set up. First a brief introduction to the governing equations of EIT with a simplification of the equations corresponding to the usage in this thesis. Secondly, theory of the properties of B-splines will be treated and finally some extensions of the goals described in the introduction chapter.

2.1   Electrical Impedance Tomography

As explained in the introduction EIT is an experimental technique for medical imaging, where either current or voltage is applied to a number of electrodes on the boundary of a body and then the corresponding voltage or current are measured on adjacent electrodes.

Figure 2.1:   Electrodes on a chest for lung monitoring. [25]

The imaging part of the problem is to recover the conductivity distribution from the interior, since different tissue have different conductivity. Examples of different conductivities of tissue are shown in table 2.1.

Tissue:	Fat	Bone	Blood	Lung (inflated)	Heart
σ [S/m]	0.22-0.4	0.01-0.06	0.43-0.07	0.024-0.09	0.06-0.4

Table 2.1:   Specific Conductivities σ for different tissue. [17]

2.1.1   Derivation of equations

In this project 2-dimensional domains are considered, i.e. bounded domains $B \subset \mathbb{R}^2$, where $\mathbb{C}$ is associated with $\mathbb{R}^2$. This is by relating a belt of electrodes around a body, which is certainly bounded and 2-dimensional. The outside of the domain $\mathbb{R}^2 \setminus \overline{B}$ is defined as an electrical insulator. It has been chosen in this project to evaluate the case where the measurements are the voltages with regards to the applied current, which are the more common in medical EIT, since control of the maximum applied current can be desirable for safety reasons. An assumption is that the applied current is alternating, since the direction of the current has to be reversed within a sufficiently short time, otherwise it could result in transportation of ions, which could mean stimulation of nerves [20]. Another consequence could be electrode degredation from build up of charge. Simple EIT systems operates within a fixed frequency using an oscillator to produce a sinusoidal current. The measurement then starts when the transient part has decayed so it becomes negligible which is hereby assumed in the next derivation. [20] The time harmonic electric and magnetic vector fields

$$\mathcal{E}(x,t) = \text{Re}\left(\boldsymbol{E}(x,\omega)e^{i\omega t}\right), \tag{2.1.1}$$

$$\mathcal{H}(x,t) = \text{Re}\left(\boldsymbol{H}(x,\omega)e^{i\omega t}\right), \tag{2.1.2}$$

where $\text{Re}(f)$ denotes the real part of the complex function f. (2.1.1)-(2.1.2) satisfies Maxwell's equations, at a fixed angular frequency ω, given by

$$\nabla \times \boldsymbol{E} = -i\omega\boldsymbol{B} \tag{2.1.3}$$

$$\nabla \times \boldsymbol{H} = \boldsymbol{J} + i\omega\boldsymbol{D}, \tag{2.1.4}$$

where $\boldsymbol{J}$ is the current density, $\boldsymbol{D}$ is the electric displacement and $\boldsymbol{B}$ is the magnetic flux which relates by the material properties

$$\boldsymbol{J} = \sigma\boldsymbol{E},\ \boldsymbol{D} = \epsilon\boldsymbol{E},\ \boldsymbol{B} = \mu\boldsymbol{H}, \tag{2.1.5}$$

for conductivity σ, permittivity ϵ, and permeability μ. Plugged into (2.1.3)-(2.1.4) yields

$$\nabla \times \boldsymbol{E} = -i\omega\mu\boldsymbol{H} \tag{2.1.6}$$

$$\nabla \times \boldsymbol{H} = \sigma\boldsymbol{E} + i\omega\epsilon\boldsymbol{E}. \tag{2.1.7}$$

Setting up the non-dimensional form for the problem to evaluate parameter scale, i.e. set $\boldsymbol{E} = [\boldsymbol{E}]\,\tilde{\boldsymbol{E}}$, $\boldsymbol{H} = [\boldsymbol{H}]\,\tilde{\boldsymbol{H}}$, $\boldsymbol{x} = [\boldsymbol{x}]\,\tilde{\boldsymbol{x}}$ and $\nabla\times = [\boldsymbol{x}]^{-1}\,\tilde{\nabla}\times$, where the values in brackets are scalars carrying the units and the parameters with tilde are the nondimensional equivalence. Now (2.1.6)-(2.1.7) evaluates to

$$\tilde{\nabla} \times \tilde{\boldsymbol{E}} = -i\frac{\omega\mu\,[\boldsymbol{x}]\,[\boldsymbol{H}]}{[\boldsymbol{E}]}\tilde{\boldsymbol{H}} \tag{2.1.8}$$

$$\tilde{\nabla} \times \tilde{\boldsymbol{H}} = \sigma\frac{[\boldsymbol{x}]\,[\boldsymbol{E}]}{[\boldsymbol{H}]}\tilde{\boldsymbol{E}} + i\omega\epsilon\frac{[\boldsymbol{E}]\,[\boldsymbol{x}]}{[\boldsymbol{H}]}\tilde{\boldsymbol{E}}, \tag{2.1.9}$$

and choosing $[\boldsymbol{E}]$ and $[\boldsymbol{H}]$ such that $\sigma\frac{[\boldsymbol{x}][\boldsymbol{E}]}{[\boldsymbol{H}]} = 1$ gives

$$\tilde{\nabla} \times \tilde{\boldsymbol{E}} = -i\omega\mu\sigma\,[\boldsymbol{x}]^2\,\tilde{\boldsymbol{H}} \tag{2.1.10}$$

$$\tilde{\nabla} \times \tilde{\boldsymbol{H}} = \tilde{\boldsymbol{E}} + i\omega\sigma^{-1}\epsilon\tilde{\boldsymbol{E}}. \tag{2.1.11}$$

From [4] normal EIT systems work in a range where $\omega\mu\sigma\,[\boldsymbol{x}]^2$ is negligible, hence neglecting the right hand side in (2.1.10) corresponds to neglecting right hand side in (2.1.3). Hereby concluding that the electric field is the gradient of a scalar potential, e.g.

$$\boldsymbol{E} = -\nabla u, \tag{2.1.12}$$

where u is the electrical potential. The equation

$$\nabla(\sigma + i\epsilon\omega)\nabla u = 0, \tag{2.1.13}$$

comes from taking the divergence on both sides in (2.1.7) and inserting (2.1.12), here $\eta = \sigma + i\omega\epsilon$ is the complex conductivity. Now reviewing the applied current to the equations, which is adding an additional electric field as

$$\boldsymbol{E}_{\text{tot}} = \boldsymbol{E}_{\text{app}} + \boldsymbol{E}_0 \tag{2.1.14}$$

where $\boldsymbol{E}_{\text{app}} = \eta^{-1}\boldsymbol{J}^{\text{app}}$. Thus the equation for the magnetic field $\boldsymbol{H}$ now yields

$$\nabla \times \boldsymbol{H} = \boldsymbol{J}^{\text{app}} + \eta\boldsymbol{E}_0, \tag{2.1.15}$$

here $\boldsymbol{E}_0$ is relating to the previous derivation and hence using (2.1.12) and taking the divergence on both sides, gives

$$0 = \nabla(\boldsymbol{J}^{\text{app}} - \eta\nabla u) \Leftrightarrow \nabla \cdot \eta\nabla u = \nabla\boldsymbol{J}^{\text{app}},$$

integrating on both sides over a square Ω_δ with side length δ containing a part of the boundary ∂B, and using the divergence theorem yields when $\delta \to 0$,

$$\int_{\Omega_\delta} \nabla \cdot \eta\nabla u\, dx = \int_{\Omega_\delta} \nabla\boldsymbol{J}^{\text{app}}dx \Rightarrow$$

$$\lim_{\delta \to 0} \int_{\partial\Omega_\delta} \eta\nabla u \cdot \nu\, dS = \lim_{\delta \to 0} \int_{\partial\Omega_\delta} \boldsymbol{J}^{\text{app}} \cdot \nu\, dS \Rightarrow$$

$$\eta_{\text{out}}\partial_\nu u - \eta_{\text{in}}\partial_\nu u = \boldsymbol{J}^{\text{app}}_{\text{out}} \cdot \nu - \boldsymbol{J}^{\text{app}}_{\text{in}} \cdot \nu,$$

here ν is the unit normal and ∂_ν the normal derivative. Assuming now that the conductivity η_{out} is negligible and no internal current sources. From this, with abuse of notation $\eta_{\text{in}} = \eta$ and $\boldsymbol{J}^{\text{app}}_{\text{out}} = \boldsymbol{J}^{\text{app}}$, it follows

$$\eta\partial_\nu u = -\boldsymbol{J}^{\text{app}} \cdot \nu = g, \tag{2.1.16}$$

where g is defined as the function for the applied current, which is one of the important parameters in this problem. From the conservation of charge, which tells that there is no build up of charge in the body, and must therefore satisfy

$$\int_{\partial\Omega} g\, ds = 0. \tag{2.1.17}$$

The equations are now, given a potential $u \in H^1(B)$ and induced current $g \in H^{-1/2}(\partial B)$

$$\nabla \cdot \eta\nabla u = 0, \quad x \in B$$
$$\eta\partial_\nu u = g, \quad x \in \partial B, \tag{2.1.18}$$

where the Sobolev function spaces are described in Appendix A.1. The problem of obtaining the conductivity distribution from boundary measurements is in mathematical speaking a severely ill-posed problem. Hadamards three criteria defining a well-posed problem

1. For all admissible data, a solution exists.

2. For all admissible data, a solution is unique.

3. The solution depends continuously on the data.

For the existence of solutions to a non-linear problem like this. From the assumption of applied current to a conducting medium, which means that there must exist some potential which can be measured, corresponding to some conductivity distribution. The third criteria is what makes the problem severely ill-posed, since low-frequency electrical imaging can have difficulty measuring large changes in conductivity as explained in [12]. Since the main problem of this project is to try to implement shape optimization of an inclusion with different conductivity than the background. Therefore the non-linear partial differential equation has been simplified to a linear partial differential equation with assumptions on the conducting inclusion, which makes the problem more well-posed.

2.1.2   Simplification of the problem

The main simplification in this project has been to make an assumption on the complex conductivity η, which is assumed to only get contribution from the real conductivity part σ and for an inclusion U, where $\partial B \cap \bar{U} = \emptyset$, the conductivity is defined as

$$\sigma(x) = \begin{cases} 1, & x \in B \setminus \bar{U} \\ \infty, & x \in U. \end{cases} \tag{2.1.19}$$

Setting the conductivity to infinity corresponds to saying that the inclusion is perfectly conducting, i.e. the difference in potential across any path I through this inclusion gives

$$u_2 - u_1 = -\int \boldsymbol{E} dI = -\int \sigma^{-1} \boldsymbol{J} dI = 0 \Leftrightarrow u_2 = u_1 = c, \tag{2.1.20}$$

here c is a constant. To ground the potential or make a reference potential is like setting this constant to zero, i.e. corresponds to setting a boundary condition on $\partial U = \Sigma$ as

$$u|_\Sigma = 0. \tag{2.1.21}$$

The equations with Δ acting as Laplace operator in 2-dimensions $\Delta = \frac{\partial^2}{\partial x^2} + \frac{\partial^2}{\partial y^2}$. Setting $\partial B = \Gamma$ and defining $\Omega = B \setminus U$, with boundary $\partial\Omega = \partial B \cup \partial U = \Sigma \cup \Gamma$ gives

$$\Delta u(x) = 0, \quad x \in \Omega \tag{2.1.22}$$
$$\partial_\nu u(x) = g(x), \quad x \in \Gamma \tag{2.1.23}$$
$$u(x) = 0, \quad x \in \Sigma. \tag{2.1.24}$$

The problem is shown in figure 2.2.

The trace of the function u to the boundary Γ corresponds to the measured voltage distribution on the outer boundary, i.e.

$$u|_\Gamma = f, \tag{2.1.25}$$

where the trace $f \in H^{1/2}(\Gamma)$ as $u \in H^1(\Omega)$. The following proves uniqueness for the simplified problem

Theorem 2.1.1 *(Uniqueness) The solution $u \in H^1(\Omega)$ to (2.1.22)-(2.1.24) is unique.*
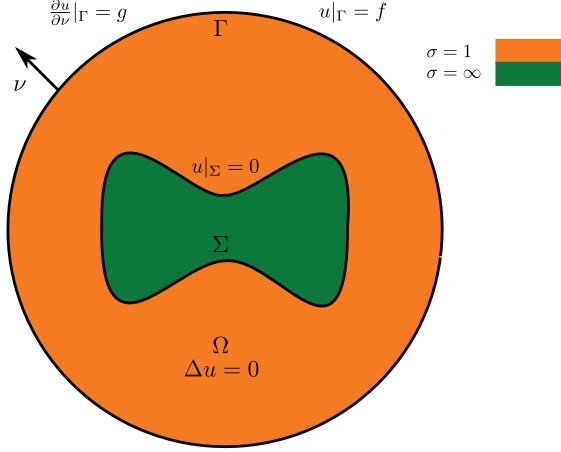
Figure 2.2: The simplified problem, with an inclusion.

Proof Let $w = u - v$ and assume that $u, v \in H^1(\Omega)$ both solves (2.1.22)-(2.1.24), then since Δ is a linear operator and using the boundary conditions gives

$$\Delta w(x) = \Delta u(x) - \Delta v(x) = 0, \quad x \in \Omega \tag{2.1.26}$$

$$\partial_\nu w(x) = \partial_\nu u(x) - \partial_\nu v(x) = g(x) - g(x) = 0, \quad x \in \Gamma \tag{2.1.27}$$

$$w(x) = u(x) - w(x) = 0, \quad x \in \Sigma. \tag{2.1.28}$$

Now take (2.1.26) and multiply w on both sides and integrate over the domain Ω then use Green's first theorem, (theorem 6.3 in [15]) together with the boundary conditions (2.1.27) and (2.1.28) gives

$$0 = -\int_\Omega \Delta w(x) \cdot w(x) dx = \int_\Omega \nabla w(x) \cdot \nabla w(x) dx - \int_{\partial\Omega} w(x) \frac{\partial w}{\partial\nu}(x) ds(x) \Leftrightarrow \tag{2.1.29}$$

$$0 = \int_\Omega |\nabla w(x)|^2 dx - \int_\Gamma w(x) \frac{\partial w}{\partial\nu}(x) ds(x) - \int_\Sigma w(x) \frac{\partial w}{\partial\nu}(x) ds(x) \Leftrightarrow \tag{2.1.30}$$

$$0 = \int_\Omega |\nabla w(x)|^2 dx. \tag{2.1.31}$$

Now this implies for a.e. $x \in \Omega$ that for a constant C

$$\nabla w(x) = 0 \Leftrightarrow w(x) = C, \tag{2.1.32}$$

and from the boundary condition (2.1.28) this implies $w(x) = 0 \Leftrightarrow u(x) = v(x)$ for a.e. $x \in \Omega$.

∎

The existence of solutions have been shown for an annular region in Appendix A.2 by separation of variables.

2.2 B-splines

In this section *B-splines* or *Basis-splines* and their basic properties are described with regards to the usage, which will relate to domain approximation and approximation of the governing functions. For further reading the reader is refered to [19].

A general curve on parametric form $\gamma : \mathbb{R} \to \mathbb{R}^2$ can be described by $n+1$ *control points* $\boldsymbol{p}_i \in \mathbb{R}^2$ and $n+1$ degree d, with order $k = d+1$, basis splines $\mathcal{N}_i^k : \mathbb{R} \to \mathbb{R}$, i.e.

$$\gamma(t) = (x(t)\,,\,y(t)) = \sum_{i=0}^n \boldsymbol{p}_i \mathcal{N}_i^k(t). \tag{2.2.1}$$

The values of $t = t_0, t_1, \ldots, t_m$ are called the *knots* and the vector $\boldsymbol{\Xi} = [t_0, t_1, \ldots, t_m]$ is called the *knot vector*, where $\{t_i\}$ is a monotonically increasing sequence. The B-spline is therefore defined for $t \in [t_0, t_m]$. Furthermore the functions $\mathcal{N}_i^k(t)$ are functions with minimal support and continuity properties corresponding to the degree, e.g. a degree $d = 2$, order $k = 3$ would have C^1 continuity at the knots and C^∞ continuity everywhere else. Now definitions and some important properties of the B-splines will be treated, along with the definition of the space of linear combinations of the B-splines. First the B-splines is defined by a recursion formula given by

Definition 2.2.1 *(Cox-de Boor algorithm) The definition of the B-splines as polynomials can be done by a recursion formula, where they are defined with regards to a strictly increasing sequence of knots $\{t_i\}$, e.g.*

$$\mathcal{N}_i^k(t) = \begin{cases} 1 & if \quad t \in [t_i, t_{i+k}) \\ 0 & otherwise \end{cases},$$

here for the order $k = 1$, and for higher orders of $k = 2, 3, \ldots$

$$\mathcal{N}_i^k(t) = \alpha_i^{k-1} \mathcal{N}_i^{k-1}(t) + \left(1 - \alpha_{i+1}^{k-1}\right) \mathcal{N}_{i+1}^{k-1}(t)$$

with parameter α_i^{k-1} which describes the support of $\mathcal{N}_i^{k-1}(t)$ given as

$$\alpha_i^{k-1} = \frac{t - t_i}{t_{i+k} - t_i}.$$

The following important properties of the B-splines as seen in [19] for a given knot vector $\boldsymbol{\Xi}$ are

1. The B-splines forms a partition of unity

$$\sum_{i=0}^n 1 \cdot \mathcal{N}_i^k(t) = 1, \quad \text{for} \quad t \in [t_{k-1}, t_{n+1}]. \tag{2.2.2}$$

2. The B-splines are positive over the interior of their support

$$\mathcal{N}_i^k(t) > 0, \quad \text{for} \quad t \in (t_i, t_{i+k}).$$

3. The B-splines have compact support

$$\text{supp}\,\mathcal{N}_i^k = [t_i, t_{i+k}].$$

4. Any segment of a spline curve $\gamma(t)$, $t \in [t_i, t_{i+1}]$ lies in the convex hull of its k control points $\boldsymbol{p}_{i-k}, \ldots, \boldsymbol{p}_i$.

The definition of the space of linear combination of the B-splines are

Definition 2.2.2 *Let $\boldsymbol{\Xi} = \left\{t_0, \ldots, t_{n_{cp}+k-1}\right\}$ be the knot vector, for n_{cp} B-splines and control points, then the linear combinations $\mathbb{S}_k^{\boldsymbol{\Xi}}$ of all such B-splines of order k, is defined by*

$$\mathbb{S}_k^{\boldsymbol{\Xi}} = span\left\{\mathcal{N}_0^k(t), \ldots, \mathcal{N}_{n_{cp}}^k(t)\right\} = \left\{\sum_{i=0}^{n_{cp}} \boldsymbol{p}_i \mathcal{N}_i^k(t) \,|\, \boldsymbol{p}_i \in \mathbb{R}^2, for\ 0 \le i \le n_{cp}\right\}.$$

An element in this space is a spline curve in $\mathbb{R}^2$ of order k. The B-splines $\mathcal{N}_i^k(t)$ can over each knot interval compute any polynomial of the same degree. Since they are linearly independent, i.e. a spline function is only 0 if all the coefficients are zero vectors, they form a basis for the space of polynomials of degree $k-1$ over each knot. From *Weierstrass approximation theorem* [5] any continuous function on a closed interval can be uniformly approximated by polynomials, which means that B-spline approximation to a given boundary curve of a certain regularity will also be a uniform approximation. Now for the purpose of simple connected inclusions, some theory for periodic B-splines is examined.

2.2.1 Uniform periodic B-splines

A knot vector for a B-spline is said to be *uniform* if the knots are uniformly distributed i.e. $t_0 < t_1 < t_2 < \cdots < t_m$ with equal spacing in between. For the meaning of periodicity of a B-spline is that the B-spline curve end-points are connected. Looking at a B-spline of order $k = 3$ degree $d = 2$ with uniform knot distribution, i.e.

$$\gamma(t) = \sum_{i=0}^{n_{cp}} p_i \mathcal{N}_i^3(t) \tag{2.2.3}$$

as shown in figure 2.3.
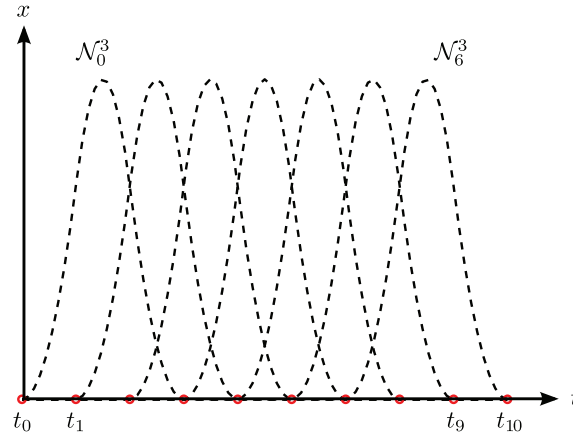
Figure 2.3: B-spline of order 3 with 7 basis functions and control points and uniform knot vector with 11 elements.

Evaluating the case above for number of

$$\text{Control points}: \quad 0 \ldots n_{cp}\,(n_{cp} + 1)$$
$$\text{Basis functions}: \quad n_{cp} + 1\,(\text{using } k + 1 = 4\,\text{knots each})$$
$$\text{Total knots}: \quad n_{cp} + k + 1 = n_{cp} + 4.$$

Seeing that between each pair of knots (bays) there are a different number of basis functions defined. Over the first and last $k - 1 = 2$ bays there are fewer basis functions, which imply that the spline is not defined over these bays as seen in figure 2.4, where the fully defined domain is highlighted. This corresponds to

$$\text{Defined Knots}: \quad (n_{cp} + 4) - 2(k - 1) = n_{cp}$$
$$\text{Defined Bays}: \quad n_{cp} - 1 \tag{2.2.4}$$
$$\text{Parameter t}: \quad t_2 \leq t \leq t_{n_{cp}+2}.$$
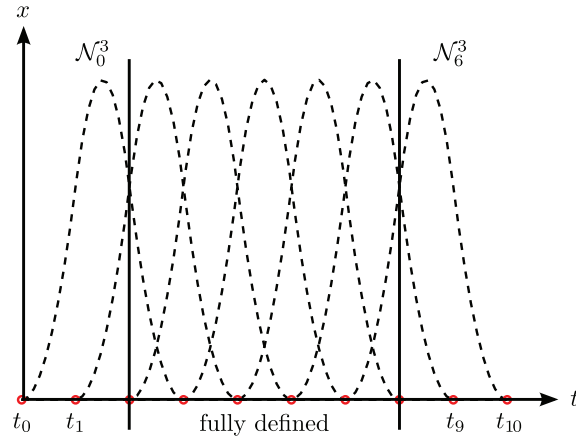
Figure 2.4: Fully defined area of B-spline curve with corresponding knots.

From (2.2.4) and figure 2.4 it is evident that the B-spline does not start at the first control point or end at the last point. When creating a periodic B-spline curve this has to be accounted for, and can be accomplished by input of socalled *phantom control points*.

The phantom control points are named as such, since they are normally not shown in graphical interpretations. The method is simply if the goal is to create a periodic spline curve of order 3, the requirement is that the first and last two control points are the same. This will relate to the defined area of the knots for the curve. An example for a periodic spline curve, setup with the MATLAB function spmak from [6], which will be further discussed in the implementation part of the report.

Example Consider the inclusion as a circle with radius 0.5 approximated by B-splines of order $k = 3$ degree $d = 2$, with a regular control polygon with $n_{cp} = 4$ coefficients. Since it is supposed to be periodic, it is not going through the first or last control point, which is overcome by repeating it, so for this problem, there will be $n_{cp} = 6$ control points, but will only be defined in 4, that is

$$\texttt{coefs} = \begin{bmatrix} 0.5 & 0.5 & -0.5 & -0.5 & 0.5 & 0.5 \\ -0.5 & 0.5 & 0.5 & -0.5 & -0.5 & 0.5 \end{bmatrix}.$$

The same for the knot vector which will have 4 phantom knots and the B-spline will be defined for $t_2 \leq t \leq t_6$, the knot vector is therefore

$$\texttt{knots} = \begin{bmatrix} -0.5 & -0.25 & 0.0 & 0.25 & 0.5 & 0.75 & 1.0 & 1.25 & 1.5 \end{bmatrix},$$

which is obviously uniformly spaced. Now in MATLAB taking sp = spmak(knots,coefs) and using the plot function, in the interval $[0, 1]$ e.g. fnplt(sp,[0 1]) is seen in figure 2.5.

In figure 2.5 is seen a periodic spline curve, which has 4 polynomial pieces. Now some tools for the shape optimization has been seen, and a reformulation of the goals stated in the introduction can be done.
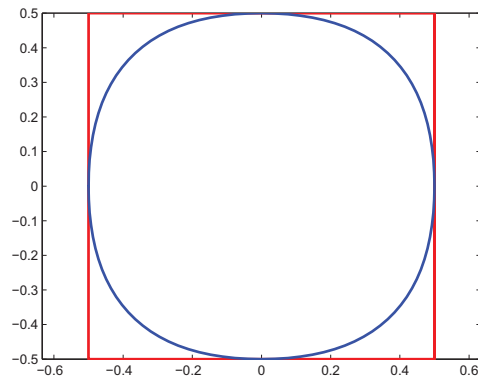
Figure 2.5: The order 3 uniform periodic B-spline (blue) with corresponding control polygon (red).

2.3 Specification of goals

The previously stated goals were a little bit vague formulated, since a limited knowledge of the equations and the tools were known. Now with the simplification of the problem along with the knowledge of B-splines, the goals can be further specified. In this project the main and only problem discussed is the linear partial differential equation (2.1.22)-(2.1.24) with the perfectly conducting inclusion, this simplification has been determined since the main focus will lie on the aspect of optimizing the shape of an inclusion and not to determine the conductivity distribution, the approximation will be with regards to third order, second degree periodic B-splines with uniform knots. The goal is hereby to obtain a map from Neumann data (current) to Dirichlet data (voltage) with respect to a perfectly conducting inclusion, which is the forward problem. Then set up the problem of determining the shape of the boundary of the inclusion from the Cauchy-data, which is the socalled inverse problem.

Concentric Inclusion

In this chapter the Boundary Value Problem (BVP) is set up for an annular region. The *Neumann function* for the unit disc is derived and used as a kernel for a Boundary Integral Equation (BIE) representation of the harmonic function. Green's identities will be used for this setup. Furthermore the socalled *jump relation* coming from the fundamental solution of Laplace equation will be treated. The reason for this setup has been to represent the harmonic function by the boundaries of the domain, since the inverse problem will consist of detecting and approximating such boundary. The domain now considered is an annulus where $\overline{D}_a := \{x \in \mathbb{C} \mid r_i \leq |x| \leq 1\}$ and r_i is the inclusion radius as shown in figure 3.1.
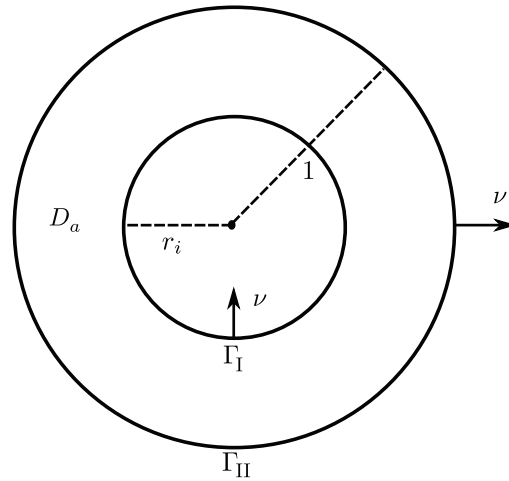
Figure 3.1:   The problem where the inclusion is a circle with radius r_i.

The setup for the problem is

$$
\begin{aligned}
\Delta u &= 0, \quad x \in D_a \\
u &= 0, \quad x \in \Gamma_{\mathrm{I}}, \quad (\Gamma_{\mathrm{I}} := \{x \in \mathbb{C} \mid |x| = r_i\}) \\
\frac{\partial u}{\partial \nu} &= g, \quad x \in \Gamma_{\mathrm{II}}, \quad (\Gamma_{\mathrm{II}} := \{x \in \mathbb{C} \mid |x| = 1\}).
\end{aligned}
\tag{3.0.1}
$$

the functions are defined in the function spaces $u \in H^1(D_a)$, $g \in H^{-1/2}(\Gamma_{\mathrm{II}})$ respectively. The following sets are defined as $\partial D_a := \Gamma_{\mathrm{I}} \cup \Gamma_{\mathrm{II}}$, for $\Gamma_{\mathrm{I}} \cap \Gamma_{\mathrm{II}} = \emptyset$.

3.1   Neumann function for the unit disc

The Neumann function used for (3.0.1) is with respect to the Neumann part of the problem, and can be interpreted as a problem for the unit disc. Hence it is supposed to, for a fixed

$y \in \mathbb{D} := \{x \in \mathbb{C} \,|\, |x| < 1\}$, to satisfy

$$\Delta N(x,y) = \delta(x-y), \quad x \in \mathbb{D}$$
$$\frac{\partial N(x,y)}{\partial \nu_x} = C, \quad x \in \partial \mathbb{D} := \{x \in \mathbb{C} \,|\, |x| = 1\}, \tag{3.1.1}$$

where δ is the dirac delta measure and $\frac{\partial}{\partial \nu_x}$ is the normal derivative w.r.t. the x-variable. C is a constant, which comes from the solvability condition from Green's identity using $u \equiv 1$ and N defined as in (3.1.1)

$$\int_{\mathbb{D}} u\Delta N - N\Delta u \, dx = \int_{\partial \mathbb{D}} u\frac{\partial N}{\partial \nu} - N\frac{\partial u}{\partial \nu} \, ds \Leftrightarrow$$
$$\int_{\mathbb{D}} \delta(x-y) \, dx = \int_{\partial \mathbb{D}} \frac{\partial N}{\partial \nu} \, ds \Leftrightarrow$$
$$1 = \int_0^{2\pi} C \, d\eta \Leftrightarrow$$
$$1 = 2\pi C. \tag{3.1.2}$$

This is satisfied if and only if $C = \dfrac{1}{2\pi}$ or more generally if $C = |\partial \Omega|^{-1}$, where Ω is the given domain.

Theorem 3.1.1 *(Neumann function) The function satisfying (3.1.1) with (3.1.2) is given by*

$$N(x,y) = \begin{cases} \frac{1}{2\pi} \left(\log\left(|x-y|\right) + \log\left(|y||x-y^*|\right) \right) & : y \in \mathbb{D} \setminus \{0\} \\ \frac{1}{2\pi} \log\left(|x|\right) & : y = 0 \end{cases} \tag{3.1.3}$$

where y^* is the reflection of y through the boundary $\partial \mathbb{D}$.

Proof : The first part of the Neumann function is the fundamental solution for the Laplace equation in 2D: $\Phi(x,y) = \dfrac{1}{2\pi} \log|x-y|$, which satisfies

$$\Delta \Phi(x,y) = \delta(x-y), \quad x \in \mathbb{D},$$
$$\frac{\partial \Phi(x,y)}{\partial \nu_x} = \frac{(x-y)\cdot x}{2\pi|x-y|^2}, \quad x \in \partial \mathbb{D}, \tag{3.1.4}$$

for a fixed $y \in \mathbb{D}$.

In the unit disc the normal w.r.t. x is just the vector x, since it has length 1 and points outwards of the unit circle. The second part of $N(x,y)$ is found by the method of reflection as shown in figure 3.2.
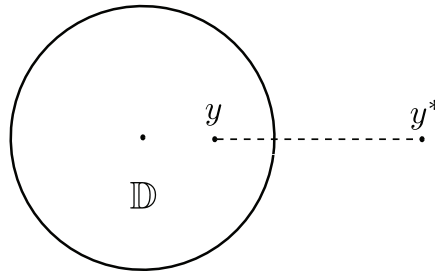

Figure 3.2:   The method of reflection, $y = r_y e^{i\eta}$ and $y^* = \frac{1}{r_y} e^{i\eta}$.

The reflections satisfies $|y||y^*| = 1$, $y^* = \frac{1}{r_y^2}y$. Let $x = re^{i\theta}$ and define $\rho = |x - y|$, $\rho^* = |x - y^*|$, then for $x \in \Gamma_{\mathrm{II}} \Rightarrow r_y\rho^* = \rho$, for further convincing that this holds the reader is refered to [22], where the corresponding Green's function for the unit disc is derived. Hence the Neumann function is given as

$$N(x, y) = \Phi(x, y) + H(x, y) \tag{3.1.5}$$

where

$$H(x, y) = \frac{1}{2\pi} \log(|y||x - y^*|) = \frac{1}{2\pi}\left(\log|x - y^*| + \log|y|\right),$$

which is harmonic in $\mathbb{D}$, since

$$\Delta_x H(x, y) = \nabla \cdot \frac{(x - y^*)}{2\pi|x - y^*|^2} = \frac{1}{2\pi}\left(\frac{2}{|x - y^*|^2} - 2\frac{|x - y^*|^2}{|x - y^*|^4}\right) = 0.$$

Now it is checked that the boundary condition in (3.1.1) is fulfilled, by using polar coordinates $|x| = r$, $|y| = r_y$.

The first part, where $y \in \mathbb{D}$ and $x \in \partial\mathbb{D}$ and knowing that the outward normal derivative is given by the radial derivative in polar coordinates, yields

$$\frac{\partial \Phi}{\partial \nu_x}(x, y)\Big|_{|x|=1} = \frac{1}{2\pi}\frac{\partial}{\partial \nu_x}\log|x - y|\Big|_{|x|=1} = \frac{1}{4\pi}\frac{\partial}{\partial r}\log(r^2 + r_y^2 - 2rr_y\cos(\theta - \eta))\Big|_{r=1} \tag{3.1.6}$$

$$= \frac{1}{2\pi}\frac{r - r_y\cos(\theta - \eta)}{\rho^2}\Big|_{r=1} = \frac{1}{2\pi}\frac{1 - r_y\cos(\theta - \eta)}{\rho^2}. \tag{3.1.7}$$

Second part

$$\frac{\partial H}{\partial \nu_x}(x, y)\Big|_{|x|=1} = \frac{1}{2\pi}\frac{\partial}{\partial \nu_x}\left(\log|x - y^*| + \log|y|\right)\Big|_{|x|=1} \tag{3.1.8}$$

$$= \frac{1}{4\pi}\frac{\partial}{\partial r}\log(r^2 + \frac{1}{r_y^2} - 2r\frac{1}{r_y}\cos(\theta - \eta))\Big|_{r=1} = \frac{1}{2\pi}\frac{r - \frac{1}{r_y}\cos(\theta - \eta)}{\rho^{*2}}\Big|_{r=1} \tag{3.1.9}$$

$$= \frac{1}{2\pi}\frac{\frac{1}{r_y^2}(r_y^2 - r_y\cos(\theta - \eta))}{\frac{1}{r_y^2}\rho^2} = \frac{1}{2\pi}\frac{r_y^2 - r_y\cos(\theta - \eta)}{\rho^2}. \tag{3.1.10}$$

The normal derivative of the Neumann function is therefore

$$\frac{\partial N}{\partial \nu_x}(x, y)\Big|_{|x|=1} = \frac{\partial \Phi}{\partial \nu_x}(x, y) + \frac{\partial H}{\partial \nu_x}(x, y)$$

$$= \frac{1}{2\pi}\left(\frac{1 - r_y\cos(\theta - \eta)}{\rho^2} + \frac{r_y^2 - r_y\cos(\theta - \eta)}{\rho^2}\right)$$

$$= \frac{1}{2\pi}\frac{1 + r_y^2 - 2r_y\cos(\theta - \eta)}{\rho^2} = \frac{1}{2\pi}.$$

The constant is $C = \frac{1}{2\pi}$ which satisfies (3.1.2). ∎

3.2 The boundary integral equation for the annulus

The next step is, using the Neumann function for the unit disc, to setup the integral equations for the annular region. The representation formula for the solution of the Laplace equation in an annulus, given u a solution to (3.0.1), is given by

$$u(x) = \int_{\partial D_a}\left(u(y)\frac{\partial N}{\partial \nu_y}(x, y) - \frac{\partial u}{\partial \nu_y}(y)N(x, y)\right)ds(y)$$

$$= \int_{\Gamma_{\mathrm{II}}}\left(u(y)\frac{\partial N}{\partial \nu_y}(x, y) - \frac{\partial u}{\partial \nu_y}(y)N(x, y)\right)ds(y)$$

$$+ \int_{\Gamma_{\mathrm{I}}}\left(u(y)\frac{\partial N}{\partial \nu_y}(x, y) - \frac{\partial u}{\partial \nu_y}(y)N(x, y)\right)ds(y).$$

Using the boundary conditions from (3.0.1) gives

$$u(x) = \int_{\Gamma_{\mathrm{II}}} \left[u(y)\frac{1}{2\pi} - g(y)N(x,y) \right] ds(y) - \int_{\Gamma_{\mathrm{I}}} \frac{\partial u}{\partial \nu_y}(y)N(x,y)ds(y) \Leftrightarrow$$

$$u(x) = \frac{1}{2\pi} \int_{\Gamma_{\mathrm{II}}} u(y)ds(y) - \int_{\Gamma_{\mathrm{II}}} g(y)N(x,y)ds(y) - \int_{\Gamma_{\mathrm{I}}} \frac{\partial u}{\partial \nu_y}(y)N(x,y)ds(y). \qquad (3.2.1)$$

Now setting $\varphi(x) = \dfrac{\partial u}{\partial \nu_x}(x)\Big|_{x \in \Gamma_{\mathrm{I}}}$ and inserting into (3.2.1) gives

$$u(x) - \frac{1}{2\pi} \int_{\Gamma_{\mathrm{II}}} u(y)ds(y) = -\int_{\Gamma_{\mathrm{II}}} g(y)N(x,y)ds(y) - \int_{\Gamma_{\mathrm{I}}} \varphi(y)N(x,y)ds(y). \qquad (3.2.2)$$

For x away from Γ_{II} the first integral on the RHS is well-defined and therefore is a function of x, i.e.

$$h(x) = \int_{\Gamma_{\mathrm{II}}} g(y)N(x,y)ds(y), \quad x \in D_a. \qquad (3.2.3)$$

The second integral is a *Single layer potential* [15] with the Neumann function as a kernel, and is defined as

$$(S_N\varphi)(x) := \int_{\Gamma_{\mathrm{I}}} \varphi(y)N(x,y)ds(y), \quad x \in D_a. \qquad (3.2.4)$$

Whenever $x \in \Gamma_{\mathrm{I}}$ this integral exists as an improper integral with a weakly singular kernel from [15], the kernel is defined and continuous for all $x, y \in \Gamma_{\mathrm{I}}$, $x \neq y$, and there exists positive constants M and $\alpha \in (0,2]$ such that

$$|N(x,y)| \le M|x-y|^{\alpha-2}, \quad x, y \in \Gamma_{\mathrm{I}}, x \neq y.$$

This holds since if x is away from y, $\alpha = 2$ and the logarithm is bounded by the linear curve. If x is close to y, α can be set to 1 and the logarithm will be bounded by the reciprocal function. The integral operator with a weakly singular kernel is proved in [15] to be compact. The case of evaluating the normal derivative in the point x, is well-defined in a principal value approach and this boundary behaviour will lead to a socalled *jump relation*.

Theorem 3.2.1 *Let $D_a \subset \mathbb{R}^2$ be a bounded C^2-domain and φ a continuous function on Γ_I. Then $(S_N\varphi)(x)$ is harmonic in $\mathbb{R}^2 \backslash \Gamma_I$, continuous across Γ_I and the following jump relations holds for every $x \in \Gamma_I$, and a given $z = x - \epsilon\nu_x$, $\epsilon > 0$*

$$\lim_{\epsilon \to +0} \frac{\partial}{\partial \nu_x}(S_N\varphi)(z) = \int_{\Gamma_I} \frac{\partial}{\partial \nu_x}N(x,y)\varphi(y)ds(y) - \frac{1}{2}\varphi(x), \quad x \in \Gamma_I \qquad (3.2.5)$$

Proof Let $x \in \Gamma_{\mathrm{I}}$ and $z = x - \epsilon\nu_x \in D_a$ such that $|x - z| = |x - x + \epsilon\nu_x| = \epsilon$, now let $B_\epsilon(x)$ be a circle with center in x and radius ϵ, hence formulating a new domain $D_a' = D_a \setminus B_\epsilon(x)$ with boundary $\partial D_a' = \Gamma_{\mathrm{II}} \cup \Gamma_{\mathrm{I}}'$ where $\Gamma_{\mathrm{I}}' = \Gamma_{\mathrm{I}\backslash\epsilon} \cup \Gamma_\epsilon$, $\Gamma_{\mathrm{I}\backslash\epsilon} = \Gamma_{\mathrm{I}} \setminus (\Gamma_{\mathrm{I}} \cap B_\epsilon(x))$ and $\Gamma_\epsilon = \partial B_\epsilon(x) \cap D_a$ as illustrated in figure 3.3.

Consider the integral

$$\int_{\Gamma_{\mathrm{I}}'} \varphi(y)N(x,y)ds(y) = \int_{\Gamma_{\mathrm{I}\backslash\epsilon}} \varphi(y)N(x,y)ds(y) + \int_{\Gamma_\epsilon} \varphi(y)N(x,y)ds(y).$$

Since x is not in the domain of integration these are well-defined integrals, and therefore the normal derivative w.r.t. x is taken and trying to evaluate the integrals when $\epsilon \to +0$, i.e. first evaluating the second integral

$$\lim_{\epsilon \to 0} \frac{\partial}{\partial \nu_x} \int_{\Gamma_\epsilon} \varphi(y)N(x,y)ds(y) = \lim_{\epsilon \to 0} \int_{\Gamma_\epsilon} \varphi(y)\frac{\partial}{\partial \nu_x}N(x,y)ds(y), \qquad (3.2.6)$$
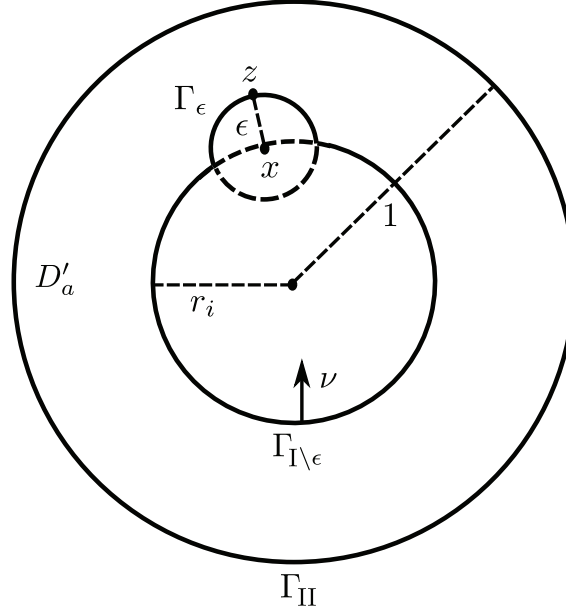
Figure 3.3: The indented annulus D_a', where x is the point of interest.

where
$$
\frac{\partial}{\partial \nu_x} N(x,y)\Big|_{y \in \Gamma_\epsilon} = \frac{1}{2\pi} \nabla_x \left(\log(|x-y|) + \log(|x-y^*|) + \log|y| \right) \cdot \nu_x = \frac{1}{2\pi} \left(\frac{(x-y) \cdot \nu_x}{|x-y|^2} + \frac{(x-y^*) \cdot \nu_x}{|x-y^*|^2} \right).
$$

For the dot product, the angle between the vectors $x-y$ and ν_x are orientated in opposite directions, inverting the vector $x-y = -(y-x)$, the vector $y-x$ gives the same direction as the normal vector ν_x, when ϵ goes to zero. Therefore $(x-y) \cdot \nu_x = -(y-x) \cdot \nu_x = -|y-x| = -\epsilon$, which inserted into (3.2.6) yields

$$
\lim_{\epsilon \to 0} \int_{\Gamma_\epsilon} \varphi(y) \frac{\partial}{\partial \nu_x} N(x,y) ds(y) = \lim_{\epsilon \to 0} \frac{1}{2\pi} \left(\int_{\Gamma_\epsilon} \varphi(y) \frac{-|y-x|}{|x-y|^2} ds(y) + \int_{\Gamma_\epsilon} \varphi(y) \frac{(x-y^*) \cdot \nu_x}{|x-y^*|^2} ds(y) \right)
$$
$$
= \lim_{\epsilon \to 0} \frac{1}{2\pi} \left(-\frac{1}{\epsilon} \int_{\Gamma_\epsilon} \varphi(y) ds(y) + \int_{\Gamma_\epsilon} \varphi(y) \frac{(x-y^*) \cdot \nu_x}{|x-y^*|^2} ds(y) \right).
$$

From the *Mean Value Theorem* the first integral can be evaluated together with the arclength of Γ_ϵ which can be found from the equation for a corde of a circle $K = 2r \sin(v/2) = \epsilon$, where the angle is between the two endpoints of the corde, i.e. looking at isosceles triangles, the arclength of the boundary is $\ell(\Gamma_\epsilon) = \epsilon \left(\pi + 2 \arcsin\left(\frac{\epsilon}{2r_i} \right) \right)$, which leads to

$$
\lim_{\epsilon \to 0} \frac{1}{2\pi} \left(-\frac{1}{\epsilon} \epsilon \left(\pi + 2 \arcsin\left(\tfrac{\epsilon}{2r_i} \right) \right) \varphi(x) + \int_{\Gamma_\epsilon} \varphi(y) \frac{(x-y^*) \cdot \nu_x}{|x-y^*|^2} ds(y) \right), \tag{3.2.7}
$$

because the functions in the integral in (3.2.7) are bounded, it will go to zero when $\epsilon \to 0$. The limit is
$$
\lim_{\epsilon \to 0} -\frac{1}{2\pi\epsilon} \epsilon \left(\pi - 2 \arcsin\left(\tfrac{\epsilon}{2r_i} \right) \right) \varphi(x) = -\frac{\varphi(x)}{2}. \tag{3.2.8}
$$
Since the boundary is smooth and the functions are well-defined away from x, the other integral, when taking the normal derivative and letting $\epsilon \to 0$, the boundary $\Gamma_{I \setminus \epsilon}$ will go towards the boundary of the original inclusion Γ_I, i.e.
$$
\lim_{\epsilon \to 0} \frac{\partial}{\partial \nu_x} \int_{\Gamma_{I \setminus \epsilon}} \varphi(y) N(x,y) ds(y) = \int_{\Gamma_I} \varphi(y) \frac{\partial}{\partial \nu_x} N(x,y) ds(y). \tag{3.2.9}
$$

Combining (3.2.8) and (3.2.9), the jump relation for the single layer potential is given by

$$\lim_{\epsilon \to 0} \frac{\partial}{\partial \nu_x}(S_N \varphi)(z) = \int_{\Gamma_{\mathrm{I}}} \frac{\partial}{\partial \nu_x} N(x,y)\varphi(y)ds(y) - \frac{1}{2}\varphi(x),$$

where

$$\frac{\partial}{\partial \nu_x}(S_N \varphi)(z) = \nabla_x (S_N \varphi)(x - \epsilon \nu_x) \cdot \nu_x.$$

The second jump relation, which is when z is in the inner circle, is derived in a similar way. ■

Considering the integral equation given by

$$u(x) - \frac{1}{2\pi} \int_{\Gamma_{\mathrm{II}}} u(y)ds(y) = -h(x) - (S_N \varphi)(x). \tag{3.2.10}$$

Using the limit and the normal derivative w.r.t. x on the inner boundary on both sides in (3.2.10) and Theorem 3.2.1, where $z = x - \epsilon \nu_x$ gives

$$\frac{\partial u}{\partial \nu_x}(x)\Big|_{x \in \Gamma_{\mathrm{I}}} = -\frac{\partial h}{\partial \nu_x}(x)\Big|_{x \in \Gamma_{\mathrm{I}}} - \lim_{\epsilon \to 0} \frac{\partial}{\partial \nu_x}(S_N \varphi)(z)\Big|_{x \in \Gamma_{\mathrm{I}}} \Leftrightarrow$$

$$\varphi(x) = -\frac{\partial h}{\partial \nu_x}(x)\Big|_{x \in \Gamma_{\mathrm{I}}} - \left(\int_{\Gamma_{\mathrm{I}}} \frac{\partial}{\partial \nu_x} N(x,y)\Big|_{x \in \Gamma_{\mathrm{I}}} \varphi(y)ds(y) - \frac{1}{2}\varphi(x) \right) \Leftrightarrow$$

$$\frac{1}{2}\varphi(x) = -\frac{\partial h}{\partial \nu_x}(x)\Big|_{x \in \Gamma_{\mathrm{I}}} - \int_{\Gamma_{\mathrm{I}}} \frac{\partial}{\partial \nu_x} N(x,y)\Big|_{x \in \Gamma_{\mathrm{I}}} \varphi(y)ds(y) \tag{3.2.11}$$

On the right hand side the two integrals w.r.t. the normal derivatives can be expressed explicitly, since the domain and the Neumann function are known. Here the inner radius is defined as $|x| = |y| = r_i$, and now the two normal derivatives can be derived first for $y \in \Gamma_{\mathrm{I}}$

$$\frac{\partial}{\partial \nu_x} N(x,y)\Big|_{x \in \Gamma_{\mathrm{I}}} = -\frac{1}{4\pi} \frac{\partial}{\partial r}\left(\log(r^2 + r_i^2 - 2rr_i \cos(\theta - \eta)) + \log(r^2 + \tfrac{1}{r_i^2} - 2r\tfrac{1}{r_i}\cos(\theta - \eta)) + \log(r_i) \right)\Big|_{r=r_i}$$

$$= -\frac{1}{2\pi}\left(\frac{r - r_i \cos(\theta - \eta)}{r^2 + r_i^2 - 2rr_i \cos(\theta - \eta)} + \frac{r - \tfrac{1}{r_i}\cos(\theta - \eta)}{r^2 + \tfrac{1}{r_i^2} - 2r\tfrac{1}{r_i}\cos(\theta - \eta)} \right)\Big|_{r=r_i}$$

$$= -\frac{1}{2\pi}\left(\frac{r_i(1 - \cos(\theta - \eta))}{2r_i^2(1 - \cos(\theta - \eta))} + \frac{r_i - \tfrac{1}{r_i}\cos(\theta - \eta)}{r_i^2 + \tfrac{1}{r_i^2} - 2\cos(\theta - \eta)} \right)$$

$$= -\frac{1}{2\pi}\left(\frac{1}{2r_i} + \frac{r_i - \tfrac{1}{r_i}\cos(\theta - \eta)}{r_i^2 + \tfrac{1}{r_i^2} - 2\cos(\theta - \eta)} \right)$$

seeing that the singularity is eliminated.

And now for $y \in \Gamma_{\mathrm{II}} \Rightarrow y = e^{iv} = y^*$

$$\frac{\partial}{\partial \nu_x} N(x,y)\Big|_{x \in \Gamma_{\mathrm{I}}} = -\frac{1}{4\pi} \frac{\partial}{\partial r}\left(\log(r^2 + 1 - 2r\cos(\theta - \eta)) + \log(r^2 + 1 - 2r\cos(\theta - \eta)) \right)\Big|_{r=r_i}$$

$$= -\frac{1}{\pi}\left(\frac{r - \cos(\theta - \eta)}{r^2 + 1 - 2r\cos(\theta - \eta)} \right)\Big|_{r=r_i}$$

$$= -\frac{1}{\pi}\left(\frac{r_i - \cos(\theta - \eta)}{r_i^2 + 1 - 2r_i \cos(\theta - \eta)} \right)$$

inserting into (3.2.11) gives

$$\frac{1}{2}\varphi(x) = \frac{1}{\pi} \int_{\Gamma_{\mathrm{II}}} g(y) \frac{r_i - \cos(\theta - \eta)}{r_i^2 + 1 - 2r_i \cos(\theta - \eta)} ds(y)$$

$$+ \frac{1}{2\pi} \int_{\Gamma_{\mathrm{I}}} \varphi(y) \left(\frac{1}{2r_i} + \frac{r_i - \tfrac{1}{r_i}\cos(\theta - \eta)}{r_i^2 + \tfrac{1}{r_i^2} - 2\cos(\theta - \eta)} \right) ds(y),$$

and the boundary integral equation on operator form is hereby

$$\left(\frac{1}{2}I - K_N\right)(\varphi) = \frac{1}{\pi}\int_{\Gamma_{\text{II}}} g(y)\frac{r_i - \cos(\theta - \eta)}{r_i^2 + 1 - 2r_i\cos(\theta - \eta)}ds(y), \tag{3.2.12}$$

where

$$(K_N\varphi)(x) = \frac{1}{2\pi}\int_0^{2\pi}\varphi(y)\left(\frac{1}{2r_i} + \frac{r_i - \frac{1}{r_i}\cos(\theta - \eta)}{r_i^2 + \frac{1}{r_i^2} - 2\cos(\theta - \eta)}\right)r_i d\eta$$

$$= \frac{1}{2\pi}\int_0^{2\pi}\varphi(y)\left(\frac{1}{2} + \frac{r_i^2 - \cos(\theta - \eta)}{r_i^2 + \frac{1}{r_i^2} - 2\cos(\theta - \eta)}\right)d\eta,$$

using the Jacobian to change the integration variables to polar coordinates, $|\boldsymbol{J}| = r_i$.

3.3 Verification of the BIE

In this section a known solution to the problem will be plugged into the equations to verify that these are satisfied for the true circular inclusion. A function which satisfy the true inclusion is taken as one of the solution derived in Appendix A.2, i.e. a function in polar coordinates

$$u(r,\theta) = \left(\left(\frac{r}{r_i}\right)^n - \left(\frac{r_i}{r}\right)^n\right)(\cos(n\theta) + \sin(n\theta))$$

which satisfy

$$\begin{aligned}
\Delta u &= 0, \quad x \in D_a, \\
u(r_i, \theta) &= 0, \quad x \in \Gamma_{\text{I}}, \\
\frac{\partial u}{\partial r}(r_i, \theta) &= -\frac{2n(\cos(n\theta) + \sin(n\theta))}{r_i} = \varphi(\theta), \quad x \in \Gamma_{\text{I}}, \\
u(1, \theta) &= \left(\frac{1}{r_i^n} - r_i^n\right)(\cos(n\theta) + \sin(n\theta)) = f(\theta), \quad x \in \Gamma_{\text{II}}, \\
\frac{\partial u}{\partial r}(1, \theta) &= \left(\frac{1}{r_i^n}n + r_i^n n\right)(\cos(n\theta) + \sin(n\theta)) = g(\theta), \quad x \in \Gamma_{\text{II}}.
\end{aligned} \tag{3.3.1}$$

Now MATLAB is used for the comparison of LHS and RHS in (3.2.12). The numerical integration is done using the trapezoidal rule, which is implemented in the function `trapezrule` from [9]. The function uses the integrands as function handles, the implementation of the integrand functions in MATLAB are seen below

```
1  function y = intTrialK(phi_handle,t,s,ri)
2  % Integrand for LHS integral with phi(theta)
3  y = phi_handle(t).*(1/2+(ri^2-cos((s-t)))./(ri^2+(1/ri^2)-2*cos((s-t))));
```

```
1  function y = intTrialH(g_handle,t,s,ri)
2  % Integrand for RHS integral, with g(theta)
3  y = g_handle(t).*((ri-cos((s-t)))./(ri^2+1-2*ri*cos((s-t))));
```

Setting up the LHS and RHS with $\boldsymbol{K}$ and $\boldsymbol{H}$ (RHS integral) found using the trapezoidal rule

$$\text{LHS:} \quad \frac{1}{2}\varphi(x) - \frac{1}{2\pi}(K_N\varphi)(x),$$

$$\text{RHS:} \quad \frac{1}{\pi}H.$$

Computing the infinity-norm of the difference between LHS and RHS, using 100 discretization points and different values of n results in the following table

n	2	4	6	8	10
$\|\text{LHS} - \text{RHS}\|_\infty$	8.88e-15	3.02e-14	1.29e-13	1.20e-12	4.41e-12

this is almost the machine number 2.22e-16, which is interpreted as 0, which shows that the boundary integral equations is set up correct.

3.4   Conclusion

The scope of this project is to try to evaluate u on the outer boundary with regards to an approximation of the inner boundary using B-splines. This chapter was an overview of the setup of the equations and to verify that they are correct, if the true inclusion is a circle. Therefore a generalized system of equations has to be set up, where it is taken into account that the inner boundary is approximated using B-splines.

General Inclusion

In this chapter the generalized problem is set up using the theory from [15], for the setup of the boundary integral equations to use in the boundary element method. To remember which boundaries the variables in the integrals are over respectively, the following single and the normal derivative of the single layer potential are introduced

$$(S_N^{(\Phi,\Psi)}u)(x) := \int_{\Phi} u(y)N(x,y)ds(y), \quad x \in \Psi$$

$$(K_N^{(\Phi,\Psi)}u)(x) := \frac{\partial}{\partial\nu_x}(S_N^{(\Phi,\Psi)}u)(x) = \int_{\Phi} u(y)\frac{\partial}{\partial\nu_x}N(x,y)ds(y), \quad x \in \Psi,$$

where the pair $\Phi, \Psi \in \{\Gamma_{\mathrm{I}}, \Gamma_{\mathrm{II}}\}$ according to which boundary the density function u is integrated over.

When $\Phi \neq \Psi$ the integrals are bounded and therefore continuous. When $\Phi = \Psi$ the notation will be for the two respectively, with regards to jump relations as explained in the previous chapter, that is

$$(S_N^{(\Phi)}u)(x) := \int_{\Phi} u(y)N(x,y)ds(y), \quad x \in \Phi$$

$$\lim_{\epsilon \to +0} \frac{\partial}{\partial\nu_x}(S_N^{\Phi}u)(z) = (K_N^{(\Phi)}u)(x) - \frac{1}{2}u(x) := \int_{\Phi} u(y)\frac{\partial}{\partial\nu_x}N(x,y)ds(y) - \frac{1}{2}u(x), \quad x \in \Phi,$$

where $z = x - \epsilon\nu_x$, $\epsilon > 0$.

4.1 Setup of the general boundary integral equations

The forward problem is stated as follows. Given an induced current $g \in H^{-1/2}(\Gamma_{\mathrm{II}})$ on the outer boundary

$$\frac{\partial u}{\partial\nu}(x) = g(x), \quad x \in \Gamma_{\mathrm{II}},$$

as $u \in H^1(\Omega)$, where Ω denotes the open domain between Γ_{I} and Γ_{II}. Solve the generalized boundary integral equation, $x \in \Gamma_{\mathrm{I}}$

$$\left(\frac{1}{2}I + K_N^{(\Gamma_{\mathrm{I}})}\right)(\varphi)(x) = -\left(K_N^{(\Gamma_{\mathrm{II}},\Gamma_{\mathrm{I}})}g\right)(x) \tag{4.1.1}$$

for $\varphi(x) \in H^{-1/2}(\Gamma_{\mathrm{I}})$ and $K_N^{(\Gamma_{\mathrm{II}},\Gamma_{\mathrm{I}})} : H^{-1/2}(\Gamma_{\mathrm{II}}) \to H^{-1/2}(\Gamma_{\mathrm{I}})$, $K_N^{(\Gamma_{\mathrm{I}})} : H^{-1/2}(\Gamma_{\mathrm{I}}) \to H^{-1/2}(\Gamma_{\mathrm{I}})$ and let the inner boundary be approximated by B-splines. Then the representation formula (3.2.1) is used, to find an approximation to the measured voltage distribution $f \in H^{1/2}(\Gamma_{\mathrm{II}})$. That is to find an approximation

$$u(x) = f(x), \quad x \in \Gamma_{\mathrm{II}},$$

using the formula for $x \in \Gamma_{\mathrm{II}}$

$$u(x) - \frac{1}{2\pi} \int_{\Gamma_{\mathrm{II}}} u(y) ds(y) = - \left(S_N^{(\Gamma_{\mathrm{II}})} g \right)(x) - \left(S_N^{(\Gamma_{\mathrm{I}}, \Gamma_{\mathrm{II}})} \varphi \right)(x).$$

The LHS is the function minus the average value of the function on the outer boundary, and letting this be defined as

$$\hat{f}(x) := u(x) - \frac{1}{2\pi} \int_{\Gamma_{\mathrm{II}}} u(y) ds(y).$$

The problem is now, find φ in (4.1.1) to obtain $\hat{f}$ from

$$\hat{f}(x) = - \left(S_N^{(\Gamma_{\mathrm{II}})} g \right)(x) - \left(S_N^{(\Gamma_{\mathrm{I}}, \Gamma_{\mathrm{II}})} \varphi \right)(x). \tag{4.1.2}$$

The equations (4.1.1) and (4.1.2) can be set up as a linear system of boundary integral equations, using the following matrix notation

$$\begin{bmatrix} \frac{1}{2} I + K_N^{(\Gamma_{\mathrm{I}})} & 0 \\ S_N^{(\Gamma_{\mathrm{I}}, \Gamma_{\mathrm{II}})} & I \end{bmatrix} \begin{bmatrix} \varphi \\ \hat{f} \end{bmatrix} = \begin{bmatrix} -K_N^{(\Gamma_{\mathrm{II}}, \Gamma_{\mathrm{I}})} g \\ -S_N^{(\Gamma_{\mathrm{II}})} g \end{bmatrix}, \tag{4.1.3}$$

where I is the identityoperator and 0 is the null operator. This relation can be used when the integrals and domains have been discretized. A discretization is necessary to evaluate this, since I is only compact if it maps finite dimensional spaces.

4.2 Discretization of the geometry

The geometry is discretized by letting the inner boundary Γ_{I} be approximated by a B-spline curve

$$\Gamma_{\mathrm{I}} := \left\{ \gamma(t) \in \mathbb{S}_k^{\boldsymbol{\Xi}} \mid t \in [0, 1] \right\},$$

where the curve is defined by a number of control points $\boldsymbol{p}_i$, knot vector $\boldsymbol{\Xi}$ and B-spline pieces $\mathcal{N}_i^k(t)$ of order k, e.g.

$$\gamma(t) = \sum_i \boldsymbol{p}_i \mathcal{N}_i^k(t).$$

Using this in (4.1.1) and letting $x = \gamma(s)$ for some fixed $s \in [0, 1]$, and evaluating the normal derivative of the Neumann function for an arbitrary regular inner boundary and for the circular outer boundary, where $x \in \Gamma_{\mathrm{I}}$, i.e.

$$\frac{\partial}{\partial \nu_x} N(x, y) = \frac{1}{2\pi} \left(\frac{x - y}{|x - y|^2} + \frac{x - y^*}{|x - y^*|^2} \right) \cdot \nu_x, \quad y \in \Gamma_{\mathrm{I}}$$

$$\frac{\partial}{\partial \nu_x} N(x, y) = \frac{1}{\pi} \left(\frac{x - y}{|x - y|^2} \right) \cdot \nu_x, \quad y \in \Gamma_{\mathrm{II}}. \tag{4.2.1}$$

The Jacobian for the integral on the inner boundary is $|\boldsymbol{J}| = |\dot{\gamma}(t)|$ and for the outer boundary $|\boldsymbol{J}| = 1$. The normal vector w.r.t. x is therefore $\nu_x = \dfrac{\hat{\dot{\gamma}}(s)}{|\dot{\gamma}(s)|}$, the first part of the system of equations is now for $x \in \Gamma_{\mathrm{I}}$

$$\left(\frac{1}{2} I + K_N^{(\Gamma_{\mathrm{I}})} \right)(\varphi)(x) = - \left(K_N^{(\Gamma_{\mathrm{II}}, \Gamma_{\mathrm{I}})} g \right)(x)$$

$$\frac{1}{2} \varphi(x) + \int_{\Gamma_{\mathrm{I}}} \varphi(y) \frac{\partial}{\partial \nu_x} N(x, y) ds(y) = - \int_{\Gamma_{\mathrm{II}}} g(y) \frac{\partial}{\partial \nu_x} N(x, y) ds(y)$$

where the approximated spline γ is included and this evaluates to

$$\frac{1}{2}\varphi(\gamma(s)) + \frac{1}{2\pi}\int_0^1 \varphi(\gamma(t)) \left(\frac{\gamma(s)-\gamma(t)}{|\gamma(s)-\gamma(t)|^2} + \frac{\gamma(s)-\gamma^*(t)}{|\gamma(s)-\gamma^*(t)|^2} \right) \cdot \frac{\hat{\dot{\gamma}}(s)}{|\dot{\gamma}(s)|}|\dot{\gamma}(t)|dt$$

$$= -\frac{1}{\pi}\int_{\Gamma_{II}} g(y) \left(\frac{\gamma(s)-y}{|\gamma(s)-y|^2} \right) \cdot \frac{\hat{\dot{\gamma}}(s)}{|\dot{\gamma}(s)|}ds(y). \qquad (4.2.2)$$

The second part, where $x \in \Gamma_{II}$, is given by

$$\hat{f}(x) = -\left(S_N^{(\Gamma_{II})}g \right)(x) - \left(S_N^{(\Gamma_I, \Gamma_{II})}\varphi \right)(x) \qquad (4.2.3)$$

$$= -\frac{1}{\pi}\int_{\Gamma_{II}} g(y)\log|x-y|ds(y) - \frac{1}{2\pi}\int_0^1 \varphi(\gamma(t))\left(\log|x-\gamma(t)| + \log(|\gamma(t)||x-\gamma^*(t)|)\right)dt.$$

The boundary has now been discretized by piecewise polynomials which the B-spline curve are. The outer boundary is fixed and this is discretized by

$$\Gamma_{II} := \left\{ z(t) = e^{i2\pi t} \,|\, t \in [0,1] \right\},$$

or using corresponding $\mathbb{R}^2$ terminology as $z(t) = (x(t), y(t)) = (\cos(2\pi t), \sin(2\pi t))$. The boundary element method is now, to take a finite number of control points, which approximates the inner boundary by polynomial pieces and then evaluate the functions on each of these pieces using a discretization scheme. In this project quadratic polynomial pieces are used.

4.3 Boundary Element Method

The Boundary Element Method is used for solving these kinds of integral equations as seen in [3]. It is done here by a collocation scheme, where the functions are evaluated on a finite set. This means to project the problem of functions in infinite dimensional Hilbert spaces to a finite dimensional space and require that equality of the functions are satisfied on this finite set. As explained for the geometry $\gamma \in \mathbb{S}_3^{\Xi}$. Now choose collocation points uniformly $\{0 = t_1 < t_2 \cdots < t_{n_{el}-1} < t_{n_{el}} = 1\}$ and $\boldsymbol{t} = (t_1, \ldots, t_{n_{el}})^T$. Like the geometry also the functions φ and $\hat{f}$ can be discretized using B-splines. In this case the approximation is done with piecewise constant functions $\varphi, \hat{f} \in \mathbb{S}_1^{\boldsymbol{t}}$, where the constant coefficients $\varphi(\gamma(s_i)) = \tilde{\varphi}_i$ and $\hat{f}(z(s_i)) = \hat{f}_i$ with $s_i = \dfrac{t_i + t_{i+1}}{2}$ is taken as the value at the midpoint between two discretization points and hence

$$\varphi(x) = \varphi(\gamma(t)) = \sum_{i=1}^{n_{el}-1} \tilde{\varphi}_i \mathcal{N}_i^1(t) = \sum_{i=1}^{n_{el}-1} \tilde{\varphi}_i \mathbb{1}_{[t_i, t_{i+1}]}(t)$$

$$\hat{f}(x) = \hat{f}(z(t)) = \sum_{i=1}^{n_{el}-1} \hat{f}_i \mathcal{N}_i^1(t) = \sum_{i=1}^{n_{el}-1} \hat{f}_i \mathbb{1}_{[t_i, t_{i+1}]}(t). \qquad (4.3.1)$$

Using (4.3.1) on the integral equations for a fixed $x = \gamma(s_i)$, the first integral equation gives

$$\frac{1}{2}\tilde{\varphi}_i + \frac{1}{2\pi}\sum_{j=1}^{n_{el}-1} \tilde{\varphi}_j \int_{t_j}^{t_{j+1}} \left(\frac{\gamma(s_i)-\gamma(t)}{|\gamma(s_i)-\gamma(t)|^2} + \frac{\gamma(s_i)-\gamma^*(t)}{|\gamma(s_i)-\gamma^*(t)|^2} \right) \cdot \frac{\hat{\dot{\gamma}}(s_i)}{|\dot{\gamma}(s_i)|}|\dot{\gamma}(t)|dt$$

$$= -2\int_0^1 g(y(t)) \left(\frac{\gamma(s_i)-y(t)}{|\gamma(s_i)-y(t)|^2} \right) \cdot \frac{\hat{\dot{\gamma}}(s_i)}{|\dot{\gamma}(s_i)|}dt.$$

The second integral equation is given by

$$\hat{f}_i = -2\int_0^1 g(y(t))\log|x(s_i) - y(t)|dt - \frac{1}{2\pi}\sum_{j=1}^{n_{el}-1}\tilde{\varphi}_j\int_{t_j}^{t_{j+1}}\log|x(s_i) - \gamma(t)| + \log(|\gamma(t)||x(s_i) - \gamma^*(t)|)dt \iff$$

$$\frac{1}{2\pi}\sum_{j=1}^{n_{el}-1}\tilde{\varphi}_j\int_{t_j}^{t_{j+1}}\log|x(s_i) - \gamma(t)| + \log(|\gamma(t)||x(s_i) - \gamma^*(t)|)dt + \hat{f}_i = -2\int_0^1 g(y(t))\log|x(s_i) - y(t)|dt.$$

$$(4.3.2)$$

The above two equations can be set up as two coupled linear system of equations as

$$\left(\frac{1}{2}\boldsymbol{I} + \frac{1}{2\pi}\boldsymbol{K}\right)\tilde{\boldsymbol{\varphi}} = -2\boldsymbol{H},$$

$$\frac{1}{2\pi}\boldsymbol{S}\tilde{\boldsymbol{\varphi}} + \hat{\boldsymbol{f}} = -2\boldsymbol{G},$$

$$(4.3.3)$$

which can be combined using matrix notation as

$$\begin{bmatrix} \frac{1}{2}\boldsymbol{I} + \frac{1}{2\pi}\boldsymbol{K} & \boldsymbol{0} \\ \frac{1}{2\pi}\boldsymbol{S} & \boldsymbol{I} \end{bmatrix}\begin{bmatrix} \tilde{\boldsymbol{\varphi}} \\ \hat{\boldsymbol{f}} \end{bmatrix} = \begin{bmatrix} -2\boldsymbol{H} \\ -2\boldsymbol{G} \end{bmatrix}$$

$$(4.3.4)$$

where $\boldsymbol{I}$ is the identitymatrix and $\boldsymbol{0}$ the null matrix of only zeros, which both are of size $(n_{el} - 1) \times (n_{el}-1)$, $\tilde{\boldsymbol{\varphi}} = (\tilde{\varphi}_1, \ldots, \tilde{\varphi}_{n_{el}-1})^T$, $\hat{\boldsymbol{f}} = \left(\hat{f}_1, \ldots, \hat{f}_{n_{el}-1}\right)^T$. $\boldsymbol{K}$, $\boldsymbol{S}$ are matrices of size $(n_{el}-1)\times(n_{el}-1)$ and $\boldsymbol{H}$, $\boldsymbol{G}$ are vectors sized $(n_{el} - 1) \times 1$ with elements given by

$$K_{i,j} = \int_{t_j}^{t_{j+1}}\left(\frac{\gamma(s_i) - \gamma(t)}{|\gamma(s_i) - \gamma(t)|^2} + \frac{\gamma(s_i) - \gamma^*(t)}{|\gamma(s_i) - \gamma^*(t)|^2}\right) \cdot \frac{\hat{\dot{\gamma}}(s_i)}{|\dot{\gamma}(s_i)|}|\dot{\gamma}(t)|dt \qquad (4.3.5)$$

$$S_{i,j} = \int_{t_j}^{t_{j+1}}\log|x(s_i) - \gamma(t)| + \log(|\gamma(t)||x(s_i) - \gamma^*(t)|)dt \qquad (4.3.6)$$

$$H_i = \int_0^1 g(y(t))\left(\frac{\gamma(s_i) - y(t)}{|\gamma(s_i) - y(t)|^2}\right) \cdot \frac{\hat{\dot{\gamma}}(s_i)}{|\dot{\gamma}(s_i)|}dt \qquad (4.3.7)$$

$$G_i = \int_0^1 g(y(t))\log|x(s_i) - y(t)|dt. \qquad (4.3.8)$$

When $i = j$ in (4.3.5) some problems, related to singularities in the integral, might occur. Therefore some singularity evaluation must be taken into account, but as seen in the previous chapter and from [15] improper integrals are in fact compact and therefore bounded, implying that the singularity can be evaluated.

4.3.1   Singularity evaluation

The above mentioned singularity for $\boldsymbol{K}$ occurs $s_i \in [t_j, t_{j+1}]$ which means s_j and comes from the part of the integral related to the fundamental solution of Laplace equation.

$$\int_{t_j}^{t_{j+1}}\left(\frac{\gamma(s_j) - \gamma(t)}{|\gamma(s_j) - \gamma(t)|^2} + \frac{\gamma(s_j) - \gamma^*(t)}{|\gamma(s_j) - \gamma^*(t)|^2}\right) \cdot \frac{\hat{\dot{\gamma}}(s_j)}{|\dot{\gamma}(s_j)|}|\dot{\gamma}(t)|dt \iff$$

$$\int_{t_j}^{t_{j+1}}\left(\frac{\gamma(s_j) - \gamma(t)}{|\gamma(s_j) - \gamma(t)|^2}\right) \cdot \frac{\hat{\dot{\gamma}}(s_j)}{|\dot{\gamma}(s_j)|}|\dot{\gamma}(t)|dt + \int_{t_j}^{t_{j+1}}\left(\frac{\gamma(s_j) - \gamma^*(t)}{|\gamma(s_j) - \gamma^*(t)|^2}\right) \cdot \frac{\hat{\dot{\gamma}}(s_j)}{|\dot{\gamma}(s_j)|}|\dot{\gamma}(t)|dt$$

This corresponds to the first integral, since the second is bounded and therefore continuous. In order to evaluate the singularity a Taylor expansion is performed around the source point s_j, $\langle\cdot,\cdot\rangle$

and $\cdot$ will be used to represent the same inner product in $\mathbb{R}^2$. The little "o" notation is used. For simplicity s is now written instead of s_j

$$\gamma(t) = \gamma(s) + \dot{\gamma}(s)(t - s) + \frac{1}{2}\ddot{\gamma}(s)(t - s)^2 + o\left((t - s)^3\right) \Leftrightarrow$$

$$\gamma(s) - \gamma(t) = \dot{\gamma}(s)(s - t) - \frac{1}{2}\ddot{\gamma}(s)(s - t)^2 + o\left((s - t)^3\right) \Leftrightarrow$$

$$(\gamma(s) - \gamma(t)) \cdot \hat{\dot{\gamma}}(s) = -\frac{1}{2}\ddot{\gamma}(s) \cdot \hat{\dot{\gamma}}(s)(s - t)^2 + o\left((s - t)^3\right) \tag{4.3.9}$$

Taking the norm squared on both sides and using the inner product rules for $\mathbb{R}^2$ gives

$$|\gamma(s) - \gamma(t)|^2 = \left\langle \dot{\gamma}(s)(s - t) - \frac{1}{2}\ddot{\gamma}(s)(s - t)^2 + o\left((s - t)^3\right), \dot{\gamma}(s)(s - t) - \frac{1}{2}\ddot{\gamma}(s)(s - t)^2 + o\left((s - t)^3\right) \right\rangle$$

$$= |\dot{\gamma}(s)|^2(s - t)^2 + \left\langle \dot{\gamma}(s)(s - t), -\frac{1}{2}\ddot{\gamma}(s)(s - t)^2 \right\rangle + \left\langle -\frac{1}{2}\ddot{\gamma}(s)(s - t)^2, \dot{\gamma}(s)(s - t) \right\rangle + o\left((s - t)^4\right)$$

$$= |\dot{\gamma}(s)|^2(s - t)^2 - \dot{\gamma}(s) \cdot \ddot{\gamma}(s)(s - t)^3 + o\left((s - t)^4\right). \tag{4.3.10}$$

Combining (4.3.9) and (4.3.10), the following holds

$$\frac{(\gamma(s) - \gamma(t)) \cdot \hat{\dot{\gamma}}(s)}{|\gamma(s) - \gamma(t)|^2} = \frac{-\frac{1}{2}\ddot{\gamma}(s) \cdot \hat{\dot{\gamma}}(s)(s - t)^2 + o\left((s - t)^3\right)}{|\dot{\gamma}(s)|^2(s - t)^2 - \dot{\gamma}(s) \cdot \ddot{\gamma}(s)(s - t)^3 + o\left((s - t)^4\right)}$$

$$= \frac{-\frac{1}{2}\ddot{\gamma}(s) \cdot \hat{\dot{\gamma}}(s)(s - t)^2 + o\left((s - t)^3\right)}{|\dot{\gamma}(s)|^2(s - t)^2 \left(1 - \frac{\dot{\gamma}(s) \cdot \ddot{\gamma}(s)(s - t)^3}{|\dot{\gamma}(s)|^2(s - t)^2} + o\left((s - t)^2\right)\right)} \tag{4.3.11}$$

using the geometric sequence $\sum_i x^{i-1} = \frac{1}{1 - x}$, where $|x| < 1$, for the expansion in (4.3.11)

$$\frac{(\gamma(s) - \gamma(t)) \cdot \hat{\dot{\gamma}}(s)}{|\gamma(s) - \gamma(t)|^2} = -\frac{1}{2}\frac{\ddot{\gamma}(s)\hat{\dot{\gamma}}(s) + o\left((s - t)\right)}{|\dot{\gamma}(s)|^2}\left(1 + \frac{\dot{\gamma}(s)\ddot{\gamma}(s)(s - t)}{|\dot{\gamma}(s)|^2} + o\left((s - t)^2\right)\right)$$

$$= -\frac{1}{2}\frac{\ddot{\gamma}(s)\hat{\dot{\gamma}}(s)}{|\dot{\gamma}(s)|^2} + o\left((s - t)\right) \Leftrightarrow$$

$$\frac{(\gamma(s) - \gamma(t)) \cdot \hat{\dot{\gamma}}(s)}{|\gamma(s) - \gamma(t)|^2|\dot{\gamma}(s)|} = -\frac{1}{2}\frac{\ddot{\gamma}(s) \cdot \hat{\dot{\gamma}}(s)}{|\dot{\gamma}(s)|^3} + o\left((s - t)\right). \tag{4.3.12}$$

The last term in the kernel is

$$|\dot{\gamma}(t)| = |\dot{\gamma}(s) + \ddot{\gamma}(s)(t - s) + o\left((t - s)^2\right)|$$

$$\leq |\dot{\gamma}(s)| + |\ddot{\gamma}(s)||s - t| + o\left(|s - t|^2\right), \tag{4.3.13}$$

from triangle inequality, which combined with (4.3.11) gives the following constant approximation to the kernel whenever s is in the domain of integration, i.e.

$$\frac{(\gamma(s) - \gamma(t))}{|\gamma(s) - \gamma(t)|^2} \cdot \frac{\hat{\dot{\gamma}}(s)|\dot{\gamma}(t)|}{|\dot{\gamma}(s)|} = -\frac{1}{2}\frac{\ddot{\gamma}(s) \cdot \hat{\dot{\gamma}}(s)|\dot{\gamma}(s)|}{|\dot{\gamma}(s)|^3} + o\left((s - t)\right)$$

$$= -\frac{1}{2}\frac{\ddot{\gamma}(s) \cdot \hat{\dot{\gamma}}(s)}{|\dot{\gamma}(s)|^2} + o\left((s - t)\right) \tag{4.3.14}$$

The consideration here is that the approximation of the function φ and $\hat{f}$ is by piecewise constant functions, which means that it should be reasonable to approximate the kernel by a constant as well. When x is in the domain of integration the computation of the matrix $\boldsymbol{K}$ is given by

$$K_{j,j} = C_j(t_{j+1} - t_j) + \int_{t_j}^{t_{j+1}} \left(\frac{\gamma(s_j) - \gamma^*(t)}{|\gamma(s_j) - \gamma^*(t)|^2}\right) \cdot \frac{\hat{\dot{\gamma}}(s_j)}{|\dot{\gamma}(s_j)|}|\dot{\gamma}(t)|dt \tag{4.3.15}$$

where C_j is the constant coming from the RHS in (4.3.14). The next section shows the implementation of the forward problem.

4.4   Implementation of the Forward problem

In this section the MATLAB implementation of the forward problem is described. To simplify and evaluate the validicity of the equations set up, there has been used already implemented methods for numerical integration and use of MATLAB's spline Toolbox [6].

For the implementation of the geometry the function `spmak` is used to make the spline approximation of the boundary. The function takes as inputs a matrix with coefficients for the control polygon and a knot vector, where the knots are specified for the spline, it returns a `struct` form which specifies the form as basis form, the knot vector, the coefficient matrix, the number of polynomial pieces, the order of the spline and the corresponding dimensions. For evaluating the derivative of the spline curve the function `fnder` is used, which takes as input a spline, created by `spmak` and gives out the corresponding differentiated spline curve of degree one less than the original.

The implementation of the forward problem, is to set up the system of linear equations based on the discretization of the integral equations. First the integrands are set up in different MATLAB functions, which is done for the matrix system given in (4.3.4). The implementation and relation for the integrands to the implemented solver is seen in figure 4.1.
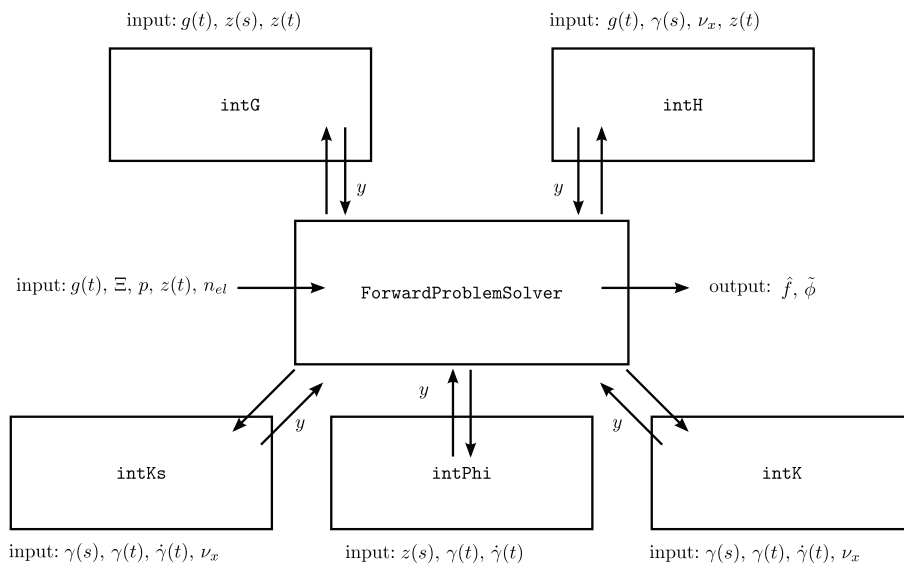
Figure 4.1:   The implemented solver and relation to the integrands.

A MATLAB function has been implemented and called `ForwardProblemSolver` to solve the forward problem as suggested by the name. The full code can be reviewed in Appendix B.2 and it is described in Algorithm 4.1. It takes as input the function $g(t)$ as a function handle for the induced current, it then takes either a coefficient matrix $\boldsymbol{p}$ of control points and a knot vector Ξ for creation of the spline inclusion otherwise the values for number of control points n_{cp}, the order k of the spline and the radius r_i of the circular inclusion. It also takes the number of discretization points n_{el} and the outer boundary in a function handle $z(t)$.

In Algorithm 4.1 use of the backslash operator $\backslash$ implemented in MATLAB to solve the linear system of equations to get the vector $\tilde{\boldsymbol{\varphi}}$ and $\hat{\boldsymbol{f}}$ of constants. The next section describes the results of the implementation.

Algorithm 4.1 Forward Problem Solver

Require: $g(t)$, knots $\boldsymbol{\Xi}$, coefs $\boldsymbol{P}$, points n_{el}
 1: Create spline boundary using `spmak` and discretization points `t` and `s`
 2: Setup of the splines and the constant C derived from Taylor expansion (4.3.14)
 3: $\gamma(s), \dot{\gamma}(s), \ddot{\gamma}(s), \nu(\gamma(s)), |\dot{\gamma}(s)|, C$
 4: Compute $\boldsymbol{H}$ and $\boldsymbol{G}$ using (4.3.7),(4.3.8) and `trapezrule`
 5: Allocate full arrays $\boldsymbol{K}$ and $\boldsymbol{S}$
 6: **for** j=1 to `length(s)` **do**
 7:     Compute K(j,j) for x in domain of integration using (4.3.15) and `trapezrule`
 8:     Compute K(i,j) $i \neq j$ using (4.3.5) and `trapezrule`
 9:     Compute S(:,j) using (4.3.6) and `trapezrule`
10: **end for**
11: Setup $\boldsymbol{A} = [1/2\boldsymbol{I} + 1/(2\pi)\boldsymbol{K}, \, \boldsymbol{0}; 1/(2\pi)\boldsymbol{S}, \, \boldsymbol{I}]$ and $\boldsymbol{b} = [-2\boldsymbol{H}; -2\boldsymbol{G}]$
12: $\boldsymbol{c} = \boldsymbol{A} \backslash \boldsymbol{b}$
13: $\tilde{\boldsymbol{\varphi}} = \boldsymbol{c}(1 : n_{el} - 1)$
14: $\hat{\boldsymbol{f}} = \boldsymbol{c}(n_{el} : end)$

4.5 Results

The first example is regarding knowledge of the inclusion as a circle, which is approximated by order $k = 3$ B-splines pieces like example 2.2.1 where like previous example using the function coming from separation of variables found in Appendix A.2, therefore it is possible to compare to the real values of φ and f from (3.3.1). For reminder the Cauchy-data and calculated values for φ and f are given by

$$g(\theta) = n \left(\frac{1}{r_i^n} + r_i^n \right) (\cos(n\theta) + \sin(n\theta))$$

$$f(\theta) = \left(\frac{1}{r_i^n} - r_i^n \right) (\cos(n\theta) + \sin(n\theta)) \qquad (4.5.1)$$

$$\varphi(\theta) = -\frac{2n \left(\cos(n\theta) + \sin(n\theta) \right)}{r_i},$$

where $\theta \in [0, 2\pi]$. The integral of f over the outer boundary is 0, so no information of the signal is lost in the approximation, when comparing with the approximated $\hat{f}$. Setup of the spline by making 4 and 12 control point as the corners of a regular polygon where the incircle corresponds to the true inclusion, there will therefore be 4 and 12 polynomial pieces which will not be an exact circle, but an approximation using quadratic B-splines. Using `ForwardProblemSolver` to solve with $n_{el} = 40$ discretization points, gives the following piecewise constant approximation $\tilde{\varphi}$ and $\hat{f}$ with the relative error for $\hat{f}$ evaluated in the discretization points.

Figure 4.2 shows the approximations of φ. It is seen that it approximates the analytical solution better as the number of control points increases, which is because the inclusion spline is closer to the real circle. The corresponding approximate $\hat{f}$ of f is seen in figure 4.3

Figure 4.3 again shows a close approximation to the real values. To get an idea of how close a plot of the relative error in each discretization point is shown in figure 4.4

From figure 4.4 it is seen that the relative error from the use of 4 control points is between $2.7 \cdot 10^{-2}$ and $4.5 \cdot 10^{-2}$, when the number of control points are increased the error is between $1.8 \cdot 10^{-5}$ and $6.5 \cdot 10^{-3}$, the difference in the error between the number of control point suggests a closer approximation of the circle will decrease the corresponding error. Actually after a certain number of control points the error is not decreasing anymore and the sum of the errors will be steady at around 10^{-4}, which could suggest that a less simplified method could be better.

(a) $n_{cp} = 4$, $r_i = 0.5$, $n_{el} = 40$ and $n = 1$

(b) $n_{cp} = 12$, $r_i = 0.5$, $n_{el} = 40$ and $n = 1$
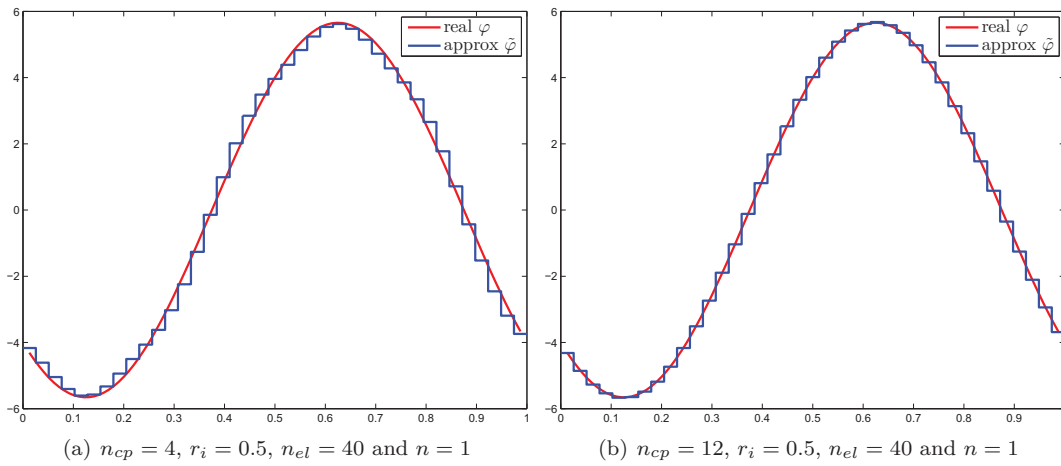
Figure 4.2: The piecewise constant function $\tilde{\varphi}$ and the analytical φ for 4 and 12 control points

(a) $n_{cp} = 4$, $r_i = 0.5$, $n_{el} = 40$ and $n = 1$

(b) $n_{cp} = 12$, $r_i = 0.5$, $n_{el} = 40$ and $n = 1$
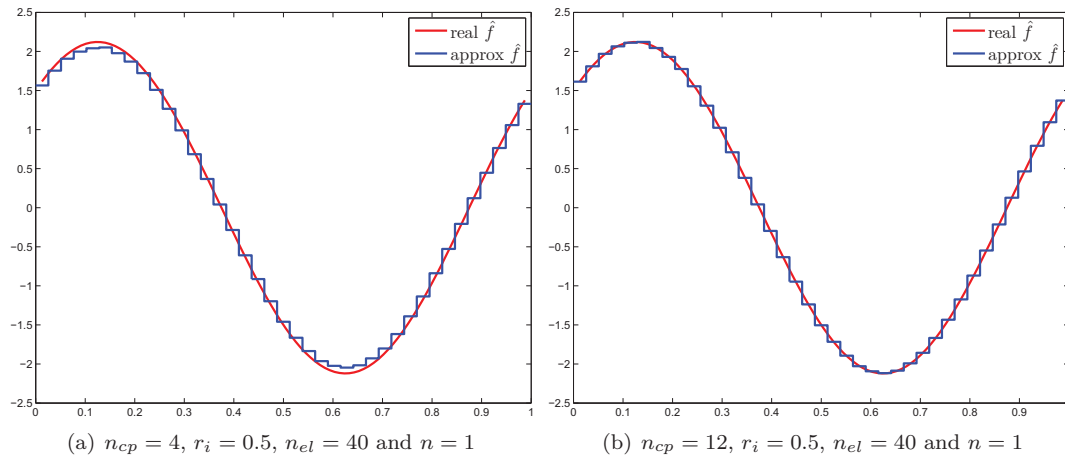
Figure 4.3: The piecewise constant function $\hat{f}$ and the analytical f for respectively 4 and 12 control points

(a) $n_{cp} = 4$, $r_i = 0.5$, $n_{el} = 40$ and $n = 1$

(b) $n_{cp} = 12$, $r_i = 0.5$, $n_{el} = 40$ and $n = 1$
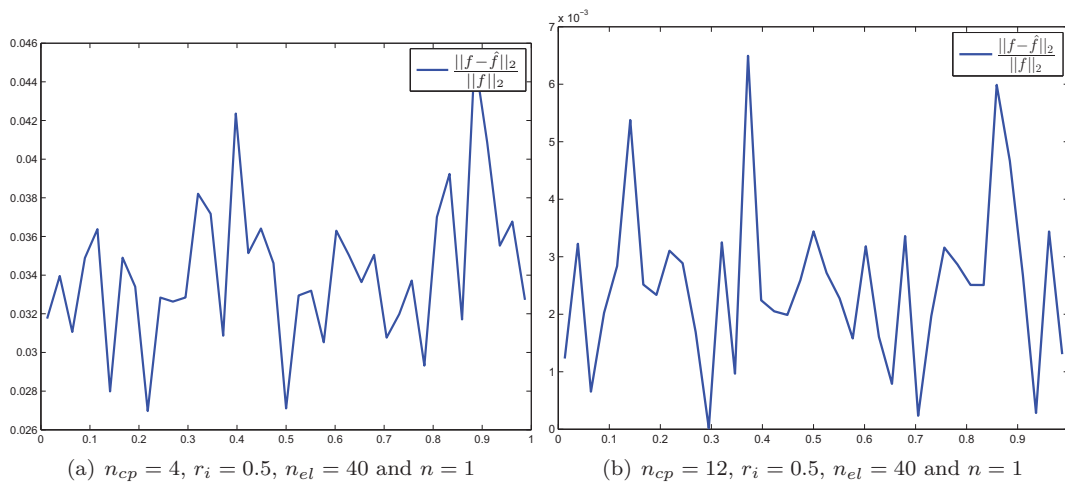
Figure 4.4: The relative error for the approximated $\hat{f}$ and f.

4.6   Conclusion

A method of obtaining the Neumann to Dirichlet map using boundary integral equations, with the boundary element method, has been set up and examined using the solution obtained from separation of variables. It should be mentioned that the linear system of equations is close to singular, from the matrix $\frac{1}{2}\boldsymbol{I}$, since the determinant of this is $\det\left(\frac{1}{2}\boldsymbol{I}\right) = \frac{1}{2^{n_{el}-1}}$, which means that when more elements is added the determinant of the full matrix will get closer to zero. The condition number of the matrix is though stable at around 2. The almost singular matrix, could imply that it would get wrong solutions or none at all, but theory from [15] states that these kind of operators has in fact a compact inverse, and therefore continuing with the solutions given from this, without making any regularization of the matrix. The method of integration is chosen, since the already implemented quadrature rules were not satisfying for a periodic function. A method where the quadrature is based on fourier series or from new research of quadrature of potentials [14], could have been a better choice, but this is left for discussion. The equations has been set up and implemented as given any type of spline inclusion and an induced current it will return the dirichlet data minus the average value of it. Since test Cauchy data is only analytically found for a concentric circular inclusion, it is necessary to find a way to determine Cauchy data for other types of inclusions.

Chapter 5
Conformal mapping

In this chapter theory from complex analysis will be utilized, with regards to the previously calculated annular domain. The goal of this chapter is to find a way to obtain Cauchy-data representing other types of inclusions. The annulus has an important property coming from the Riemann mapping theorem for doubly connected domains, which states that any doubly connected domain are conformally equivalent to the annulus. This means that given an inclusion of arbitrarily shape there exists a conformal map which takes the boundary of the inclusion to a concentric circle. First some preliminaries of complex funtion theory, where the text book used is [21].

5.1 Analytic functions

There exists some of the same properties for complex valued functions as for real valued function, i.e. same reasoning for continuity and differentiability, there are though some additional properties. For example with differentiability a complex valued function f on an open set Ω of complex numbers is said to be holomorphic (or analytic) at the point $z_0 \in \Omega$ if the limit of the qoutient

$$f'(z_0) = \lim_{h \to 0} \frac{f(z_0 + h) - f(z_0)}{h},$$

exists, here $h \in \mathbb{C}$, $h \neq 0$ and $z_0 + h \in \Omega$. The difference from real valued functions are here that h is a complex number and can approach zero from any direction. Let $z = x + iy$ with $i = \sqrt{-1}$, be a complex number and $\bar{z} = x - iy$ denoting the complex conjugate for x, y and $f(z) = f(x, y) = u(x, y) + iv(x, y)$ where u, v are real functions, if f is holomorphic the important *Cauchy-Riemann* equations are given by

$$\frac{\partial u}{\partial x} = \frac{\partial v}{\partial y} \quad \text{and} \quad \frac{\partial u}{\partial y} = -\frac{\partial v}{\partial x}.$$

Then defining two differential operators

$$\frac{\partial}{\partial z} = \frac{1}{2}\left(\frac{\partial}{\partial x} + \frac{1}{i}\frac{\partial}{\partial y}\right) \quad \text{and} \quad \frac{\partial}{\partial \bar{z}} = \frac{1}{2}\left(\frac{\partial}{\partial x} - \frac{1}{i}\frac{\partial}{\partial y}\right).$$

Now proving exercise 12, chapter 2 in [21] which states that any real-valued twice differentiable harmonic function defined in the unit disc $\mathbb{D} := \{z \in \mathbb{C} \mid |z| < 1\}$ is the real part of a holomorphic function in the same region.

Theorem 5.1.1 *Let $u \in C^2(\mathbb{D})$ be harmonic, where $\mathbb{D}$ is the unit disc, that is*

$$\Delta u(x, y) = 0,$$

for all $(x, y) \in \mathbb{D}$. Then $\exists f$ holomorphic on $\mathbb{D}$ s.t.

$$Re(f) = u.$$

Proof : Using the two differential operators

$$\frac{\partial}{\partial \bar{z}}\frac{\partial}{\partial z} = \frac{1}{2}\left(\frac{\partial}{\partial x} - \frac{1}{i}\frac{\partial}{\partial y}\right)\frac{1}{2}\left(\frac{\partial}{\partial x} + \frac{1}{i}\frac{\partial}{\partial y}\right) \tag{5.1.1}$$

$$= \frac{1}{4}\left(\frac{\partial^2}{\partial x^2} + \frac{\partial^2}{\partial y^2}\right). \tag{5.1.2}$$

Now let $g(z) = 2\frac{\partial u}{\partial z}$ then $\frac{\partial g}{\partial \bar{z}} = 2\frac{\partial}{\partial \bar{z}}\frac{\partial}{\partial z}u = 0$, since u is harmonic. From theorem 2.4 in [21] shows that g is holomorphic in the disc, since it satisfies Cauchy-Riemann equations. Hence from theorem 2.1 in [21], which states that a holomorphic function in an open disc has a primitive in that disc, e.g. $\exists F$ s.t. $F' = g$. Then

$$\frac{\partial Re(F)}{\partial z} = \frac{1}{2}\frac{F}{\partial z} = \frac{1}{2}g = \frac{\partial u}{\partial z}, \tag{5.1.3}$$

by proposition 2.3 on page 12 [21]. From (5.1.3) $Re(F)$ differs from u by a constant u_0, then if $f(z) = F(z) - u_0$, f is holomorphic and the real part $Re(f) = u$. ■

This shows that any harmonic function is the real part of a holomorphic function, which can be utilized for the problem in this project.

Now what is interesting is conformal mappings or biholomorphic mappings. Which is defined as a bijective holomorphic mapping $f : U \to V$ is called a conformal map or a biholomorphism.

5.2   Automorphisms of the unit disc

In this project the outer boundary has been assumed to be $\partial \mathbb{D}$. To move the inclusion to either a non-concentric circle or an inclusion of another shape, considering the conformal mappings known as automorphisms $Aut(\mathbb{D})$ which are conformal mappings which maps the open disc to itself. For the unit disc there is obviously the identity map $z \mapsto z$ but also rotations of the form $z \mapsto e^{i\theta}z$ with inverse $z \mapsto e^{-i\theta}z$. For not so simple mappings, consider the group of Möbius transformations, given by

Definition 5.2.1 *(Möbius Transformation) Let* $\mathbb{CP} = \mathbb{C} \cup \{\infty\}$, *and* $\Phi : \mathbb{CP} \to \mathbb{CP}$, *then* Φ *is a Möbius transformation if it has the form with corresponding matrix formulation*

$$\Phi(z) = \frac{az+b}{cz+d} \sim \begin{bmatrix} a & b \\ c & d \end{bmatrix}\begin{bmatrix} z \\ 1 \end{bmatrix} = \begin{bmatrix} az+b \\ cz+d \end{bmatrix}, \tag{5.2.1}$$

where $a, b, c, d \in \mathbb{C}$ *and* $\det\left(\begin{bmatrix} a & b \\ c & d \end{bmatrix}\right) = ad - bc \neq 0.$

The Möbius transformation given by

$$\Psi_\alpha(z) = \frac{\alpha - z}{1 - \bar{\alpha}z}, \tag{5.2.2}$$

where $\alpha \in \mathbb{C}$ with $|\alpha| < 1$ is of special interest. Here it is not apparent that $\Psi_\alpha \in Aut(\mathbb{D})$ but as a short explanation from the book if $|z| = 1$, then $z = e^{i\theta}$ and

$$\Psi_\alpha(e^{i\theta}) = \frac{\alpha - e^{i\theta}}{1 - \bar{\alpha}e^{i\theta}} = e^{-i\theta}\frac{\alpha - e^{i\theta}}{e^{-i\theta} - \bar{\alpha}} = e^{-i\theta}\frac{w}{\bar{w}} \Rightarrow \tag{5.2.3}$$

$$|\Psi_\alpha(e^{i\theta})| = |e^{-i\theta}\frac{w}{\bar{w}}| = 1. \tag{5.2.4}$$

From the maximum modulus principle, concluding that $|\Psi_\alpha(z)| < 1$ for all $z \in \mathbb{D}$, which means that it maps $\mathbb{D} \to \mathbb{D}$. Furthermore it is self-inverse, here another approach compared to the book,

where the matrix representation of the Möbius transform is observed, where the first row are the values to the nominator a, b and the second row b, d correspond to the denominator

$$\Psi_\alpha(z) = \frac{\alpha - z}{1 - \bar{\alpha}z} \sim \begin{bmatrix} -1 & \alpha \\ -\bar{\alpha} & 1 \end{bmatrix} \begin{bmatrix} z \\ 1 \end{bmatrix} = \begin{bmatrix} \alpha - z \\ 1 - \bar{\alpha}z \end{bmatrix} \tag{5.2.5}$$

and by matrix multiplications, this leads to

$$\Psi_\alpha(\Psi_\alpha(z)) = \begin{bmatrix} -1 & \alpha \\ -\bar{\alpha} & 1 \end{bmatrix} \begin{bmatrix} \alpha - z \\ 1 - \bar{\alpha}z \end{bmatrix} = \begin{bmatrix} z - \alpha + \alpha - |\alpha|^2 z \\ -|\alpha|^2 + \bar{\alpha}z + 1 - \bar{\alpha}z \end{bmatrix} = \begin{bmatrix} (1 - |\alpha|^2)z \\ 1 - |\alpha|^2 \end{bmatrix} = \begin{bmatrix} z \\ 1 \end{bmatrix} = z. \tag{5.2.6}$$

This shows that Ψ_α is an automorphism of the unit disc with itself as inverse. From Theorem 2.2 in [21] it is shown that if f is an automorphism of the disc then $\exists \theta \in \mathbb{R}$ and $\alpha \in \mathbb{D}$ s.t.

$$f(z) = e^{i\theta} \frac{\alpha - z}{1 - \bar{\alpha}z}. \tag{5.2.7}$$

A property of the Möbius transformations are that they map circles to circles and lines to lines.

Lemma 5.2.2 *Möbius transformations maps circles to circles.*

Proof The lemma is proven by a direct computation. The equation for a circle in the plane is given by

$$x^2 + y^2 + ax + by + c = 0,$$

for some choices of a, b and c. Now set $z = x + iy \neq 0$ and $\frac{1}{z} = u + iv$, then

$$u = Re\left(\frac{1}{x + iy}\right) = Re\left(\frac{x - iy}{x^2 + y^2}\right) = \frac{x}{x^2 + y^2}$$

$$x = Re\left(\frac{1}{u + iv}\right) = Re\left(\frac{u - iv}{u^2 + v^2}\right) = \frac{u}{u^2 + v^2}$$

$$v = Im\left(\frac{1}{x + iy}\right) = Im\left(\frac{x - iy}{x^2 + y^2}\right) = \frac{-y}{x^2 + y^2}$$

$$y = Im\left(\frac{1}{u + iv}\right) = Re\left(\frac{u - iv}{u^2 + v^2}\right) = \frac{-v}{u^2 + v^2},$$

which is inserted into the equation for a circle, e.g.

$$\frac{u^2}{(u^2 + v^2)^2} + \frac{v^2}{(u^2 + v^2)^2} + \frac{au}{u^2 + v^2} + \frac{-bv}{u^2 + v^2} + c = 0 \Leftrightarrow$$

$$\frac{u^2 + v^2 + au(u^2 + v^2) - bv(u^2 + v^2)}{(u^2 + v^2)^2} + c = 0 \Leftrightarrow$$

$$\frac{1 + au - bv}{u^2 + v^2} + c = 0 \Leftrightarrow$$

$$1 + au - bv + c(u^2 + v^2) = 0,$$

which is again a circle if $c \neq 0$, if $c = 0$ this is a line, but saying that lines equal circles connected at ∞. This means that the Möbius transform $z \mapsto 1/z$ maps circles which does not pass through the origin to circles and circles which goes through the origin to lines. ∎

5.3 Relation to the forward problem

The previously observed problem of an inclusion which is a concentric circle is of special importance, since the Riemann mapping theorem for doubly connected domains (Theorem 1.2 in

[23]) states that any doubly connected domain can be conformally mapped to an annulus. This can be used to map our previously annular problem to a problem with a different inclusion if the conformal map is known. Let D_a denote the annulus $D_a := \{z \in \mathbb{C} \mid r_i < |z| < 1\}$ and set the two circles $C_{\mathrm{I}} := \{z \in \mathbb{C} \mid |z| = r_i\}$ and $C_{\mathrm{II}} := \{z \in \mathbb{C} \mid |z| = 1\}$ as the boundaries of the annulus. Let Γ_{I} and Γ_{II} denote the boundaries of another doubly connected domain, then there exist a conformal map Ψ, which maps C_{I} to Γ_{I} and C_{II} to Γ_{II}. Now let $\Psi_\alpha \circ \theta = \gamma \circ \psi$, where θ is w.r.t. C_{II}, i.e. given by $\theta(t) := \{e^{it} \mid t \in [0, 2\pi]\}$ and γ relates to the boundary of Γ_{II}, since from the previous section Ψ_α maps the boundary of the unit disc to itself, or can equivalently be set as θ, therefore

$$e^{i\psi(t)} = \Psi_\alpha(e^{it}) \Leftrightarrow \psi(t) = \frac{1}{i} \log\left(\frac{\alpha - e^{it}}{1 - \bar{\alpha}e^{it}}\right). \tag{5.3.1}$$

Now let $\alpha = \rho e^{is}$ where $0 \le \rho < 1$ and $s \in [0, 2\pi]$ and plug in, with some none trivial calculations using trigonometric equations, this evaluates to

$$\psi(t) = s + 2\arctan\left(\frac{1+\rho}{1-\rho}\tan\left(\frac{1}{2}(t-s)\right)\right), \tag{5.3.2}$$

with corresponding derivative

$$\psi'(t) = \frac{1-\rho^2}{1+\rho^2 - 2\rho\cos(t-s)}. \tag{5.3.3}$$

Now if u is the real part of a holomorphic function h, which is harmonic in the annulus and satisfying the boundary conditions and it is conformally mapped to another domain, then $k = \Psi_\alpha \circ h$ will be holomorphic in this region, where $v = Re(k)$ will be a harmonic function, which satisfies the transfered boundary conditions. The new Cauchy-data $\tilde{f} = f \circ \psi$ and $\tilde{g} = (g \circ \psi)\psi'$, which comes from the chain rule combined with Cauchy-Riemann equations as explained in [1]. This mapping is uniquely determined up to rotation for this non-concentric circle inclusion, the new problem is shown in figure 5.1.
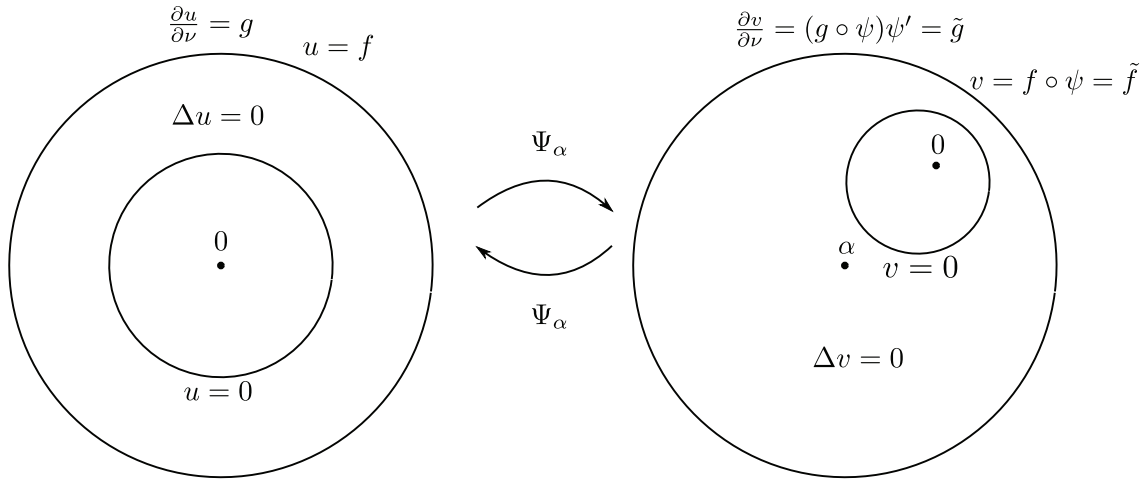

Figure 5.1:   The mapping of the annular problem to the problem with a non-concentric circle inclusion.

Regarding this transformed problem, it is possible to solve the forward problem with this new inclusion and see how the corresponding Cauchy-data will interact compared to the analytically derived.

5.4 Results

The forward problem is transfered from the domain of an annular region to a region with a non-concentric circle. This is done as in figure 5.1, as a solution to the annular region, using (3.3.1) for f and g, e.g. the transfered Cauchy-data are given by

$$\tilde{f}(\theta) = f(\psi(\theta)) = \left(\frac{1}{r_i^n} - r_i^n\right)\left(\cos(n\psi(\theta)) + \sin(n\psi(\theta))\right) \tag{5.4.1}$$

$$\tilde{g}(\theta) = g(\psi(\theta))\psi'(\theta) = n\left(\frac{1}{r_i^n} + r_i^n\right)\left(\cos(n\psi(\theta)) + \sin(n\psi(\theta))\right)\psi'(\theta), \tag{5.4.2}$$

where ψ and ψ' are as defined in (5.3.2) and (5.3.3) and r_i are the radius of the inclusion of the inclusion of the annular domain. In MATLAB the first thing is to transform the control points of the B-spline curve $\gamma(t)$, since $\mathbb{R}^2$ are associated with $\mathbb{C}$ the control points can be changed with a function handle, first define $\alpha = \rho e^{is}$ and then set up the function handle as

```
1  alpha = rho*exp(1i*s);
2  psi_alpha = @(z)(alpha*ones(length(z),1)-z)./(1-conj(alpha)*ones(length(z),1).*z);
```

Example Let $\alpha = 0.6e^{i\pi/2}$ and make 6 control point as a hexagon, where the incircle is the circle of radius $r_i = 0.3$, can be done with the implemented MATLAB function `regPol(p,ri)`, where $p = 6$ here. The corresponding control points including phantom control points are now

$$\text{coefs} = \begin{bmatrix} 0.3000 & 0.3000 & 0.0000 & -0.3000 & -0.3000 & 0.0000 & 0.3000 & 0.3000 \\ -0.1732 & 0.1732 & 0.3463 & 0.1732 & -0.1732 & -0.3463 & -0.1732 & 0.1732 \end{bmatrix},$$

with corresponding knot vector for uniform knots with 10 knots

$$\text{knots} = \begin{bmatrix} -0.3333 & -0.1667 & 0.0000 & \dots & 0.5000 & \dots & 1.000 & 1.1667 & 1.3333 \end{bmatrix}.$$

The transformation of this example is shown in figure 5.2.

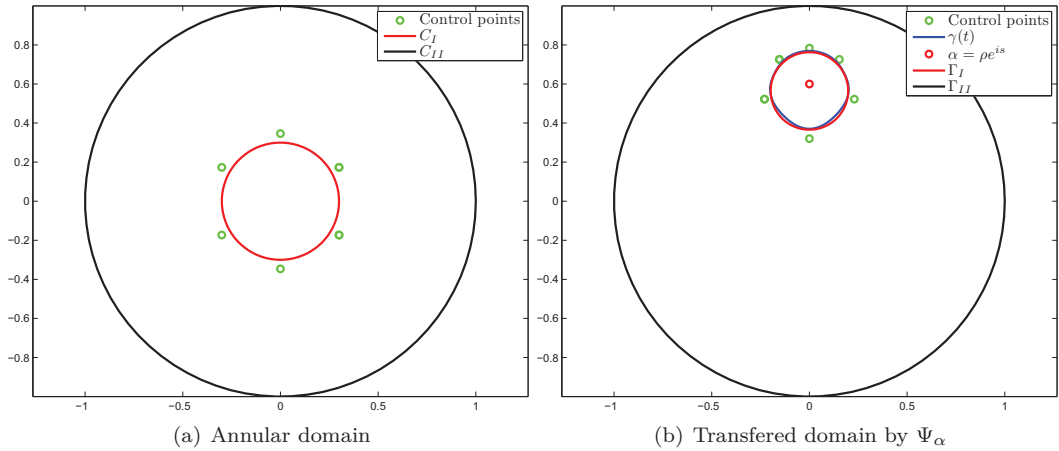(a) Annular domain   (b) Transfered domain by Ψ_α

Figure 5.2: The mapping of 6 control points by $\alpha = 0.6e^{i\pi/2}$, where $\gamma(t)$ is the quadratic B-spline representation of Γ_I.

Now to the solution of the forward problem, with these new control points, knot vector and $\tilde{g}$ defined as in (5.4.2) along with a number of discretization points here $n_{el} = 80$ and choose a $n = 1$. Then as explained in the chapter of the generalised inclusion, the $\hat{f}$ which is computed is actually

$$\hat{f}(x) = u(x) - \frac{1}{2\pi} \int_{\Gamma_{\text{II}}} u(x) ds(x),$$

where x is the restriction of u to Γ_{II}. Which means that the comparison is between this and the difference, with abuse of notation

$$\tilde{f}(t) = \tilde{f}(t) - \int_0^1 \tilde{f}(t) dt,$$

where $t \in [0, 1]$ and the integral is computed using the trapezoidal rule. This is implemented in MATLAB as

```
1   %The angular transformation
2   phi =@(t)s+2*atan((1+rho)/(1-rho)*tan(pi*t-1/2*s));
3   dphi = @(t)(1-rho^2)./(1-2*rho*cos((2*pi*t)-s)+rho^2);
4   % Induced current and analytical voltage on outer boundary
5   n1 = 1;
6   g = @(t,ri) (1/(ri^(n1))*n1+ri^n1*n1)*(cos(n1*phi(t))+sin(n1*phi(t)))*dphi(t);
7   f =@(t,ri)(1/(ri^(n1))-ri^n1)*(cos(n1*phi(t))+sin(n1*phi(t)));
8   % Taking integral using trapezrule to evaluate
9   intf = trapezrule(@(t)real(f(t,ri)),0,1,1000);
10  freal = real(f(tm1,ri))-intf;
```

The piecewise constant approximation $\hat{f}$ and $\tilde{f}$ are plotted in figure 5.3(b) and the 2-norm difference in the evaluated points are shown in figure 5.3(a).
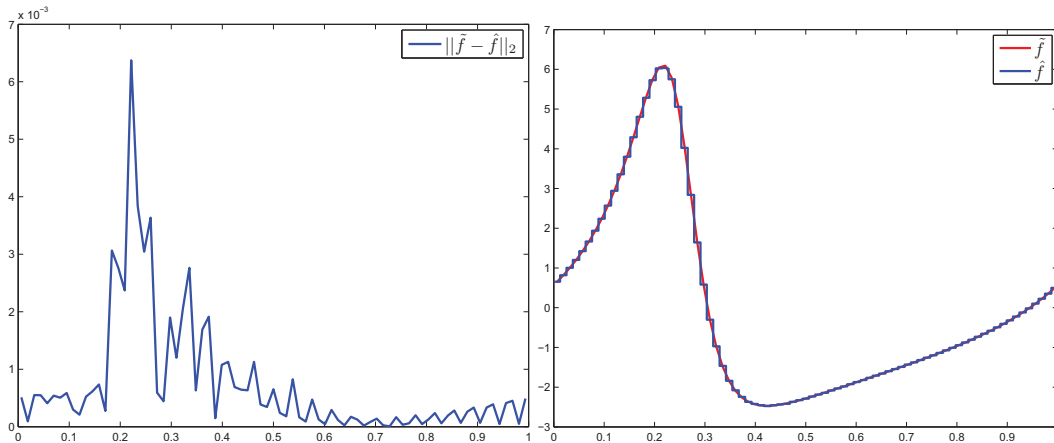
(a) The 2-norm difference between the computed $\hat{f}$ and the calculated $\tilde{f}$.

(b) Piecewise constant approximation $\hat{f}$ to $\tilde{f}$

Figure 5.3:   Comparing the computed $\hat{f}$ and the corresponding $\tilde{f}$ for $\alpha = 0.6e^{i\pi/2}$ and 80 discretization points $n = 1$.

The biggest difference comes when the function changes the most, and the maximal norm difference is $6.37 \cdot 10^{-3}$, which can have something to do that the B-spline curve does not make a perfect circle and integration errors.

The next is a collage with different transformations, i.e. for different choices of α and n holding $r_i = 0.3$ and $n_{el} = 80$ constant.

(a) $\alpha = 0.5e^{i\pi}$.
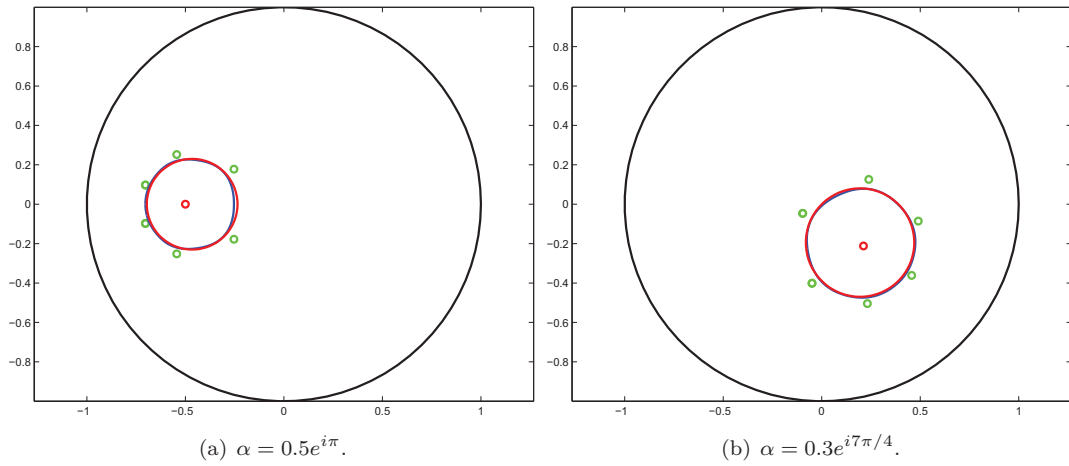
(b) $\alpha = 0.3e^{i7\pi/4}$.

Figure 5.4: Transformed annulus for different values of α

(a) 2-norm difference, $n = 1$

(b) $\hat{f}$ and $\tilde{f}$, $n = 1$.

(c) 2-norm difference, $n = 3$

(d) $\hat{f}$ and $\tilde{f}$, $n = 3$.
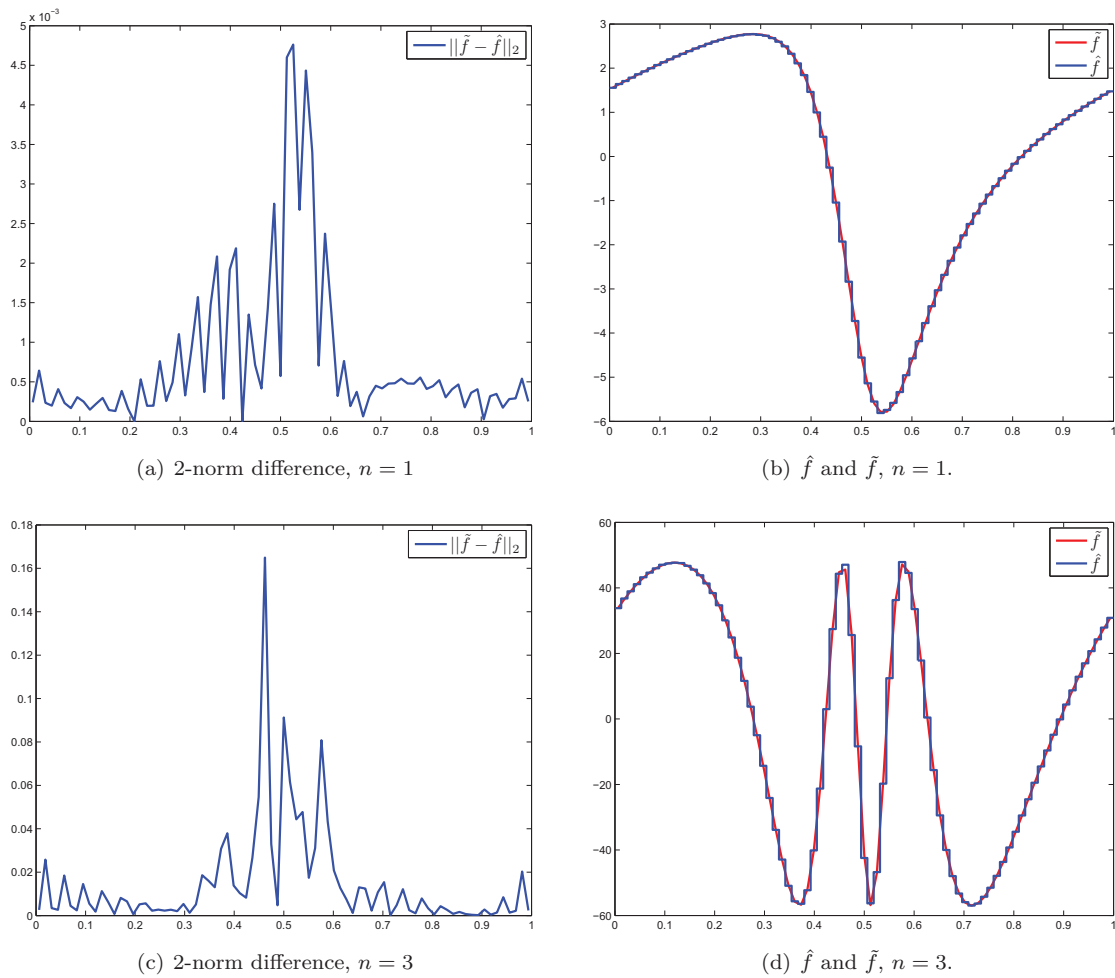
Figure 5.5: Transformed problem $\alpha = 0.5e^{i\pi}$ for $n = 1, 3$ in (5.4.2)

(a) 2-norm difference, $n = 1$

(b) $\hat{f}$ and $\tilde{f}$, $n = 1$.

(c) 2-norm difference, $n = 3$

(d) $\hat{f}$ and $\tilde{f}$, $n = 3$.
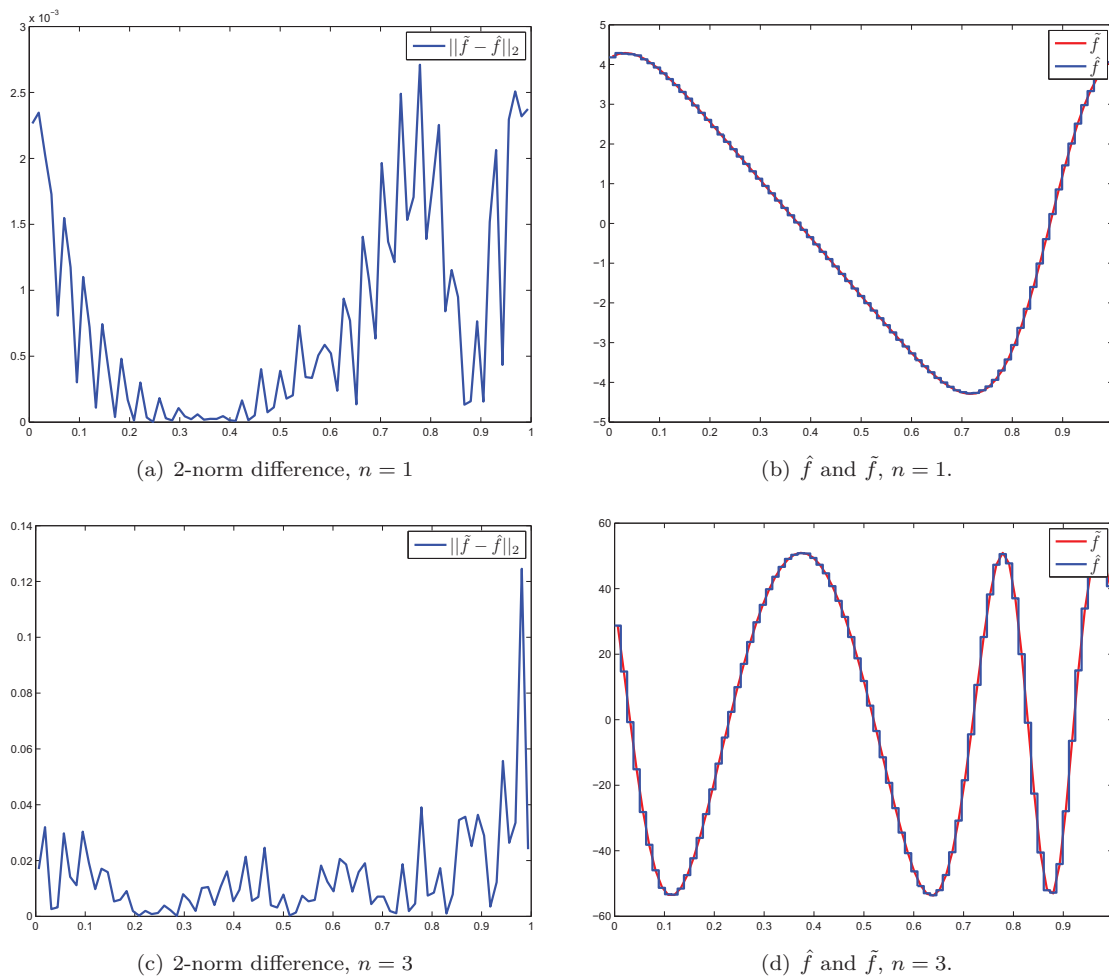
Figure 5.6: Transformed problem $\alpha = 0.3e^{i7\pi/4}$ for $n = 1, 3$ in (5.4.2)

The figures 5.5 and 5.6 shows the approximation computed by the `ForwardProblemSolver` for different transformations and different chosen frequencies. When n gets higher the function values are becoming higher and higher, this is with regards to the part $\frac{1}{r_i^n}$, where $r_i < 1$ for $n = 1$ the function values are in the first case between 3 and -6 where in the other case are between 5 and -5 going further to the case where $n = 3$ the values are between 60 and -60 for both of them, which is ten times higher. Which will say that high frequent signals will give a high valued function, which will therefore also enhance noise a lot more than low-frequent signals.

5.5 Conclusion

The conformal mapping of an annulus to another domain to present new Cauchy-data is seen to be working. Another combination with a holomorphic map could determine Cauchy-data for other types of inclusions. A holomorphic map, since it is holomorphic can be evaluated in a power series, and to get some sort of other inclusion, it would be possible to do the same thing as was done in this chapter for different inclusions. Now there are Cauchy-data corresponding to non-concentric circle inclusions. This will now lead to the inverse problem of given the data, find the inclusion and shape of the inclusion, which will be considered in the next chapter.

In this chapter the inverse problem of detecting and approximating by B-splines the boundary of the perfectly conducting inclusion from measurements of boundary potentials. First a simple case when the known inclusion is a concentric circle, where the minimizer is the radius of the B-spline approximation to the circle given a fixed number of control points. Further investigations leads to minimization of control points for concentric and non-concentric circular inclusions, both examples, with and without a certain noise ratio on the measurement. For computing the optimal shape MATLABs built in solver `fmincon`, has been used, for non-linear programming which is from the Optimization framework [13]. The functions for comparison has been chosen for the optimization of radius and control points as the solution to the solution of the annular problem from Appendix A.2 used for the concentric case and for the non-concentric case the functions found in the chapter of conformal mappings. For the concentric case

$$f(\theta) = \left(\frac{1}{r_i^n} - r_i^n\right)(\cos(n\theta) + \sin(n\theta)) \tag{6.0.1}$$

$$g(\theta) = n\left(\frac{1}{r_i^n} + r_i^n\right)(\cos(n\theta) + \sin(n\theta)), \tag{6.0.2}$$

and for the non-concentric case

$$\tilde{f}(\theta) = f(\psi(\theta)) = \left(\frac{1}{r_i^n} - r_i^n\right)(\cos(n\psi(\theta)) + \sin(n\psi(\theta))) \tag{6.0.3}$$

$$\tilde{g}(\theta) = g(\psi(\theta))\psi'(\theta) = n\left(\frac{1}{r_i^n} + r_i^n\right)(\cos(n\psi(\theta)) + \sin(n\psi(\theta)))\psi'(\theta), \tag{6.0.4}$$

where ψ and ψ' are given by (5.3.2) and (5.3.3). And since the setup of boundary integral equations finds the dirichlet data minus the average, the function compared with are

$$\check{f}(\theta) = \tilde{f}(\theta) - \frac{1}{2\pi}\int_0^{2\pi}\tilde{f}(\theta)d\theta.$$

It is known that for the concentric case the integral is zero, but for the non-concentric case this are taken into account. First part of this chapter is the introduction to noise in the system, which is highly likely in a problem like this.

6.1 Noise

In empirical experiments, measurements of the potential difference will be affected by an amount of noise, where three of the main sources of signal variability [16] are

(i) current drive random noise

(ii) measurement amplifier random noise

(iii) transimpedance flucctuations-dominated by physiological signals and noise

where the current drive can be represented by a constant current generator I_k, k denotes the electrode number and a noise current generator I_n, and similarly for the measurement amplifier can be represented by an additional voltage source V_k. The transimpedance R is the convertion from current to voltage by Ohm's law w.r.t. the domain, i.e. the observed potential difference can be expressed as

$$V_{\text{obs}} = (I_k + I_n)R + V_k$$

Assuming the induced current is noiseless, and then assuming that the noise V_k can be interpreted as gaussian noise and should be compared to the signal. So mathematically speaking the noise can be interpreted as

$$\boldsymbol{f}_{\text{obs}} = \boldsymbol{f}_{\text{real}} + \boldsymbol{f}_{\text{noise}},$$

where $\boldsymbol{f}_{\text{noise}}$ is a noise vector with the size of $\boldsymbol{f}_{\text{real}}$, which is the real measurements taken in an amount of collocation points. First let $\boldsymbol{e}$ be a vector of gaussian noise, and normalize it to $\boldsymbol{e}_1 = \frac{\boldsymbol{e}}{\|\boldsymbol{e}\|_2}$ then scale it compared to the norm of the real signal by a scaling factor β so that the desired measure of the noise is given by

$$\boldsymbol{f}_{\text{noise}} := \beta \|\boldsymbol{f}_{\text{real}}\|_2 \frac{\boldsymbol{e}}{\|\boldsymbol{e}\|_2},$$

so the observed signal is given by

$$\boldsymbol{f}_{\text{obs}} = \boldsymbol{f}_{\text{real}} + \beta \|\boldsymbol{f}_{\text{real}}\|_2 \frac{\boldsymbol{e}}{\|\boldsymbol{e}\|_2}, \tag{6.1.1}$$

where the scaling factor is a measure of the relative error of the observed signal and the real signal, which can be seen by this short computation

$$\|\boldsymbol{f}_{\text{real}} - \boldsymbol{f}_{\text{obs}}\|_2 = \|\beta \|\boldsymbol{f}_{\text{real}}\|_2 \frac{\boldsymbol{e}}{\|\boldsymbol{e}\|_2}\| = \beta \|\boldsymbol{f}_{\text{real}}\|_2 \Leftrightarrow \beta = \frac{\|\boldsymbol{f}_{\text{real}} - \boldsymbol{f}_{\text{obs}}\|_2}{\|\boldsymbol{f}_{\text{real}}\|_2}.$$

This is implemented in MATLAB using the function randn for computing of $\boldsymbol{e}$.

6.2   Optimization of radius

In this section considering knowing that the inclusion is a concentric circle with radius $0 < r_i < 1$ then defining the functional

$$J(r_i) = \int_{\Gamma_{\text{II}}} |f - \hat{f}(r_i)|^2 ds \to inf \tag{6.2.1}$$

where f are the measured voltages at the surface and $\hat{f}(r_i)$ is the computed voltage distribution, which comes by solving the forward problem with a circle inclusion approximated by second degree B-splines for a fixed number of control points. As explained the problem is solved using MATLABs function fmincon, which takes as input a number of different variables, first it takes in an objective function, which is here implemented as objfunri, which is a function of the objective of the minimization and is seen in appendiks B.2. Since the collocation scheme is over a certain amount of discretization points the functional (6.2.1) is discretized so the evaluation of the real function and computed function is over an amount of elements n_{el} as

$$J(r_i) \approx \sum_{j=1}^{n_{el}-1} \int_{t_j}^{t_{j+1}} |f(s_j) - \tilde{f}(r_i, s_j)|^2 dt = \sum_{j=1}^{n_{el}-1} |f(s_j) - \tilde{f}(r_i, s_j)|^2 h_j \tag{6.2.2}$$

where $s_j = \dfrac{t_{j+1} + t_j}{2}$ and $h_j = t_{j+1} - t_j$, since $h_j = h_{j+1} = \cdots h_{n_{el}-1} = h$, and the minimization is over the midpoint sum of the squared absolute values of the difference in the same points. Start by setting the options of the minimization algorithm to the *interior-point method*, then setting an initial guess, i.e. it is reasonable to set the inclusion within the unit disc, therefore this is set as $r_i^0 = 0.7$. Furthermore no constraints are utilized, neither equality nor inequality constraints, only constraints is for the variable set as

$$0.1 \le r_i \le 0.9.$$

The following matlab code run the minimization algorithm

```
1  options = optimset('Algorithm','interior-point');
2  rimin = fmincon(@objfunri,0.7,[],[],[],[],0.1,0.9,[],options);
```

The algorithm runs and stops saying it has reach a local minimum. The plot for no noise and an inclusion with radius $r_i = 0.3$ for respectively 40 discretization points and 4 and 12 control points is displayed in figure 6.1

(a) $n_{cp} = 4$, $\beta = 0$ (b) $n_{cp} = 12$ $\beta = 0$
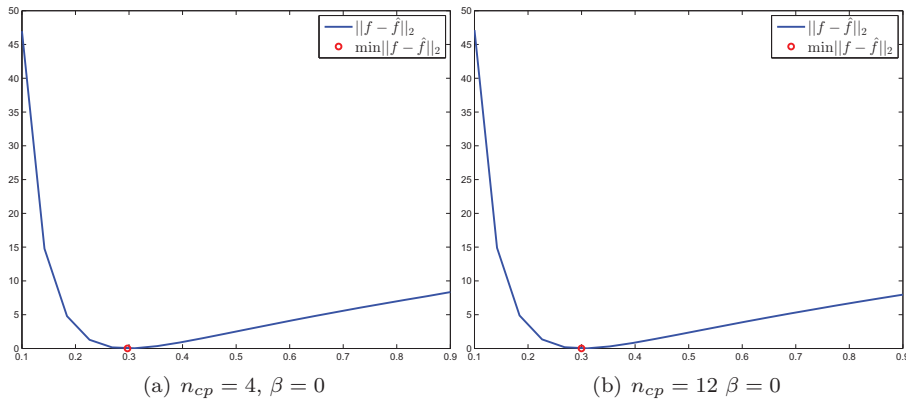
Figure 6.1: For 4 control points $r_i^* = 0.2972$ and for 12 control points the minimal $r_i^* = 0.2999$.

Trying with different values of β and n_{el} is seen in table 6.1, to see how much the noise affect the result

β, n_{el}	1%, 40	5%, 40	5%, 80	10%, 80
$r_i^* : n_{cp} = 4$	0.2972	0.2975	0.2957	0.2942
$r_i^* : n_{cp} = 12$	0.2999	0.3002	0.2983	0.2968

Table 6.1: Minimum r_i^* found for different β and n_{el}.

To visualise the effect of the noise, the corresponding B-spline curves are plotted with respect to the radius found by 10% noise and $n_{el} = 80$, shown in figure 6.2

Figure 6.2 shows that even with a lot of noise, the final inclusion is really close to the exact, which suggests that the optimization of radius is really stable with regard to noise, which is probably because of the simplicity of the optimization over just one variable. The next section shows the more abstract problem of optimization with regards to the control points, which will bring more difficulties, since there are $2 \cdot n_{cp}$ amount of variables.

(a) $n_{cp} = 4$, $r_i^* = 0.2942$ (b) $n_{cp} = 12$, $r_i^* = 0.2968$

Figure 6.2:   The inclusions depicted by 10% noise and 80 points.

6.3   Optimization of control points

The optimization of control points, can be introduced as the minimization of the functional

$$J(\boldsymbol{p}) = \int_{\Gamma_{\mathrm{II}}} |\check{f} - \hat{f}(\boldsymbol{p})|^2 ds \rightarrow inf \tag{6.3.1}$$

where $\boldsymbol{p}$ is a vector of the control points. For the optimization there has again been used `fmincon` with the *interior-point* algorithm. The input is again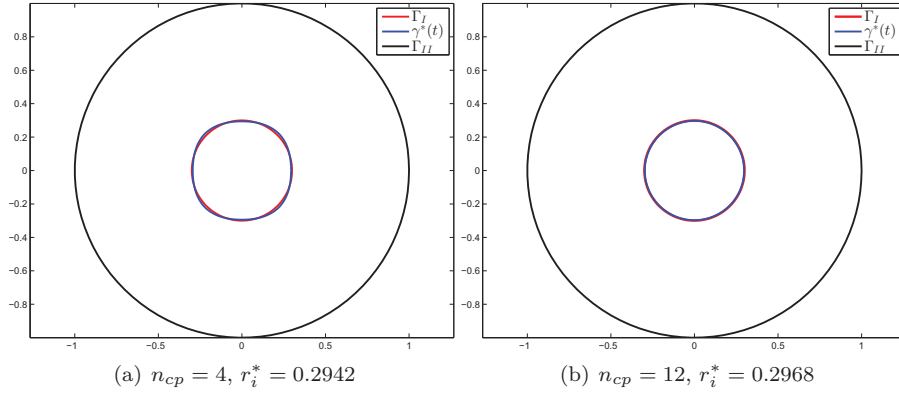 an initial guess, the objective function here implemented in `objfun` which is a function of the control points. The constraints of the control points is set so that they do not go out of the unit disc, and chosen to

$$-0.8 \leq p_{i,x} \leq 0.8$$
$$-0.8 \leq p_{i,y} \leq 0.8.$$

The initial guess will be regular polygon, where the incircle is of radius $r_i^0 = 0.7$, i.e. the initial guess of control points will be for 6 control points

$$\boldsymbol{p}_0 = \begin{bmatrix} 0.7000 & 0.7000 & 0.0000 & -0.7000 & -0.7000 & 0.0000 \\ -0.4041 & 0.4041 & 0.8083 & 0.4041 & -0.4041 & -0.8083 \end{bmatrix}.$$

Here is neglected the phantom control points but they will be added in the objective function, when the spline is created, since the spline has to be periodic, this seems reasonable, and exclude 4 variables in the minimization. So the first part of the objective function adds these phantom control points and makes the uniform knot vector for order 3 spline curve to use in the `ForwardProblemSolver`, then it defines the real Cauchy data and solves the forward problem, then it compares the two functions as explained in the optimization of the radius by

$$J(\boldsymbol{p}) \approx \sum_{j=1}^{n_{el}-1} \int_{t_j}^{t_{j+1}} |\check{f}(s_j) - \tilde{f}(\boldsymbol{p}, s_j)|^2 dt = \sum_{j=1}^{n_{el}-1} |\check{f}(s_j) - \tilde{f}(\boldsymbol{p}, s_j)|^2 h_j, \tag{6.3.2}$$

where the s_j and h_j is defined as in the previous section. without any regularization or definition of gradient the optimization is tried for $n_{cp} = 6$, $n_{el} = 40$ for respectively a concentric and non-concentric circle inclusion.

As seen in figure 6.3, the inclusions boundary has been approximated, but since there is no restrictions on where the approximated gradient will go, the behaviour of the control points are uncontrollable in the algorithm, and for the non-concentric case the optimization ends with an output of too many function evaluations (3000), which means that there has to be done some regularization of the spline curve, in order to control it.

(a) Concentric inclusion $r_i = 0.2$ with $n_{cp} = 6$

(b) Non-concentric inclusion $\alpha = 0.4e^{3\pi/2}$, $n_{cp} = 6$, $r_i = 0.2$
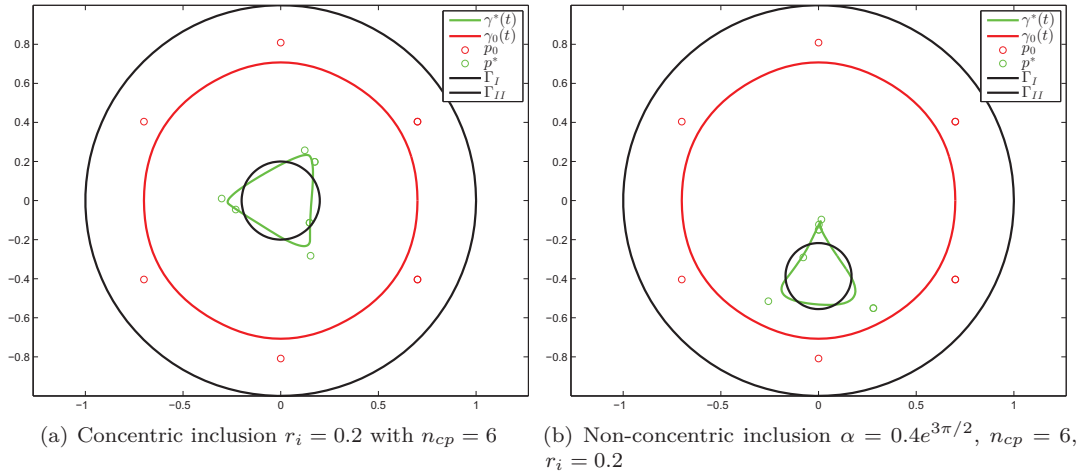
Figure 6.3: The finalized control points $\boldsymbol{p}^*$ for a concentric and non-contric circle inclusion.

6.3.1 Curve regularization

As seen in figure 6.3 there is no restriction for the control points to make a selfintersecting curve or a curve where the control points are extremely close to each other. A regularization term for the speed of the curve, compared to the mean value of the speed that is the curve length

$$L(\gamma) = \int_0^1 |\gamma'(t)| dt. \tag{6.3.3}$$

Taking the squared difference between this and the speed and integrate

$$|\gamma'(t)| - L(\gamma) \Rightarrow (|\gamma'(t)| - L(\gamma))^2 \Rightarrow \int_0^1 (|\gamma'(t)| - L(\gamma))^2 dt \Leftrightarrow \tag{6.3.4}$$

$$\int_0^1 |\gamma'(t)|^2 + L(\gamma)^2 - 2|\gamma'(t)|L(\gamma) dt = \int_0^1 |\gamma'(t)|^2 dt - 2L(\gamma) \int_0^1 |\gamma'(t)| dt + L(\gamma)^2 \Leftrightarrow \tag{6.3.5}$$

$$\int_0^1 |\gamma'(t)|^2 dt - 2L(\gamma)^2 + L(\gamma)^2 = \int_0^1 |\gamma'(t)|^2 dt - L(\gamma)^2 = \int_0^1 |\gamma'(t)|^2 dt - \left(\int_0^1 |\gamma'(t)| dt \right)^2. \tag{6.3.6}$$

This is implemented in the objective function using a function determining the integrand called `intL`

```
1   % Create spline for curve regularization
2   sp = spmak(knots,coefs);
3   s1 = fnder(sp);
4
5   L = quadl(@(t)intL(t,s1,0),0,1,1e-6);
6   S = quadl(@(t)intL(t,s1,1),0,1,1e-6);
7   K = S-L^2;
8   lambda = 1e-3;
9
10  function y = intL(t,s1,bool)
11  dgammat = fnval(s1,t);
12  if bool == 1
13      y = dgammat(1,:).^2+dgammat(2,:).^2;
```

```
14  else
15      y = sqrt(dgammat(1,:).^2+dgammat(2,:).^2);
16  end
```

where the numerical integration used is `quadl`, which is Gauss-Lobatto quadrature, which can evaluate polynomials exact. `s1` is the derivative of the spline curve and `fnval` evaluates the spline at `t`.

Adding this to the objective function, and with a regularization parameter λ our functional is now

$$J(\boldsymbol{P}) = \int_{\Gamma_{\mathrm{II}}} |\check{f} - \hat{f}(\boldsymbol{P})|^2 ds + \lambda \left(\int_0^1 |\gamma'(t)|^2 dt - \left(\int_0^1 |\gamma'(t)|dt \right)^2 \right) \rightarrow inf \qquad (6.3.7)$$

The regularization parameter will be estimated by a trial and error approach.

The effect of the regularization with respect to the previous two figures 6.3 is seen in the figures 6.4

(a) Concentric inclusion $r_i = 0.2$, $n_{cp} = 6$

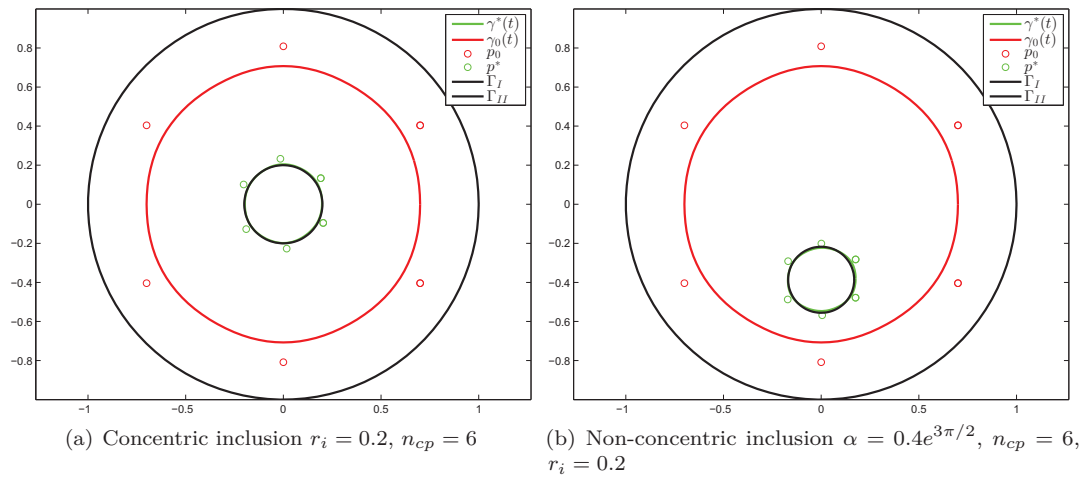(b) Non-concentric inclusion $\alpha = 0.4e^{3\pi/2}$, $n_{cp} = 6$, $r_i = 0.2$

Figure 6.4: The finalized control points $\boldsymbol{p}^*$ for a concentric and non-concentric circle inclusion with $\lambda = 10^{-3}$.

As seen in figure 6.4 the curves do not selfintersect, neither is the control points too close, and the determined circular inclusion $\gamma^*(t)$ and exact Γ_{I} is approximately equal. Further experiments with different noise levels will now be evaluated. First $\beta = 1\%$ noise and the corresponding circle with the same choice of $\lambda = 10^{-3}$ as in figure 6.4(a) is shown for $n_{el} = 40$, then trying to up the regularization and the number of elements to $n_{el} = 80$ is shown in figure 6.5

For even higher noise $\beta = 5\%$ and a non-concentric circle, there is seen to start self-intersecting, even with the regularization and number of elements as in figure 6.5(b). The corresponding figure is shown, where there again has been setup of the regularization parameter λ

The figures shows that, the optimal point is not so robust to noise, but by enhancing the regularization parameter and number of elements, can yield a better approximation to the inclusion, where the curve do not selfintersect nor does the control points get too close. Another way to stop selfintersecting could be done as in [18], where a nonlinear constraint can be set up using Bernstein polyomials. This has not been introduced, since the minimization already is a very slow process since the function needs to approximate the gradient for each step to determine in which direction the step should be performed. Furthermore it can be ended prematurely by the criteria

(a) $n_{cp} = 6$, $\lambda = 10^{-3}$, $n_{el} = 40$ (b) $n_{cp} = 6$, $\lambda = 10^{-2}$, $n_{el} = 80$
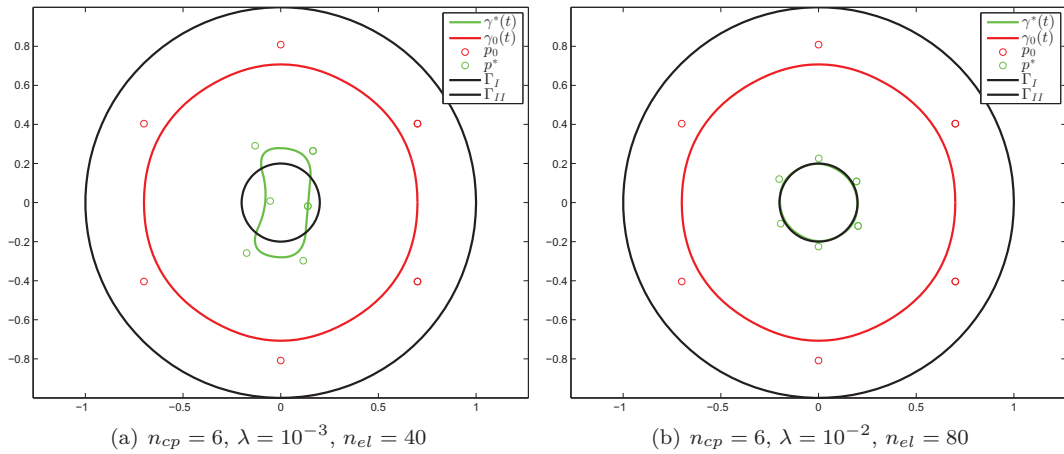
Figure 6.5: The finalized control points $\boldsymbol{p}^*$ for a concentric circle $r_i = 0.2$, with 1% noise and different λ and n_{el}.

(a) $n_{cp} = 6$, $\lambda = 10^{-2}$, $n_{el} = 80$ (b) $n_{cp} = 6$, $\lambda = 5 \cdot 10^{-2}$, $n_{el} = 80$
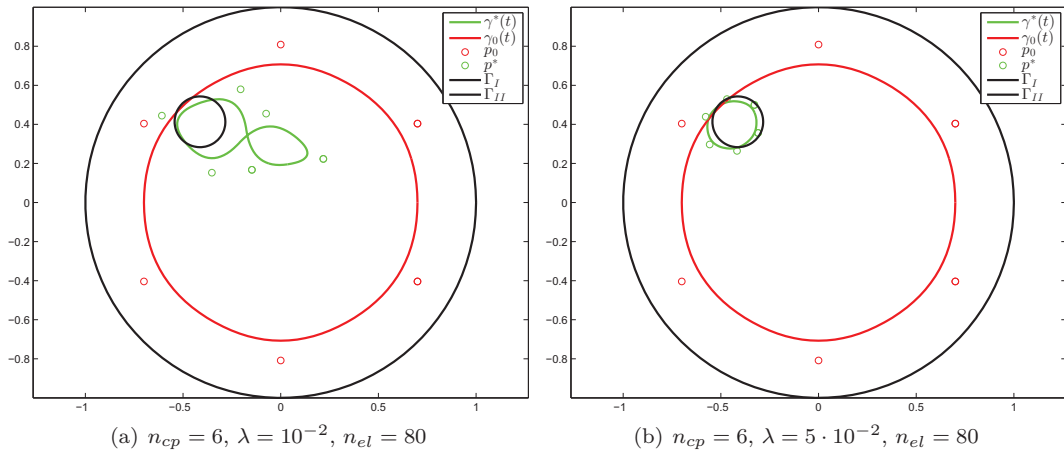
Figure 6.6: The finalized control points $\boldsymbol{p}^*$ for a non-concentric circle $\alpha = 0.6e^{3\pi/4}$, with 5% noise and different λ.

of exceeding the maximum function evaluation (default 3000), so even if the forward problem is solved fast, the optimization will still be slow.

6.4   Conclusion

The shape optimization with regards to the simple case of the inner radius is seen to be very stable to noise and finds a close approximation to the inclusion even with 10% noise. The shape optimization of control points even if it is inefficient and takes a long time to compute, the problem of blindly plug in the objective function, shows that the curve is finding the area of the inclusion, but do not compute the shape in a good way. With the regularization the curve is seen to be more stable and the control points is seen to not get too close or make a selfintersecting curve, this has been tested with different noise levels and different inclusions. The problem gets more unstable when more noise is added to the system, but some countermeasures can be taken into account from upping the regularization and number of elements. The choice of the degree of the B-splines approximating the inclusion, has been set to quadratic polynomial pieces with uniform knot vector, which is a fine choice for circle approximation, even if there is numerous of different ways to evaluate and change the splines.

Chapter **7**
Discussion

In this chapter the results will be analysed and future extensions and outlook will be discussed.

7.1   Discussion of results

The problem stated in the preliminaries is at first a really simplified case of the true non-linear severely ill-posed problem, which is suggesting that this could be an over simplification of the problem and that the true problem will require a different approach. But from the commercialized EIT system PulmoVista [8], they have been seen to use a lot of a priori information regarding the conductivity distribution from empirical experiments. A socalled reference map, which relates in a small way to the a priori knowledge of the conductivity distribution in this project.

The simplification of a perfectly conducting inclusion is for the mathematical purpose good, but in real measurements probably not something which occur on a day-to-day basis. However the scope has been to implement a shape optimization process. The result has been a way to determine circular shaped inclusion in the unit disc, which have been seen to be succesfull for a regularized functional even with different amount of noise, this again is probably not what happens in practical scenaries, unless a person swallowed a perfectly conducting coin. The important example of an annulus has been seen to be conformally mapped for determination of the Cauchy data related to non-concentric circular inclusions, this has been a way to obtain different test data, which could also have been done using a finite element solver.

The boundary integral equations has been set up to find the trace of the function withdrawn the average value on the outer boundary, which is in fact another simplification. This could result in loss of data. However the signal still yields the information needed to obtain the geometry of the inclusion, which means one of two, one, the signal could have been luckily chosen as to not lose data, when withdrawn the average value or two, the average value are insignificant for the signals knowledge of the geometry.

One way to correct the data withdrawal can be to instead of grounding the potential on the inner boundary, then grounding it on the outer boundary making the integral 0 over the outer boundary. Then keep the constant potential on the inner boundary, this will result in a little bit different setup of the integral equations, where the normal derivative has to be taken over a point, which is reflected through the boundary.

7.2   Extensions and outlook

Future extensions can be to look at other holomorphic maps, which can map the annulus to different domains to obtain Cauchy data for other shaped inclusions, this could be done as

47

in [2], where they setup an algorithm to determine the unique conformal radius of the annulus corresponding to the domain of interest. Another way could be to try the Kohn-Vogelius functional, which is the same type of problem, but the PDE is separated into two parts, a part for the Dirichlet problem and one for the Neumann problem, which has proven to be more stable compared to the least-squares functional [10]. It could also be extended to a less simplified problem known as the transmission equation using boundary integral equations as in [7]. To implement it in 3D an extension by surface patches could be obtained again using B-splines as Tensor Products. For the slow optimization an aspect of isogeometric analysis like Shape Calculus and finding derivates of the functional, would also enhance the optimization, such that the optimization algorithm does not approximate the gradient in each step. Regarding setting the B-splines to only look at quadratic uniform periodic B-spline curves is something which can easily be extended to higher or lower degree polynomials, which means that there can be implemented some optimization process regarding the B-splines for adjusting the control points and knots for B-spline curve approximation as done in [26]. Recent progress in quadrature for potentials could also have significant upside to evaluate the BIE [14].

Chapter **8**
Conclusion

In this chapter the partial conclusions throughout the chapters will be combined and the main questions from introduction and preliminaries will be answered.

The main goal of combining the different mathematical fields has been accomplished using the theory of linear integral equations with the Neumann function as kernel to obtain a forward map from Neumann to Dirichlet data minus the average value. The optimization process of determining the shape of an inclusion has been done for circular inclusions by using conformal mapping to get Cauchy-data for the non-concentric case. Then optimize a least squares functional, using the interior-point method. First with respect to the inner radius of a circular approximated B-spline curve, which has seen to be really robust to noise. Secondly by optimizing the control points with respect to the B-spline approximation of a circular inclusion, which has also seen to work, when applied curve speed regularization.

Throughout the chapters there have been done some partial conclusions, where the main aspects has been as regarding the choices made in this thesis. First choice has been to only look at quadratic uniformly periodic B-spline approximation of the geometry whereas the governing functions has been approximated by piecewise constant functions. This has seen to satisfy the set up of the boundary integral equations and evaluated close to the analytical solution obtained from separation of variables. The choice of using a conformal map to map the annular region to a region with the unit disc and a non-concentric circle has also been shown to approximate the analytical functions. Further investigations has led to the optimization problem, where a least squares functional has been set up using a regularization for the curve speed of the B-spline curve. This method has seen to find the circular inclusions even with added gaussian random noise, and approximate the boundary well which was the main goal of this thesis.

List of Appendices

A. Mathematical Theory

A.1. Function spaces

In this appendix section some important function spaces and properties is explained to the extend of the usage in this thesis. First let Ω be a bounded, open set in $\mathbb{R}^2$ equivalent with $\mathbb{C}$ then $C(\Omega)$ is the space of continuous function in Ω, hence $C_0^\infty(\Omega)$ is the space of infinitely continuously differentiable functions with compact support. For the Lebesgue measurable function spaces $1 \leq p < \infty$

$$L^p(\Omega) := \left\{ u(x) : u \text{ Lebesgue measurable}, \int_\Omega |u(x)|^p dx < \infty \right\}, \tag{.0.1}$$

with norm

$$\|u\|_{L^p\Omega} = \left(\int_\Omega |u(x)|^p dx \right)^{1/p}. \tag{.0.2}$$

Where, in this report, the most used is the Hilbert space $L^2(\Omega)$.

A short introduction to Sobolev spaces as the function spaces used in this thesis for functions which does not have too great smoothness properties the results are taken from [11] and [15], and for further study the reader is refered to these. The Sobolev spaces seen in this report is $H^1(\Omega)$, $H^{1/2}(\Gamma)$ and $H^{-1/2}(\Gamma)$, where Ω is an open bounded domain in $\mathbb{R}^2$ with boundary $\partial\Omega = \Gamma$ of class C^1, then $H^1(\Omega)$ is defined as the completion of the space $C^1(\bar{\Omega})$ of continuously differentiable functions with respect to the norm

$$\|u\|_{H^1(\Omega)} := \left(\int_\Omega |u(x)|^2 + |\nabla u(x)|^2 dx \right)^{1/2}.$$

From [15] since each Cauchy sequence w.r.t. H^1-norm is also a Cauchy sequence w.r.t. the L^2-norm, interpreting $H^1(\Omega)$ as a subspace of $L^2(\Omega)$ holds. For a harmonic function the Dirichlet integral

$$\int_\Omega |\nabla u|^2 dx,$$

represent the energy of the potential u and should be finite, when solving a BVP like the one in this thesis. Therefore u should belong to $H^1(\Omega)$. The connection between Sobolev spaces in the domain and on the boundary can be evaluated in the *trace* sense, i.e. if a function is defined on the closure $\bar{\Omega}$ and the restriction to the boundary is called the trace. The operator mapping the function to its trace is called the *trace operator*. From Corollary 8.16 in [15] stating that the trace operator can be uniquely extended as a continuous operator from $H^1(\Omega)$ into $H^{1/2}(\Gamma)$.

This leads to a weak formulation of the interior Neumann problem as to for each solution $u \in C^2(\Omega) \cup C^1(\bar{\Omega})$ to the Neumann problem $\Delta u = 0$ with $\frac{\partial u}{\partial \nu} = g$ on Γ by the Green's identity

$$\int_\Omega \nabla u \cdot \nabla v dx = \int_\Gamma gv ds$$

for all $v \in C^1(\bar{\Omega})$. The duality pairing, combined with the trace theorem, given by

$$\int_\Gamma gvds := g(v),$$

where the integral for all $g \in H^{-1/2}(\Gamma)$ and $v \in H^1(\Omega)$ is well defined. This means that the weak formulation of the Neumann problem is given as find a function $u \in H^1(\Omega)$ that satisfies

$$\int_\Omega \nabla u \cdot \nabla v dx = \int_\Gamma gvds$$

for all $v \in H^1(\Omega)$, given $g \in H^{-1/2}(\Gamma)$. The solution of this problem as the one explained in preliminaries can differ only by a constant and like in preliminaries setting the trace of the inner boundary to 0 yields a unique solution. This has been a short explanation on where the Sobolev spaces arises and for questions about weak derivatives, distribution theory and other Sobolev spaces the reader is refered to the described literature.

A.2. Laplace equation in an Annulus

In this appendix section the method of separation of variables has been used to show existence of a solution to the problem of an annulus for the Laplace equation.
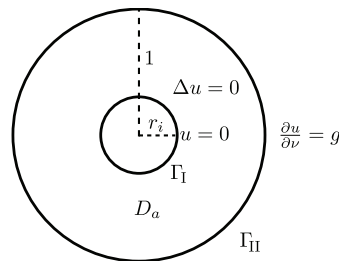
Figure A.1: The domain Ω and assertions.

The problem asserted is find a harmonic function $u \in C^2(D_a) \cup C^1(\bar{D}_a)$ satisfying Laplace equation as shown in figure A.1

$$\Delta u(x) = 0, \quad x \in D_a$$

which satisfies the following boundary conditions

$$u(x) = 0, \quad x \in \Gamma_{\text{I}}$$

$$\frac{\partial u}{\partial \nu}(x) = g(x), \quad x \in \Gamma_{\text{II}},$$

where ν is the normal to the boundary Γ_{II}.

The Laplace equation in cylindrical coordinates are given by

$$\Delta u(x) = u_{rr} + \frac{1}{r}u_r + \frac{1}{r^2}u_{\theta\theta} = 0.$$

Trying a product solution on the form $u(x) = R(r)\Theta(\theta)$, inserting into Laplace equation yields

$$R''(r)\Theta(\theta) + \frac{1}{r}R'(r)\Theta(\theta) + \frac{1}{r^2}R(r)\Theta''(\theta) = 0.$$

Separate variables by dividing with $R(r)\Theta(\theta)$ which gives

$$\frac{R''}{R} + \frac{1}{r}\frac{R'}{R} + \frac{1}{r^2}\frac{\Theta''}{\Theta} = 0 \Leftrightarrow r^2\frac{R''}{R} + r\frac{R'}{R} = -\frac{\Theta''}{\Theta}.$$

Because R and Θ are independent of each other, these will equal a constant μ, i.e.

$$r^2 \frac{R''}{R} + r \frac{R'}{R} = -\frac{\Theta''}{\Theta} = \mu.$$

Hence there are two differential equations given by

$$\Theta''(\theta) + \mu \Theta(\theta) = 0 \tag{.0.3}$$

$$r^2 R''(r) + r R'(r) - \mu R(r) = 0. \tag{.0.4}$$

The differential equation (.0.3) must have periodic boundary conditions given by

$$\Theta(0) = \Theta(2\pi)$$

$$\Theta'(0) = \Theta'(2\pi).$$

First case $\mu = \beta^2$ where $\beta > 0$ the characteristic polynomium given by $\lambda^2 + \mu = 0 \Leftrightarrow \lambda^2 = -\beta^2 \Leftrightarrow \lambda = \pm i\beta$ gives the following solution to the ODE

$$\Theta(\theta) = c_1 \cos(\beta\theta) + c_2 \sin(\beta\theta).$$

Using the periodic BC's gives

$$\Theta(0) = c_1 = c_1 \cos(\beta 2\pi) + c_2 \sin(\beta 2\pi) = \Theta(2\pi)$$

$$\Theta'(0) = c_2 = -c_1 \sin(\beta 2\pi) + c_2 \cos(\beta 2\pi) = \Theta'(2\pi).$$

Since in both cases sine needs to be zero implying $\beta = n = 1, 2, \ldots$.

Second case $\mu = -\beta^2$ where $\beta > 0$ the characteristic polynomium given by $\lambda^2 + \mu = 0 \Leftrightarrow \lambda^2 = \beta^2 \Leftrightarrow \lambda = \pm\beta$ gives the following solutions to the ODE

$$\Theta(\theta) = c_1 \cosh(\beta\theta) + c_2 \sinh(\beta\theta).$$

Using the periodic BC's gives

$$\Theta(0) = c_1 = c_1 \cosh(\beta 2\pi) + c_2 \sinh(\beta 2\pi) = \Theta(2\pi)$$

$$\Theta'(0) = c_2 = c_1 \sinh(\beta 2\pi) + c_2 \cosh(\beta 2\pi) = \Theta'(2\pi).$$

Since sinh is only 0 at sinh(0) these values of μ can be rejected.

Third case $\mu = 0$ which gives the ODE $\Theta''(\theta) = 0$ has solution $\Theta(\theta) = c_1\theta + c_2$ and for the periodic BC's the only solution is $\Theta(\theta) = c_1$ a constant, i.e. the full solution of the ODE with periodic BC's are given by

$$\Theta_n(\theta) = A_n \cos(n\theta) + B_n \sin(n\theta), \quad n = 0, 1, \ldots. \tag{.0.5}$$

For the ODE (.0.4) inserting the values of $\mu = n^2$ $n = 1, 2, \ldots$ gives

$$r^2 R''(r) + r R'(r) - n^2 R(r) = 0,$$

which is identified as an Euler type ODE, where it's reasonable to try a solution on the form $R(r) = r^\alpha$, e.g.

$$r^2 \alpha(\alpha - 1) r^{\alpha-2} + r\alpha r^{\alpha-1} - n^2 r^\alpha = 0 \Leftrightarrow (\alpha(\alpha - 1) + \alpha - n^2) r^\alpha = 0 \Leftrightarrow (\alpha^2 - n^2) r^\alpha = 0,$$

since $r > 0$ the condition $\alpha^2 - n^2 = 0 \Leftrightarrow \alpha = \pm n$ must be satisfied and since they are distinct real roots, the solution of the Euler type ODE is hereby

$$R(r) = c_1 r^n + c_2 r^{-n}, \quad n = 1, 2, \ldots.$$

For the case where $n = 0$ the ODE takes the form $r^2 R'' + rR' = 0 \Leftrightarrow r(rR'' + R') = 0$ implying $rR'' + R' = (rR')' = 0$ integrating on both sides and moving constant and r over gives $R' = \dfrac{c_1}{r}$ and integrating again gives $R(r) = c_1 \log(r) + c_2$.

The full solution for (.0.4) are therefore

$$R_n(r) = \begin{cases} C_n r^n + D_n r^{-n}, & n = 1, 2, \ldots \\ C_0 + D_0 \log(r), & n = 0. \end{cases} \tag{.0.6}$$

Combining (.0.5) and (.0.6) for all the product solutions, i.e.

$$u_n(r, \theta) = R_n(r)\Theta(\theta) = \begin{cases} A_0(C_0 + D_0 \log(r)) \\ (A_n \cos(n\theta) + B_n \sin(n\theta))(C_n r^n + D_n r^{-n}) \end{cases}$$

for $n = 0, 1, \ldots$. The full solution comes from summing over every n-solutions and by abusing notation setting $A_n = A_n C_n$, $B_n = A_n D_n$, $C_n = B_n C_n$ and $D_n = B_n D_n$ e.g.

$$u(r, \theta) = A_0 + B_0 \log(r) + \sum_{n=1}^{\infty} (A_n r^n + B_n r^{-n}) \cos(n\theta) + (C_n r^n + D_n r^{-n}) \sin(n\theta). \tag{.0.7}$$

Use orignial BC's on (.0.7) which gives for first one

$$u(r_i, \theta) = A_0 + B_0 \log(r_i) + \sum_{n=1}^{\infty} (A_n r_i^n + B_n r_i^{-n}) \cos(n\theta) + (C_n r_i^n + D_n r_i^{-n}) \sin(n\theta) = 0$$

which gives coefficients

$$\begin{aligned} A_0 + B_0 \log(r_i) = 0 &\Leftrightarrow B_0 = -\frac{A_0}{\log(r_i)} \\ A_n r_i^n + B_n r_i^{-n} = 0 &\Leftrightarrow B_n = -A_n r_i^{2n} \\ C_n r_i^n + D_n r_i^{-n} = 0 &\Leftrightarrow D_n = -C_n r_i^{2n}. \end{aligned} \tag{.0.8}$$

Inserting into (.0.7) gives

$$u(r, \theta) = A_0 \left(1 - \frac{\log(r)}{\log(r_i)}\right) + \sum_{n=1}^{\infty} r_i^n \left(\left(\frac{r}{r_i}\right)^n - \left(\frac{r_i}{r}\right)^n\right) (A_n \cos(n\theta) + C_n \sin(n\theta)). \tag{.0.9}$$

Using the second BC, where $\frac{\partial u}{\partial \nu} = \frac{\partial u}{\partial r}$ gives

$$\frac{\partial u}{\partial r}(1, \theta) = -A_0 \frac{1}{\log(r_i)} + \sum_{n=1}^{\infty} n r_i^n \left(\left(\frac{1}{r_i}\right)^n + r_i^n\right) (A_n \cos(n\theta) + C_n \sin(n\theta) = g(\theta)),$$

from the full Fourier series on the right the coefficients can be determined

$$\begin{aligned} -A_0 \frac{1}{\log(r_i)} &= \frac{1}{2\pi} \int_0^{2\pi} g(\varphi) d\varphi \Leftrightarrow A_0 = -\frac{\log(r_i)}{2\pi} \int_0^{2\pi} g(\varphi) d\varphi \\ A_n n r_i^n (r_i^{-n} + r_i^n) &= \frac{1}{\pi} \int_0^{2\pi} g(\varphi) \cos(n\varphi) d\varphi \Leftrightarrow A_n = \frac{1}{n\pi r_i^n (r_i^{-n} + r_i^n)} \int_0^{2\pi} g(\varphi) \cos(n\varphi) d\varphi \\ C_n n r_i^n (r_i^{-n} + r_i^n)) &= \frac{1}{\pi} \int_0^{2\pi} g(\varphi) \sin(n\varphi) d\varphi \Leftrightarrow C_n = \frac{1}{n\pi r_i^n (r_i^{-n} + r_i^n)} \int_0^{2\pi} g(\varphi) \sin(n\varphi) d\varphi. \end{aligned}$$

Inserting the coefficients and exploiting the relation $\cos(x) \cos(y) + \sin(x) \sin(y) = \cos(x - y)$ the solution becomes

$$u(r, \theta) = \log\left(\frac{r}{r_i}\right) \frac{1}{2\pi} \int_0^{2\pi} g(\varphi) d\varphi + \sum_{n=1}^{\infty} \left(\left(\frac{r}{r_i}\right)^n - \left(\frac{r_i}{r}\right)^n\right) \frac{1}{n\pi (r_i^{-n} + r_i^n)} \int_0^{2\pi} g(\varphi) \cos(n(\varphi - \theta)) d\varphi.$$

Now let g be given by

$$g(\theta) = m(r_i^{-m} + r_i^m)\left(\cos(m\theta) + \sin(m\theta)\right).$$

Then the first integral is zero, and the second is only different from 0, since these are orthogonal eigenfunctions, when $m = n$ and is

$$\int_0^{2\pi} \left(\cos(m\varphi) + \sin(m\varphi)\right)\cos(m(\varphi - \theta))d\varphi = \pi\left(\cos(m\theta) + \sin(m\theta)\right),$$

therefore the function satisfying the problem for this particular g and some fixed $m \in \mathbb{Z}$ is

$$u(r,\theta) = \left(\left(\frac{r}{r_i}\right)^m - \left(\frac{r_i}{r}\right)^m\right)\left(\cos(m\theta) + \sin(m\theta)\right). \tag{.0.10}$$

B. Matlab

B.1. Scripts

```matlab
1   % Script to implement the Boundary Element Method for Laplace equation
2   % using spline boundary.
3   clear all; close all; clc;
4
5   % Setting up the induced current on the outer boundary
6   n1 = 1;
7   ri = 0.5;
8   g = @(t,ri) ((1/ri)^n1*n1+ri^n1*n1)*(cos(n1*2*pi*t)+sin(n1*2*pi*t));
9
10  z1_cir = @(t)[cos(2*pi*t);sin(2*pi*t)];
11  % Making the inclusion boundary spline:
12  % Number of edges in the circumscribed polygon
13  p = 12;
14  % Coefficients of the edges of the polygon with incircle radius ri =0.5
15  [coefs, a] = regPolygon(p,ri);
16  % Making phantom coefficients for periodic spline
17  coefs = [coefs coefs(:,2)];
18  [l,n] = size(coefs);
19  k = 3; % Order of the basis functions (degree + 1)
20  % Knot vector [0,1] with phantom knots
21  knots = linspace(-2/p,(p+2)/p,n+k);
22  points = 40; % Number of discretization points
23
24  % Discretizing the spline into number of points
25  t = linspace(0,1,points);
26
27  % Find midpoint between each t and create gamma(tm)
28  tm = .5*(t(1:end-1)+t(2:end));
29
30  % Use ForwardProblem to solve for phi and f
31  [fhat phi Anew tid] = ForwardProblemSolver(g,[],[],knots,coefs,points,ri);
32
33
34  % Plot phi as a piecewise constant function and the real phi(x)
35  phi_spline = spmak(t,phi);
36  fhat_spline = spmak(t,fhat);
37
38  %real values of f and phi
39  ri_real = ri;
40  fhat_real =@(t)((1/ri_real)^n1-ri_real^n1)*(cos(n1*2*pi*t)+sin(n1*2*pi*t));
41  phi_real = @(t)-2*n1*(cos(n1*2*pi*t)+sin(n1*2*pi*t))/ri;
```

```
42
43   %Plotting the two figures
44   h = figure;
45   plot(linspace(tm(1),tm(end),100),...
46       phi_real(linspace(tm(1),tm(end),100)),'-r','linew',2), hold on
47   fnplt(phi_spline,[0 1])
48   %axis([0 1 min(c) max(c)])
49   hl = legend('real $\varphi$','approx $\tilde{\varphi}$');
50   set(hl,'interpreter','latex','fontsize',16)
51   % print(h,'-depsc','..\Images\General\cirincphi40poly12.eps');
52
53   h1 = figure;
54   plot(linspace(tm(1),tm(end),100),...
55       fhat_real(linspace(tm(1),tm(end),100)),'-r','linew',2), hold on
56   fnplt(fhat_spline,[0 1])
57   hl1 = legend('real $\hat{f}$','approx $\hat{f}$');
58   set(hl1,'interpreter','latex','fontsize',16)
59   % print(h1,'-depsc','..\Images\General\cirinc03fhat80poly12.eps');
60
61   hdiff = t(2)-t(1);
62   h2 = figure;
63   plot(tm,sqrt(abs((fhat_real(tm))-(fhat)).^2*hdiff)./sqrt(abs(fhat_real(tm)).^2*hdiff),'linew',2), hold on
64   hl2 = legend('$\frac{||f-\hat{f}||_2}{||f||_2}$');
65   set(hl2,'interpreter','latex','fontsize',20)
66   % print(h2,'-depsc','..\Images\General\cirincrelerrordiff40poly12.eps');
67
68   h3 = figure;
69   plot(tm,sqrt(abs((phi_real(tm))-(phi)).^2*hdiff)./sqrt(abs(phi_real(tm)).^2*hdiff),'linew',2), hold on
70   hl3 = legend('$\frac{||\phi-\tilde{\phi}||_2}{||\phi||_2}$');
71   set(hl3,'interpreter','latex','fontsize',20)
72   % print(h3,'-depsc','..\Images\General\cirincrelerrorphidiff40poly12.eps');
```

```
1    % Script for the forward problem for a non-concentric circle
2    clear all;close all; clc;
3    % Normal unit disc setup of circular inclusion spline of radius ri
4    p = 6;
5    ri = .3;
6    [coefs, a] = regPolygon(p,ri);
7    % Making phantom coefficients for periodic spline
8    coefs = [coefs coefs(:,2)];
9
10   % Conformal mapping of unit disc and control points with psi_alpha
11   rho = 0.3; s = -pi/4;
12   alpha = rho*exp(1i*s);
13   psi_alpha = @(z)(alpha*ones(length(z),1)-z)./(1-conj(alpha)*ones(length(z),1).*z);
14   %psi_alpha = @(z)(z-alpha)/lambda;
15   % Transform of control points
16   coefs_complex = coefs(1,:)+1i*coefs(2,:);
17   coefs_new = psi_alpha(coefs_complex(:));
18   coefs_new = [real(coefs_new)';imag(coefs_new)'];
19   [l,n] = size(coefs_new);
20   k = 3; % Order of the basis functions (degree + 1)
21   % Knot vector [0,1] with phantom knots
22   knots = linspace(-2/p,(p+2)/p,n+k);
23   points = 80;
```

```
24  % Generation of spline
25  sp = spmak(knots,coefs_new);
26  t1 = linspace(0,1,points);
27  tm1 = ((t1(2:end)+t1(1:end-1))/2)';
28
29  % Transformed values of the true problem
30  z_cir = @(t)exp(1i*t(:)*2*pi);
31  z = ri*exp(1i*t1*2*pi);
32  z1 = psi_alpha(z(:));
33  z1_cir = @(t)[real(psi_alpha(z_cir(t)))';imag(psi_alpha(z_cir(t)))'];
34  pl_cir = z1_cir(t1);
35
36  % Figure of the originally annular region
37  h1 = figure;
38  plot(coefs(1,:),coefs(2,:),'og','linew',2), hold on
39  plot(real(z),imag(z),'-r','linew',2)
40  plot(real(z_cir(t1)),imag(z_cir(t1)),'k','linew',2), axis equal
41  hl1 = legend('Control points','$C_{I}$','$C_{II}$');
42  set(hl1,'interpreter','latex','fontsize',14)
43  % print(h1,'-depsc','..\Images\annulw6CPri03.eps');
44
45  % Figure of the transformed disc with inclusion
46  h2 = figure;
47  plot(coefs_new(1,:),coefs_new(2,:),'og','linew',2), hold on
48  fnplt(sp,[0 1],'-b'),
49  plot(real(alpha),imag(alpha),'or','linew',2),
50  plot(real(z1),imag(z1),'-r','linew',2),
51  plot(real(z_cir(t1)),imag(z_cir(t1)),'k','linew',2), axis equal
52  % hl2 = legend('Control points','$\gamma(t)$',...
53  %     '$\alpha=\rho e^{i s}$','$\Gamma_{I}$','$\Gamma_{II}$');
54  % set(hl2,'interpreter','latex','fontsize',14)
55  % print(h2,'-depsc','..\Images\transfannulw6CPri03r03sminpi4.eps');
56
57  alpha1 = alpha;
58  %The angular transformation
59  phi =@(t)s+2*atan((1+rho)/(1-rho)*tan(pi*t-1/2*s));
60  dphi = @(t)(1-rho^2)./(1-2*rho*cos((2*pi*t)-s)+rho^2);
61  % Induced current and analytical voltage on outer boundary
62  n1 = 1;
63  g = @(t,ri) (1/(ri^(n1))*n1+ri^n1*n1)*(cos(n1*phi(t))+sin(n1*phi(t)))*dphi(t);
64  f =@(t,ri)(1/(ri^(n1))-ri^n1)*(cos(n1*phi(t))+sin(n1*phi(t)));
65
66  % Taking integral using trapezrule to evaluate f minus average of f
67  intf = trapezrule(@(t)real(f(t,ri)),0,1,1000);
68  freal = real(f(tm1,ri))-intf;
69
70  % Solve the forward problem and plot w.r.t. the analytical voltage minus
71  % average
72  [fhat phi1] = ForwardProblemSolver(g,[],[],knots,coefs_new,points,ri);
73  fhatapp_spl = spmak(t1,fhat);
74  h3 = figure;
75  plot(tm1,freal,'-r','linew',2), hold on
76  fnplt(fhatapp_spl,[0 1]),
77  hl3 = legend('$\tilde{f}$','$\hat{f}$');
78  set(hl3,'interpreter','latex','fontsize',16)
79  % print(h3,'-depsc','..\Images\transfannulw6CPri03fhat80r05spin5.eps');
80
```

```
81  h4 = figure;
82  plot(tm1,sqrt(abs((freal)-(fhat')).^2*(t1(2)-t1(1))),'linew',2), hold on
83  hl4 = legend('$||\tilde{f}-\hat{f}||_2$');
84  set(hl4,'interpreter','latex','fontsize',16)
85  % print(h4,'-depsc','..\Images\transfannulw6CPri03n2fhatftilde80r05spin5.eps');
```

```
1   % Minimization of the radius
2   clear all; clc;
3
4   % Setup the minimization algorithm
5   options = optimset('Algorithm','interior-point');
6   rimin = fmincon(@objfunri,0.7,[],[],[],[],0.1,0.9,[],options);
7
8   % Calculate differences for plot
9   ri =linspace(0.1,0.9,20);
10  n2new = zeros(1,length(ri));
11  for i = 1:length(ri)
12      n2new(i) = objfunri(ri(i));
13  end
14
15  h2 = figure;
16  plot(ri,n2new,'-b','linew',2), hold on
17  plot(rimin,objfunri(rimin),'or','linew',2)
18  hl = legend('$||f - \hat{f}||_2$','min$||f - \hat{f}||_2$');
19  set(hl,'interpreter','latex','fontsize',16)
20  print(h2,'-depsc','..\Images\Optim\Jri80poly12beta010.eps');
```

```
1   % Minimization of control points with fmincon
2   clear all; close all; clc;
3   p = 6;
4   x0 = regPolygon(p,0.7); x0 = x0(:,1:p); %x0(1,:) = x0(1,:)-0.3;
5   lb = -0.8.*ones(size(x0)); ub = 0.8.*ones(size(x0));
6   options = optimset('Algorithm','interior-point');
7   tic;
8   x = fmincon(@objfun,x0,[],[],[],[],lb,ub,[],options);
9   tid = toc;
10  x = [x x(:,1:2)];
11
12  % Setup of values for plotting
13  [l,n] = size(x);
14  k =3; points = 80;
15  knots = linspace(-2/p,(p+2)/p,n+k);
16  ri = .2;
17  t = linspace(0,2*pi,100);
18  z_inc = ri*exp(1i*t);
19
20  % Noncontric spline
21  rho = 0.6; s = 3*pi/4;
22  alpha = rho*exp(1i*s);
23  psi_alpha = @(z)(alpha*ones(length(z),1)-z)./(1-conj(alpha)*ones(length(z),1).*z);
24  z1 = psi_alpha(z_inc(:));
25
26  % Make the minimal spline
27  sp = spmak(knots,x);
```

```
28  % Make the spline start quess
29  x0 = [x0 x0(:,1:2)];
30  sp0 = spmak(knots,x0);
31
32  %plot the figure
33  h1 = figure;
34  fnplt(sp,[0 1],'-g'), hold on
35  fnplt(sp0,[0 1],'-r'), hold on
36  plot(x0(1,:),x0(2,:),'or')
37  plot(x(1,:),x(2,:),'og')
38  plot(real(z1),imag(z1),'-k','linew',2)
39  % plot(real(z_inc),imag(z_inc),'-k','linew',2)
40  plot(cos(linspace(0,2*pi,100)),sin(linspace(0,2*pi,100)),'-k','linew',2), axis equal,
41  hl = legend('$\gamma^*(t)$','$\gamma_0(t)$','$p_0$','$p^*$','$\Gamma_{I}$','$\Gamma_{II}$');
42  set(hl,'interpreter','latex','fontsize',14)
43  % print(h1,'-depsc','..\Images\Optim\CP6optR06s3pi4p80ri02l1e2b5e2.eps');
```

B.2. Implemented functions

```
1   function [fhat phi] = ForwardProblemSolver(g,p,k,knots,coefs,points,ri,z1_cir)
2   % Setup of the Forward problem in a linear system of equations which
3   % is solved to get phi and fhat which is piecewise constant
4   % function, and is solved from Ac=b <=> c=A\b, where c is equal to
5   % [phi;fhat] in the midpoint of the discretization interval and assumed
6   % constant over the interval.
7   %
8   %    input:
9   %           g       : Induced current as function handle
10  %           p       : Number of control points for the B-spline
11  %           k       : Order of the B-spline
12  %           knots   : Knot vector for B-spline
13  %           coefs   : Coefficient matrix for Control points [xi;yi]
14  %           points  : Number of discretization points
15  %           ri      : Inner radius of inclusion
16  %           z1_cir  : function handle of the outer circle
17  %
18  %    output:
19  %           fhat    : The trace of u to the outer boundary size(points-1)x1
20  %           phi     : The trace of  the normal derivative of u
21  %                     to the inner boundary size(points-1)x1
22  tic
23  if nargin < 5
24      %set default values
25      points = 40;
26      ri = .5;
27  end
28  % Make circular inclusion with p CP's and of order k B-spline
29  % if knot and coefficient vectors are not provided. Otherwise make spline.
30  if nargin < 4 || (~isempty(p) && ~isempty(k))
31      coefs = regPolygon(p,ri);
32      % Making phantom coefficients for periodic spline
33      coefs = [coefs coefs(:,2)];
34      [l,n] = size(coefs);
35      knots = linspace(-2/p,(p+2)/p,n+k);
```

```matlab
36         sp = spmak(knots,coefs);
37   else
38         sp = spmak(knots,coefs);
39   end
40   % Setup outer boundary
41   if nargin < 8
42         z1_cir = @(t)[cos(2*pi*t);sin(2*pi*t)];
43   end
44   % Discretization parameter
45   t = linspace(0,1,points);
46
47   % Find midpoint between each t
48   tm = .5*(t(1:end-1)+t(2:end));
49
50   % spline values
51   gammas = fnval(sp,tm);
52   % Setting up the discretization for the outer boundary
53   gamma_outers = z1_cir(tm);
54
55   % first derivative,
56   s1 = fnder(sp);
57   % second derivative
58   s2 = fnder(s1);
59
60   % Absolute value of gamma
61   absgammas = sqrt(gammas(1,:).^2+gammas(2,:).^2);
62
63   % Finding derivative and make it unitary
64   dgammas = fnval(s1,tm);
65   ddgammas = fnval(s2,tm);
66   absdgammas = sqrt(dgammas(1,:).^2+dgammas(2,:).^2);
67   unidgammas(1,:) = dgammas(1,:)./absdgammas;
68   unidgammas(2,:) = dgammas(2,:)./absdgammas;
69
70   % Normal derivatives for gammas
71   nux = -[unidgammas(2,:); -unidgammas(1,:)];
72
73   % Constant from Taylor expansion
74   % -1/2*y''(s)yh'(s)/||y'(s)||^2
75   C = -1/2*(((ddgammas(1,:).*nux(1,:)+ddgammas(2,:).*nux(2,:)))./(absdgammas));
76
77   % Initialising of matrix K and Phi
78   K = zeros(points-1);Phi = zeros(points-1);
79   % solve the two integrals on the RHS
80   H = trapezrule(@(t)intH(g,t,gammas,nux,ri,z1_cir),0,1,1000);
81   G = trapezrule(@(t)intG(g,t,gamma_outers,ri,z1_cir),0,1,1000)';
82   % Evaluating at singularity point
83   epsilon = eps/2;
84   G(points/2)=(trapezrule(@(t)intG(g,t,gamma_outers(:,points/2),ri,...
85        z1_cir),0,tm(points/2)-epsilon,10000)+trapezrule(@(t)intG(g,t,...
86        gamma_outers(:,points/2),ri,z1_cir),tm(points/2)+epsilon,1,10000));
87
88   %Solve the integrals used on LHS
89   for j = 1:length(tm)
90        Phi(:,j) = trapezrule(@(t)intPhi(t,gamma_outers,sp,s1),t(j),t(j+1),1);
91        % If x is in the domain of integration
92        K(j,j) = C(j)*(t(j+1)-t(j))+...
```

```
93           trapezrule(@(t)intKs(t,gammas(:,j),sp,s1,nux(:,j)),t(j),t(j+1),1);
94      k = j+1;
95      %If x is not in the domain of integration
96      K(1:j-1,j) = trapezrule(@(t)intK(t,gammas(:,1:j-1),sp,s1,...
97          nux(:,1:j-1)),t(j),t(j+1),1);
98      K(k:end,j) = trapezrule(@(t)intK(t,gammas(:,k:end),sp,s1,...
99          nux(:,k:end)),t(j),t(j+1),1);
100  end
101
102  % Setup A and b
103  A = 1/2*eye(size(K))+1/(2*pi)*K;
104  b = -2*H; b = b(:);
105
106  % Setting up the linear system
107  Anew = [A zeros(points-1,points-1);1/(2*pi)*Phi eye(points-1)];
108  bnew = [b;-2*G];
109
110  % Solve it
111  c = Anew\bnew;
112  phi = c(1:points-1)';
113  fhat = c(points:end)';
114  tid = toc;
```

```
1   function y = intK(t,gammas,gamma,dgamma,nux)
2   % Function within the first integral in the BIE. Setup such that it can be
3   % used as a function handle in quadl
4   %
5   %    input:
6   %            t        : Function variable
7   %            gammas   : Vector of the x-point
8   %            gamma    : B-spline approx to the inner boundary in B-form
9   %            dgamma   : Derivative of gamma also in B-form
10  %            nux      : Normal vector to x point (gammas)
11  %
12  %    output:
13  %            y        : Output function
14
15
16  % Get values for y(t) and y'(t)
17  gammat = fnval(gamma,t);
18  dgammat = fnval(dgamma,t);
19
20  % Find the reflected y*(t) = y(t)/||y(t)||^2
21  regammat = [gammat(1,:)./(gammat(1,:).^2+gammat(2,:).^2);
22              gammat(2,:)./(gammat(1,:).^2+gammat(2,:).^2)];
23
24  % The two difference vectors x-y and x-y*
25  diff1 = [gammas(1,:)-gammat(1,:);
26           gammas(2,:)-gammat(2,:)];
27  diff2 = [gammas(1,:)-regammat(1,:);
28           gammas(2,:)-regammat(2,:)];
29
30  % ||x-y||^2 and ||x-y*||^2
31  n2diff1 = diff1(1,:).^2+diff1(2,:).^2;
32  n2diff2 = diff2(1,:).^2+diff2(2,:).^2;
```

```
33
34  % ||y'(t)||
35  n2dgammat = sqrt(dgammat(1,:).^2+dgammat(2,:).^2);
36
37  % calculating the function
38  % y = ((x-y)/||x-y||^2+(x-y*)/||x-y*||^2)*v(x)*Jacobian
39  y = ((diff1(1,:)./n2diff1+diff2(1,:)./n2diff2).*nux(1,:)+...
40      (diff1(2,:)./n2diff1+diff2(1,:)./n2diff2).*nux(2,:)).*n2dgammat;
```

```
1   function y = intKs(t,gammas,gamma,dgamma,nux)
2   % The Neumann function without the fundamental solution to Laplace
3   % Equation, to setup the part when x is inside the domain of integration.
4   %
5   %   input:
6   %           t       : Function variable
7   %           gammas  : Vector of the x-point
8   %           gamma   : B-spline approx to the inner boundary in B-form
9   %           dgamma  : Derivative of gamma also in B-form
10  %           nux     : Normal vector to x point (gammas)
11  %
12  %   output:
13  %           y       : Output function
14
15  % Get values for y(t) and dy(t)
16  gammat = fnval(gamma,t);
17  dgammat = fnval(dgamma,t);
18
19  % Find the reflected y*(t)= y(t)/||y(t)||^2
20  regammat = [gammat(1,:)./(gammat(1,:).^2+gammat(2,:).^2);
21              gammat(2,:)./(gammat(1,:).^2+gammat(2,:).^2)];
22
23  % The two difference vectors x-y and x-y*
24  diff = [gammas(1,:)-regammat(1,:);
25          gammas(2,:)-regammat(2,:)];
26
27  % ||x-y||^2 and ||x-y*||^2
28  n2diff = diff(1,:).^2+diff(2,:).^2;
29
30  % ||y'(t)||
31  n2dgammat = sqrt(dgammat(1,:).^2+dgammat(2,:).^2);
32
33  % calculating the function y
34  y = (diff(1,:).*nux(1,:)+...
35      (diff(2,:)).*nux(2,:))./n2diff.*n2dgammat;
```

```
1   function y = intH(g_handle,t,gammas,nux,ri,z1_cir)
2   % Function within the RHS integral in the BIE. Setup such that it can be
3   % used as a function handle in quadl
4   %
5   %   input:
6   %           ghandle : Induced current input as function handle
7   %           t       : Function variable
8   %           gammas  : Vector of the x-point
9   %           nux     : Normal vector to x point (gammas)
```

```matlab
10  %
11  %    output:
12  %             y       : Output function
13
14  % Setup of the outer known boundary as the unit disc t in [0,1]
15  % var = [cos(2*pi*t);sin(2*pi*t)];
16  var = z1_cir(t);
17
18  % finding x-y = gamma(s)-y
19  diff = (gammas(1,:)-var(1)).^2+(gammas(2,:)-var(2)).^2;
20
21  % Output function
22  y = real(g_handle(t,ri)).*((gammas(1,:)-var(1))./diff.*nux(1,:)+...
23      (gammas(2,:)-var(2))./diff.*nux(2,:));
```

```matlab
1   function y = intG(g_handle,t,gamma0s,ri,z1_cir)
2   % Function within the RHS integral in the BIE. Setup such that it can be
3   % used as a function handle in quadl
4   %
5   %    input:
6   %             ghandle : Induced current input as function handle
7   %             t       : Function variable
8   %             gamma0s  : Vector of the x-point
9   %
10  %    output:
11  %             y       : Output function
12
13  % Setup of the outer known boundary as the unit disc t in [0,1]
14  % var = [cos(2*pi*t);sin(2*pi*t)];
15  var = z1_cir(t);
16
17  % finding |x-y|
18  diff = sqrt((gamma0s(1,:)-var(1)).^2+(gamma0s(2,:)-var(2)).^2);
19
20  % Output function
21  y = real(g_handle(t,ri)).*(log(diff));
```

```matlab
1   function y = intPhi(t,gamma0s,gamma,dgamma)
2   % Function within the RHS integral in the BIE. Setup such that it can be
3   % used as a function handle in quadl
4   %
5   %    input:
6   %             phihandle : Induced current input as function handle
7   %             t       : Function variable
8   %             gamma0s  : Vector of the x-point
9   %
10  %    output:
11  %             y       : Output function
12
13  % Get values for y(t) and y'(t)
14  gammat = fnval(gamma,t);
15  dgammat = fnval(dgamma,t);
16
17  % Find the reflected y*(t) = y(t)/||y(t)||^2
```

```
18   regammat = [gammat(1,:)./(gammat(1,:).^2+gammat(2,:).^2);
19                gammat(2,:)./(gammat(1,:).^2+gammat(2,:).^2)];
20
21   % The two difference vectors x-y and x-y*
22   diff1 = [gamma0s(1,:)-gammat(1,:);
23            gamma0s(2,:)-gammat(2,:)];
24   diff2 = [gamma0s(1,:)-regammat(1,:);
25            gamma0s(2,:)-regammat(2,:)];
26
27   % ||x-y|| and ||x-y*||
28   n2diff1 = sqrt(diff1(1,:).^2+diff1(2,:).^2);
29   n2diff2 = (sqrt(diff2(1,:).^2+diff2(2,:).^2))...
30       .*(sqrt(gammat(1,:).^2+gammat(2,:).^2));
31
32   % ||y'(t)||
33   n2dgammat = sqrt(dgammat(1,:).^2+dgammat(2,:).^2);
34
35   % calculating the function
36   % y = phi*(log |x-y|+log|x-y*|)*||y'||
37   y = (log(n2diff1)+log(n2diff2)).*n2dgammat;
```

```
1   function [coefs, a] = regPolygon(n,r)
2   % Create coefficients for edge values at the circumscribed regular polygon
3   % of order n and inradius of the circle is r
4
5   % derive circumradius R
6   R = r*sec(pi/n);
7   % derive side length a
8   a = 2*r*tan(pi/n);
9   % derive interior and exterior angle
10  alpha = (n-2)/n*pi;
11  beta = 2*pi/n;
12  % Derive x and y values on the circle
13  x = cos((0:n)*beta-pi/n);
14  y = sin((0:n)*beta-pi/n);
15  coefs = [R*x;R*y];
```

```
1    function f  = objfunri(ri)
2
3   % Setting up the induced current on the outer boundary
4   n1 = 1;
5   g = @(t,ri) ((1/ri)^n1*n1+ri^n1*n1)*(cos(n1*2*pi*t)+sin(n1*2*pi*t));
6
7   % Quadratic B-spline curve
8   k = 3;
9   % Number of discretization points
10  points = 80;
11  % Number of control points for the circumscribed polygon
12  p = 12;
13
14  % Solve the forward problem for a given radius
15  [fhat phi] = ForwardProblemSolver(g,p,k,[],[],points,ri);
16
17
```

```matlab
18  % Discretization points
19  t = linspace(0,1,points);
20
21  % Find midpoint between each t and create gamma(tm)
22  tm = .5*(t(1:end-1)+t(2:end));
23
24  % real radius of inclusion
25  ri_real = .3;
26  fhat_real =@(t)((1/ri_real)^n1-ri_real^n1)*(cos(n1*2*pi*t)+sin(n1*2*pi*t));
27
28  % Noise generation
29  randn('seed',41997);
30  e1 = randn(size(fhat_real(tm)));
31  e2 = e1./norm(e1,2);
32  beta = 1e-1;
33  e = beta*norm(fhat_real(tm),2).*e2;
34  fhat_realn = fhat_real(tm)+e;
35
36  % Step size
37  h = t(2)-t(1);
38
39  %objective function
40  f = sum(h.*abs(fhat_realn-fhat).^2);
```

```matlab
1   function f = objfun(x)
2   % Objective function for fmincon
3   p = 6; k =3; points = 80;
4   coefs =[x x(:,1:2)];
5   ri = 0.2;
6   [l,n] = size(coefs);
7   knots = linspace(-2/p,(p+2)/p,n+k);
8
9   % % concentric circular inclusion functions
10  % n1 = 1;
11  % g = @(t,ri)  ((1/ri)^n1*n1+ri^n1*n1)*(cos(n1*2*pi*t)+sin(n1*2*pi*t));
12  % fhat_real =@(t,ri)((1/ri)^n1-ri^n1)*(cos(n1*2*pi*t)+sin(n1*2*pi*t));
13
14  % nonconcentric calculated functions
15  rho = 0.6; s = 3*pi/4;
16  % alpha = rho*exp(1i*s);
17  %The angular transformation
18  phi =@(t)s+2*atan((1+rho)/(1-rho)*tan(pi*t-1/2*s));
19  dphi = @(t)(1-rho^2)./(1-2*rho*cos((2*pi*t)-s)+rho^2);
20  % Induced current and analytical voltage on outer boundary
21  n1 = 1;
22  g = @(t,ri)  (1/(ri^(n1))*n1+ri^n1*n1)*(cos(n1*phi(t))+sin(n1*phi(t)))*dphi(t);
23  f =@(t,ri)(1/(ri^(n1))-ri^n1)*(cos(n1*phi(t))+sin(n1*phi(t)));
24  % fhatint = trapezrule(@(t)real(fhat_real(t,ri)),0,1,1000);
25
26  % Solve the forward problem
27  fhat = ForwardProblemSolver(g,[],[],knots,coefs,points,ri);
28
29  % Discretization points
30  t = linspace(0,1,points);
31  tm = .5*(t(1:end-1)+t(2:end));
```

```
32
33  % Noise generation
34  randn('seed',41997);
35  e1 = randn(size(fhat_real(tm,ri)));
36  e2 = e1./norm(e1,2);
37  beta = 5e-2;
38  e = beta*norm(fhat_real(tm,ri),2).*e2;
39  fhat_realn = fhat_real(tm,ri)+e;
40  fhat_realn1 = fhat_realn-sum(fhat_realn*(t(2)-t(1)));
41
42
43  % Create spline for curve regularization
44  sp = spmak(knots,coefs);
45  s1 = fnder(sp);
46
47  L = quadl(@(t)intL(t,s1,0),0,1,1e-6);
48  S = quadl(@(t)intL(t,s1,1),0,1,1e-6);
49  K = S-L^2;
50  lambda = 5e-2;
51
52  h = t(2)-t(1);
53  %objective function
54  f = sum(h.*abs(fhat_realn1-fhat).^2)+lambda*K;
55
56  function y = intL(t,s1,bool)
57  dgammat = fnval(s1,t);
58  if bool == 1
59      y = dgammat(1,:).^2+dgammat(2,:).^2;
60  else
61      y = sqrt(dgammat(1,:).^2+dgammat(2,:).^2);
62  end
```

[9]

```
1   function  T = trapezrule(f,a,b,m)
2   % Approximate integral by trapezoidal rule
3
4   % Version 4.06.2004.  INCBOX
5
6   x = linspace(a,b,m+1);                    % grid points
7   T = (feval(f,a) + feval(f,b))/2;    % endpoint contrib.
8   for  i = 1 : m-1
9     T = T + feval(f,x(i+1));     % interior point contrib.
10  end
11  T = (b-a)/m * T;                     % multiply by  h
```

Bibliography

[1] Afraites, L., Dambrine, M. and Kateb, D.: 2006, Conformal mappings and shape derivatives for the transmission problem with a single measurement., *Preprint HAL* .

[2] Akduman, I. and Kress, R.: 2002, Electrostatic imaging via conformal mapping, *Inverse Problems* **1**8(6), 1659.

[3] Ang, K.-C.: 2008, Introducing the boundary element method with matlab, *International Journal of Mathematical Education in Science and Technology* **3**9(4), 505–519.

[4] Cheney, M., Isaacson, D. and Newell, J.: 1999, Electrical impedance tomography, *SIAM review* **4**1(1), 85–101.

[5] Christensen, O.: 2010, *Functions, Spaces, and Expansions*, 1 edn, Birkhäuser Verlag GmbH.

[6] de Boor, C.: 1999, *Spline Toolbox Matlab.*
   URL: `http://dali.feld.cvut.cz/ucebna/matlab/pdf_doc/splines/splines.pdf`

[7] Delbary, F. and Kress, R.: 2010, Electrical impedance tomography with point electrodes, *J. Integral Equations Appl* **2**2, 193–216.

[8] Dräger: 2011, Pulmovista 500.
   URL: `http://campaigns.draeger.com/pulmovista500/en/`

[9] Elden, L., Wittmeyer-Koch, L. and Nielsen, H. B.: 2004, *Introduction to Numerical Computation - analysis and Matlab illustrations*, Studentlitteratur, Lund.
   URL: `http://www2.imm.dtu.dk/pubdb/p.php?3202`

[10] Eppler, K.: 2007, *Efficient Shape Optimization Algorithms for Elliptic Boundary Value Problems*, PhD thesis, Habilitation thesis, Technische Universität Chemnitz, Germany.

[11] Evans, L. C.: 1998, *Partial Differential Equations*, Vol. 19 of *Grad. Stud. Math.*, Amer. Math. Soc., Providence, RI.

[12] Holder, D.: 2005, Electrical impedance tomography.

[13] Inc., M.: 2012, Matlab r2012a.
   URL: `http://www.mathworks.com`

[14] Klöckner, A., Barnett, A., Greengard, L. and O'Neil, M.: 2012, Quadrature by expansion: a new method for the evaluation of layer potentials, *arXiv preprint arXiv:1207.4461* .

[15] Kress, R.: 1999, *Linear integral equations*, Vol. 82, Springer Verlag.

[16] Meeson, S., Blott, B. and Killingback, A.: 1999, Eit data noise evaluation in the clinical environment, *Physiological Measurement* **17**(4A), A33.

[17] Miklavčič, D., Pavšelj, N. and Hart, F.: 2006, Electric properties of tissues, *Wiley encyclopedia of biomedical engineering* .

[18] Nguyen, D. M., Evgrafov, A. and Gravesen, J.: 2012, Isogeometric shape optimization for electromagnetic scattering problems, *Progress In Electromagnetics Research B* **45**, 117–146.

[19] Prautzsch, H., Boehm, W. and Paluszny, M.: 2002, *Bézier and B-spline techniques*, Springer.

[20] Scherzer, O.: 2010, *Handbook of mathematical methods in imaging*, Vol. 1, Springer.

[21] Stein, E. M. and Shakarchi, R.: 2003, *Princeton Lectures in Analysis II, Complex Analysis*, Princeton University Press.

[22] Strauss, W. A.: 1992, *Partial differential equations: An introduction*, Vol. 3, Wiley New York:.

[23] Wen, G. C.: 1992, *Conformal mappings and boundary value problems*, Amer Mathematical Society.

[24] Wikipedia: 2012a, Electrical impedance.
URL: http://en.wikipedia.org/wiki/Electrical_impedance_tomography

[25] Wikipedia: 2012b, Electrical impedance tomography.
URL: http://en.wikipedia.org/wiki/Electrical_impedance_tomography

[26] Yang, H., Wang, W. and Sun, J.: 2004, Control point adjustment for b-spline curve approximation, *Computer-Aided Design* **36**(7), 639–652.